HR Wallingford
Working with water

Flood risk and asset management

Report prepared for the USACE

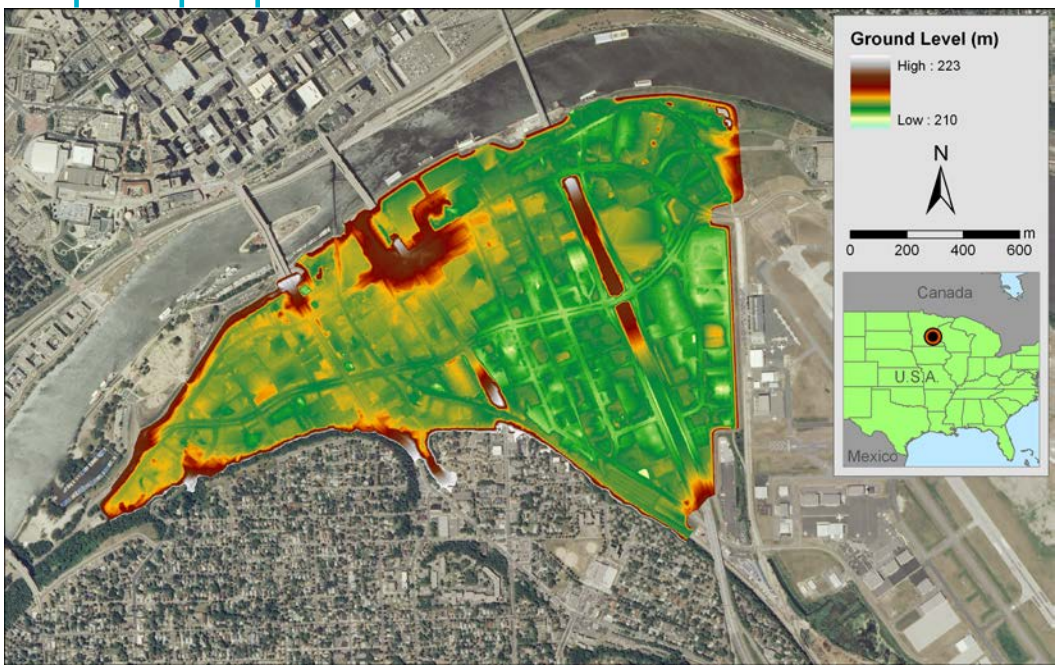

Report EX6687
Release 2.0
September 2012
Approved for Public Release; Distribution unlimited

Report Documentation Page

Form Approved
OMB No. 0704-0188

1. REPORT DATE	2. REPORT TYPE	3. DATES COVERED
SEP 2012		**00-00-2012 to 00-00-2012**

4. TITLE AND SUBTITLE	5a. CONTRACT NUMBER
Flood risk and asset management	**W911NF-10-2-0104**
	5b. GRANT NUMBER
	5c. PROGRAM ELEMENT NUMBER
6. AUTHOR(S)	5d. PROJECT NUMBER
	5e. TASK NUMBER
	5f. WORK UNIT NUMBER
7. PERFORMING ORGANIZATION NAME(S) AND ADDRESS(ES) **HR Wallingford Ltd,Howbery Park, Wallingford,Oxon, OX10 8BA, UK,**	8. PERFORMING ORGANIZATION REPORT NUMBER **; 1433-EN-01**
9. SPONSORING/MONITORING AGENCY NAME(S) AND ADDRESS(ES)	10. SPONSOR/MONITOR'S ACRONYM(S)
	11. SPONSOR/MONITOR'S REPORT NUMBER(S) **1433-EN-01**

12. DISTRIBUTION/AVAILABILITY STATEMENT
Approved for public release; distribution unlimited

13. SUPPLEMENTARY NOTES

14. ABSTRACT

15. SUBJECT TERMS

16. SECURITY CLASSIFICATION OF:			17. LIMITATION OF ABSTRACT	18. NUMBER OF PAGES	19a. NAME OF RESPONSIBLE PERSON
a. REPORT **unclassified**	b. ABSTRACT **unclassified**	c. THIS PAGE **unclassified**	**Same as Report (SAR)**	**128**	

Document Information

Project	Flood risk and Asset Management
Report title	Report prepared for the USACE
Client	USACE
Client Representative	Dave Margo
Project No.	MCR4699
Report No.	EX6687
Project Manager	Ben Gouldby
Project Director	Jonathan Simm

Document History

Date	Release	Prepared	Approved	Authorised	Notes
20/12/11	1.0	BPG	JDS	AFT	Draft
17/09/12	2.0	BPG	JDS	AFT	Draft

Prepared .....

Approved .....

Authorised .....

Summary

Flood risk and asset management

Report prepared for the USACE

Report EX6687
September 2012

Summary to be completed

Contents

1 Introduction

Over a number of years HR Wallingford and the USACE have engaged in collaboration relating to levee performance and wider flood risk management. In particular there are significant synergies in the research developments in both the US and UK focused towards the improved risk-based management of levee systems.

In September 2010, USACE commissioned HR Wallingford to undertake a collaborative project to explore the utility of the tools and techniques that have been developed at HR Wallingford and widely used by the Environment Agency, within the US context. Through pilot application, the aim was to provide a forum for detailed scientific exchange between lead researchers at HR Wallingford and in the USACE. This report presents the findings of this study.

The primary objective of the project was to:

- Support the USACE in developing and implementing robust and credible risk-based asset management analysis tools and techniques in practice.

Secondary objectives of the research were to:

- To exchange information relating to asset management science and capabilities in the US and UK
- To explore the applicability of HR Wallingford tools and techniques in the context of the US setting
- To undertake a "gap analysis" to identify a future research needs
- To outline a programme of future co-ordination and collaboration with USACE.

The project was organised as a series of tasks:

Task 1 Exchange workshops - Providing a forum to exchange asset management science and capabilities in the US and UK.

Task 2 Case study and application – Providing a pilot application of the HR Wallingford tools and techniques and to explore their utility in the US setting.

Task 3 Gap analysis – Providing an analysis of priority research needs based on the case study and on-going research elsewhere within ERDC/HEC.

Task 4 Future programme of research and development – Outline a forward programme of R&D.

To date, two exchange workshops have been held (Task 1). The first took place at HR Wallingford in January of 2011. The second took place at the HEC office in Davis, California in July of 2011. Summary information regarding the workshops is provided in Appendix 1. The primary outcomes of these workshops were the agreement of the pilot site location – St. Paul Minnesota and agreement on the models that were of interest – FRE, HR BREACH and RELIABLE.

This report describes details of the models that have been transferred to USACE and their application on the pilot site (Task 2). It also describes the details of a gap analysis (Task 3) and includes recommendations for further activities (Task 4).

2 Summary description of models

2.1 RELIABLE

Fragility curves that describe the reliability of flood defences conditional on extreme hydraulic loading conditions is a concept that originated within the US, USACE (1996) and has been adopted by the UK. These curves form a primary input to risk analysis models like HEC FDA, HEC FRM and FRE and have been the subject of recent research both in the US and UK, Schultz *et al.* (2010), Simm *et al.* (2009)

The Reliability Tool (RELIABLE) is a prototype software tool that can generate levee or flood defence specific fragility curves. The tool was developed within the FLOODsite and FRMRC research projects (FLOODsite, 2007; FLOODsite 2008). It is used to generate structure-specific fragility curves, based upon a reliability analysis of multiple potential failure modes. The logical rules that link the failure mechanisms are represented by fault trees. The ability to assess the reliability of a defence in as much detail as the engineer requires is an important feature of more local risk analysis and RELIABLE has the potential to offer this capability. It is currently a prototype software tool but could be developed into a robust software system to support asset management and flood risk activities. Further information on RELIABLE is provided in Appendix 2.

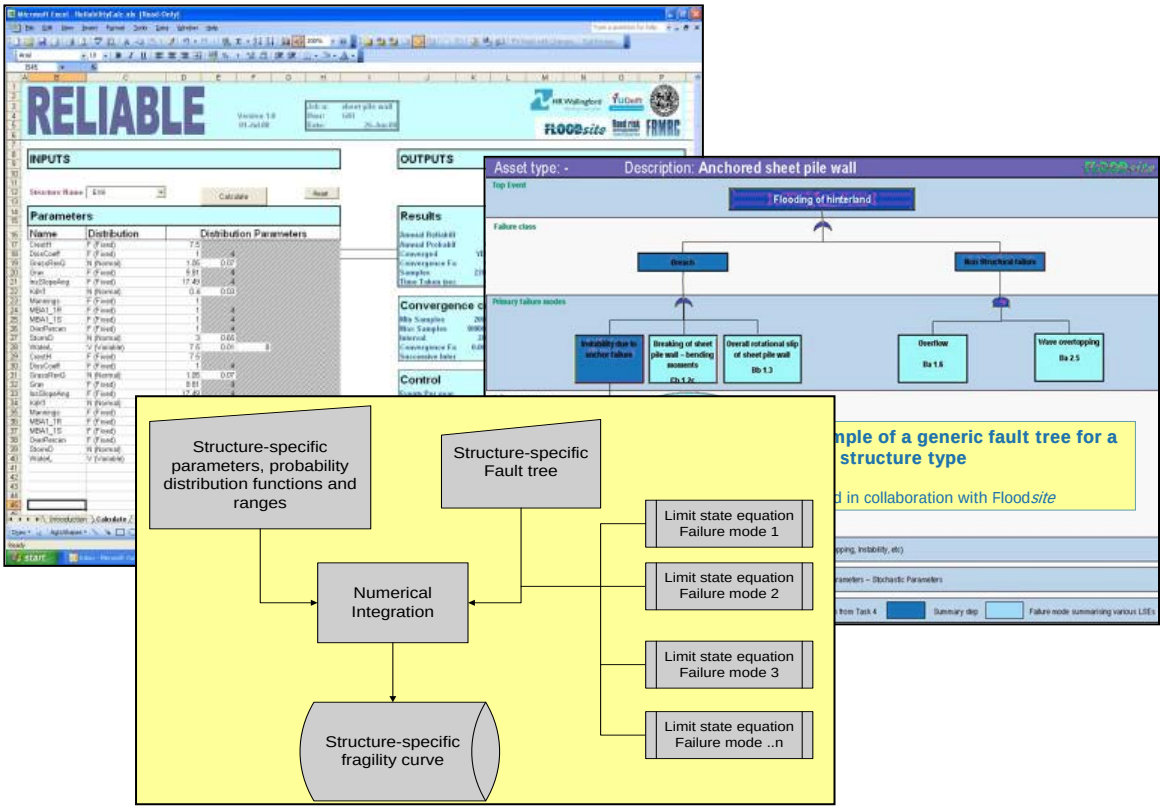

Figure 2.1 Example fault tree and RELIABLE interface

2.2 HR BREACH

A primary aspect of flood risk analysis relates to flood defence failure. The initiation of failure is handled probabilistically through the fragility curves. Another aspect is the development of breaches and the subsequent consequences associated with inundation. Whilst FRE incorporates a conceptual physics-based approach for rapid estimation of breach inflow volume, which is useful for broad-scale modelling, it may be appropriate in some cases to undertake a more rigorous physics-based breach approach locally and utilise the outputs within FRE.

Over the past 15 years, HR Wallingford has undertaken development of a breach model, called HR BREACH (See Figure 2.2). The HR BREACH model predicts breach growth through flood embankments of different material types and construction, combining hydraulics, soil mechanics and structural analysis into a single breach prediction model, Mohamed *et al* (2002). The main features include:

- breach development through piping and/or overflow;
- simulation through both cohesive and non cohesive soils;
- simulation of homogeneous or zoned structures, also including grass or rock embankment surface protection;
- breach growth simulation by surface soil erosion and head cut with discrete block failure processes (including the choice of using different sediment relationships for different embankment types); and
- probabilistic approach options to allow the user to simulate material variability/uncertainty, including full Monte Carlo simulation.

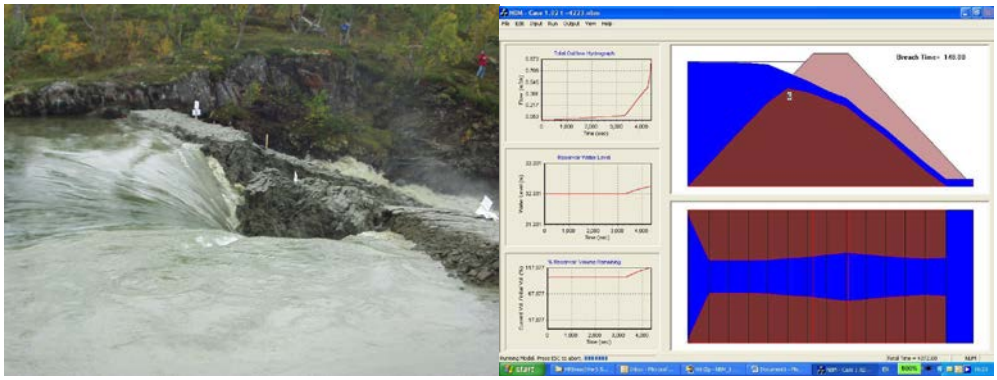

Figure 2.2 GUI of HR BREACH

The HR BREACH model was used during the EC IMPACT (www.impact-project.net; 2001 – 2004) project to compare predictions against field and laboratory test data. The model performed best (on average) in comparison with a number of other breach models from across Europe and the US.

The European FLOODsite project (www.floodsite.net) ran from 2004 – 2009 and offered an opportunity to further develop the HR BREACH model. The research programme allowed for a more rigorous analysis of the IMPACT project data, and implementation of new development work to improve model performance. Further information on HR BREACH is provided in Appendix 3.

The HR BREACH model has been also used on numerous consultancy and research studies by HR Wallingford over the last decade. On the pilot study described below, the HR BREACH model was used to derive improved breach inflow estimates.

2.3 FLOOD RISK ESTIMATOR (FRE)

FRE is a decision support toolset for quantifying economic and social impacts of flooding for present day conditions, future scenarios and different flood risk mitigation measures. It integrates information on fluvial and coastal hazards, with information on the physical flood risk system (assets, topography), and information on people and property in the floodplain, to quantify the overall flood risk.

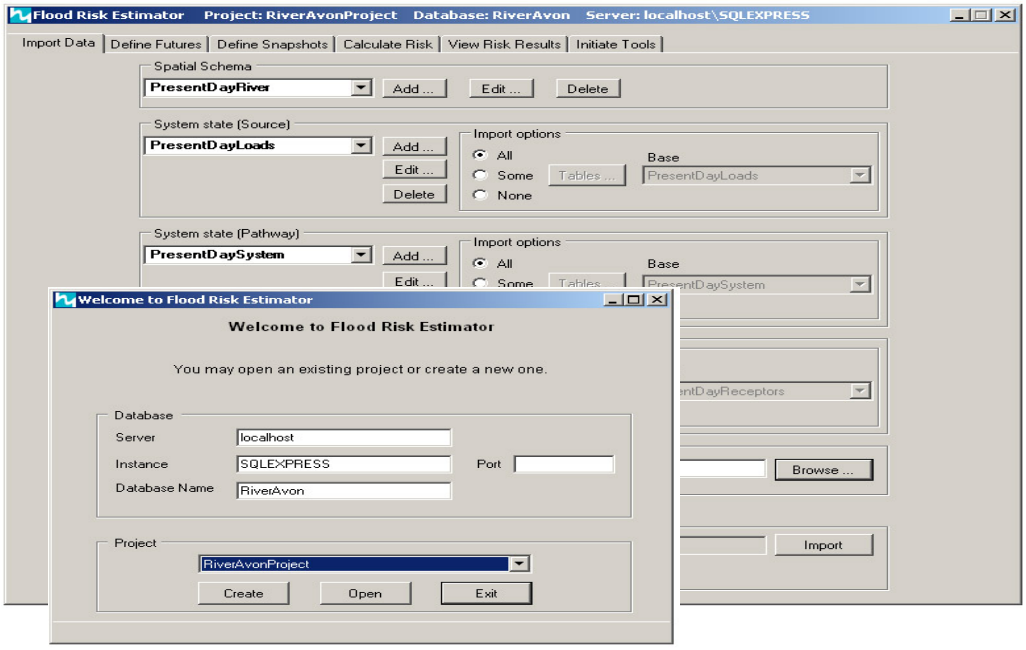

Figure 2.3 Interface of FRE

FRE, by its design, is flexible and therefore capable of supporting a wide range of flood risk management decisions. Further guidance on its use is provided in the supporting User Manual, HR Wallingford (2010).

FRE incorporates the risk analysis approach described by Gouldby *et al* (2008). The primary components are extreme value distributions to describe the hydraulic loads, fragility curves to describe the reliability of the system flood defences and depth damage functions to evaluate economic consequences. It can be used to support flood risk management support decisions relating to, for example:

- What is the existing and future risk?
- Where are the high and low risk areas?
- Which assets contribute most to risk?
- What are the key drivers of risk (probability and consequences)?
- Which mitigations measures are most effective at reducing risk?

The primary outputs of FRE are:

- Spatial distribution of risk expressed as Expected Annual Damage (EAD)

- Spatial distribution of inundation probability
- Levee contribution to risk

The methods used in FRE have been applied to establish the National Flood Risk in England and Wales over the last four years and numerous regional and local studies. The Environment Agency of England and Wales are currently being trained in the application of this approach for their own “in-house” capability in running the model.

3 Application to St Paul pilot site

3.1 INTRODUCTION

The USACE have been engaged in flood risk management activities within the St. Paul area of Minnesota for many years and they are currently undertaking analysis on this area. This area was therefore selected as the pilot site area. The following description of the site has been provided by USACE.

St. Paul levee/floodwall project is located in Ramsey County, MN between river miles 837.0 and 840.4 of the Mississippi River. The original project was authorized by the Flood Control Act of 1958 and construction was completed in 1964. Modification to this project involving a raise of the levee/floodwall of 4 feet was authorized by the Water Resources Development Act of 1986 (PL 99-662). Construction of this portion of the project was completed in 199x. The primary purpose of the project is flood risk management. It includes a recreation component as well in the form of a walking / biking trail.

The area within the line of protection is approximately 445 acres in size and the land use is primarily commercial and industrial in nature. It is located entirely within the St. Paul city limits with downtown St. Paul across the river to the north, St. Paul airport to the east, and residential/commercial neighborhoods to the south and west.

This section of the report describes the application of RELIABLE, HR BREACH and FRE to this study site.

3.2 RELIABLE

One of the primary inputs for the flood risk model, FRE, is the fragility curves associated with each of the flood defences. Within the UK a generic defence categorisation system has been developed and through reliability assessment of their different failure modes a generic set of fragility curves has been developed, (Environment Agency (2007)). These curves have been derived for broad scale analysis and are recognised as being an approximation. This approximation is necessary for regional and national scale analysis as it was considered impractical to undertake a site specific analysis for all defences within large spatial areas. These generic curves comprise approximately 60 different classes. Each class has a set of five fragility curves associated with different condition grades, 1 being very good condition and 5 being very poor condition.

When the risk analysis is being undertaken on smaller spatial scales, it is more practical to undertake site specific reliability analysis. The prototype RELIABLE model has been designed to undertake site specific reliability analysis to generate reach specific fragility cures for use in flood risk analysis models. The application of this model to the St Paul Pilot Site is described below.

During the PFMA session undertaken by the USACE and stakeholders, 13 different modes were identified as potential ways that the St. Paul levee/floodwall might fail. Some of them are grouped together based on general location along the levee alignment

and are represented by a single FIA scenario (six failure modes are represented by the "Middle" FIA scenario).

Table 3.1 shows a list of the identified failure modes, extracted from USACE 2011 and Figure 3.1 shows their location. The defence length in St Paul was also split into 8 reaches (see Figure 3.2).

Table 3.1 Potential failure mechanisms (from USACE 2011)

Performance Failure Modes		
PFM	Description	Station
E1	Embankment piping	1+00
E3	Slope instability	135+00
E5	Embankment overtopping	140+00
E6	Piping at interface	0+00
P1	Piping associated with penetration of levee	42+00
P2	Piping associated with penetration of levee	42+01
W1	I-wall - structural failure	85+00
W3	I-wall - global stability	85+00
W5	I-wall overtopping	85+00
W12	T-wall overtopping	65+00
C1	Failure to install closures	160+00
C4	Failure of Fillmore Ave closure	115+00
I1	Failure of pump station (interior flood control)	0+00

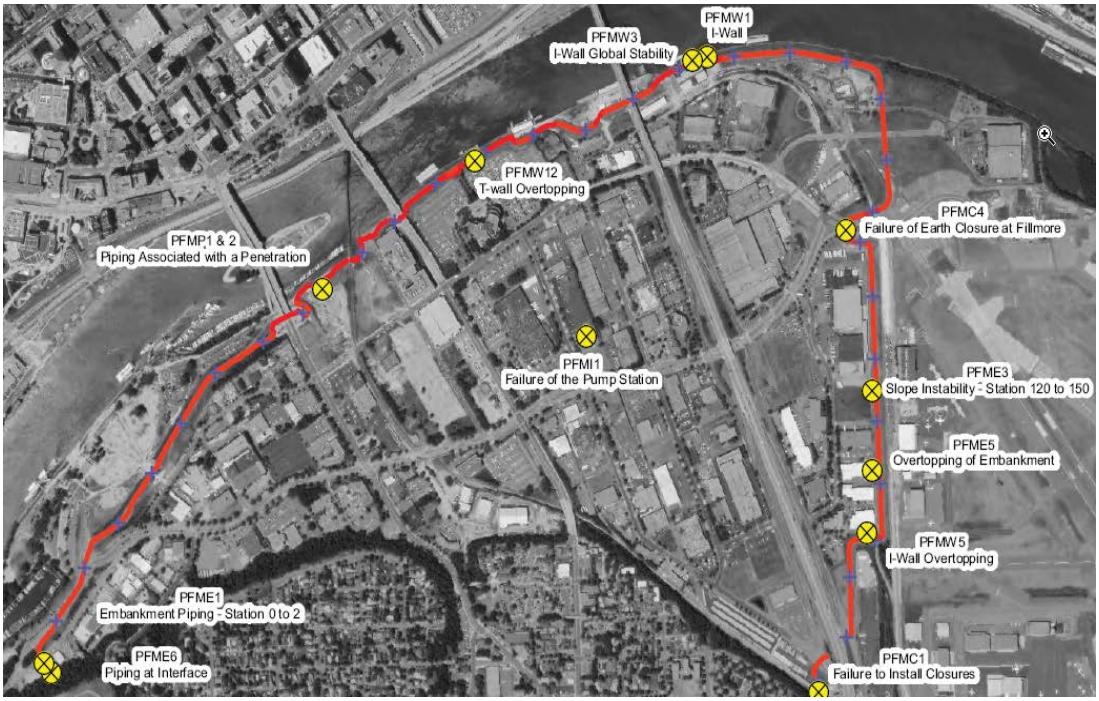

Figure 3.1 Potential failure mode locations

Table 3.2 shows the details of each defence reach. A fragility curve was provided by the USACE for each defence reach (See Figure 3.3).

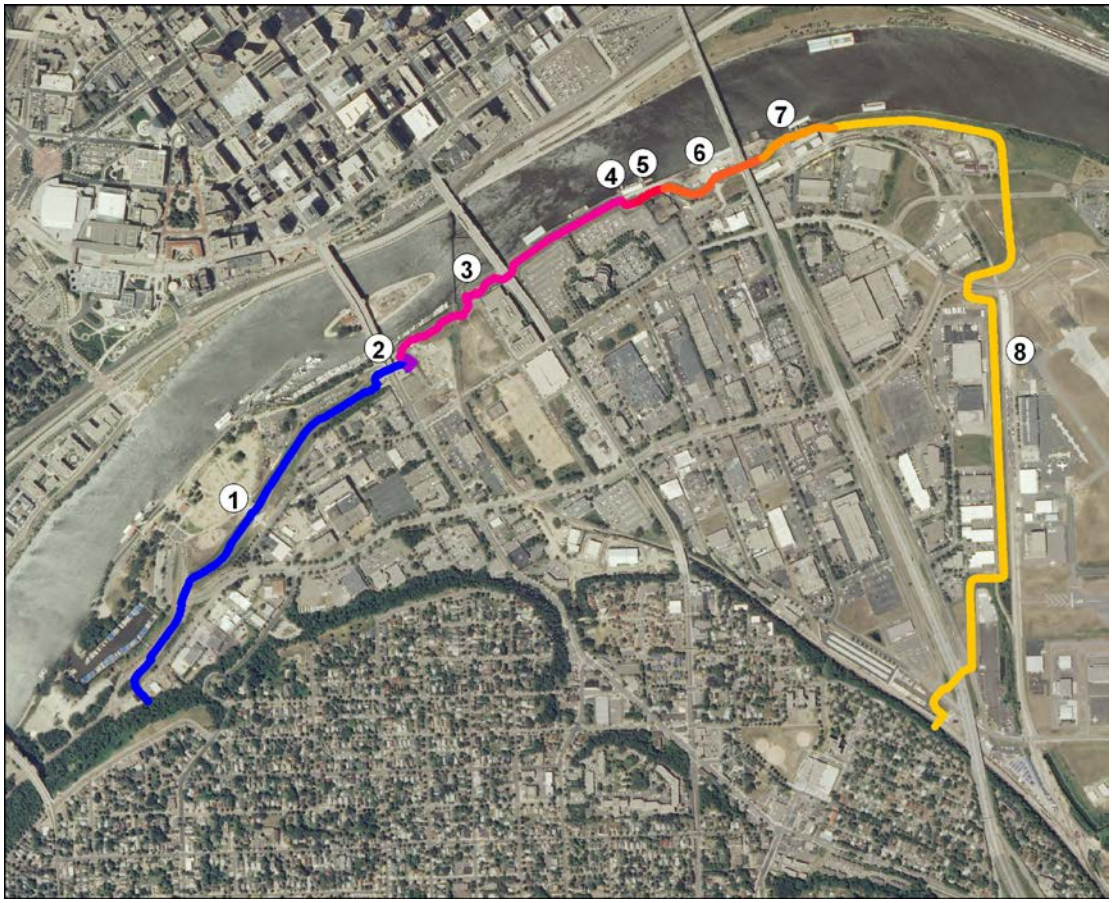

Figure 3.2 Levee reach locations

Table 3 2: Defences data in the St Paul study area

Reach	Length (m)	Elevation (m)	Reach Type*	Location
1	1,228	219.34	L	Levee from Bluff to W. Water Street Ramp
2	61	219.71	L	Levee from W. Water Street Ramp to Washaba Street
3	784	218.75	W	I-wall and T-Wall Riverfront
4	41	218.27	L	Small levee section behind Comcast
5	81	218.26	W	I -wall behind Building
6	291	218.25	L	Levee with closure under Lafayette bridge
7	216	218.13	W	Wall with pump station around Fertilzer Plant with closure
8	2,234	218.02	L	Levee around airport

*L=Levee – W=Wall

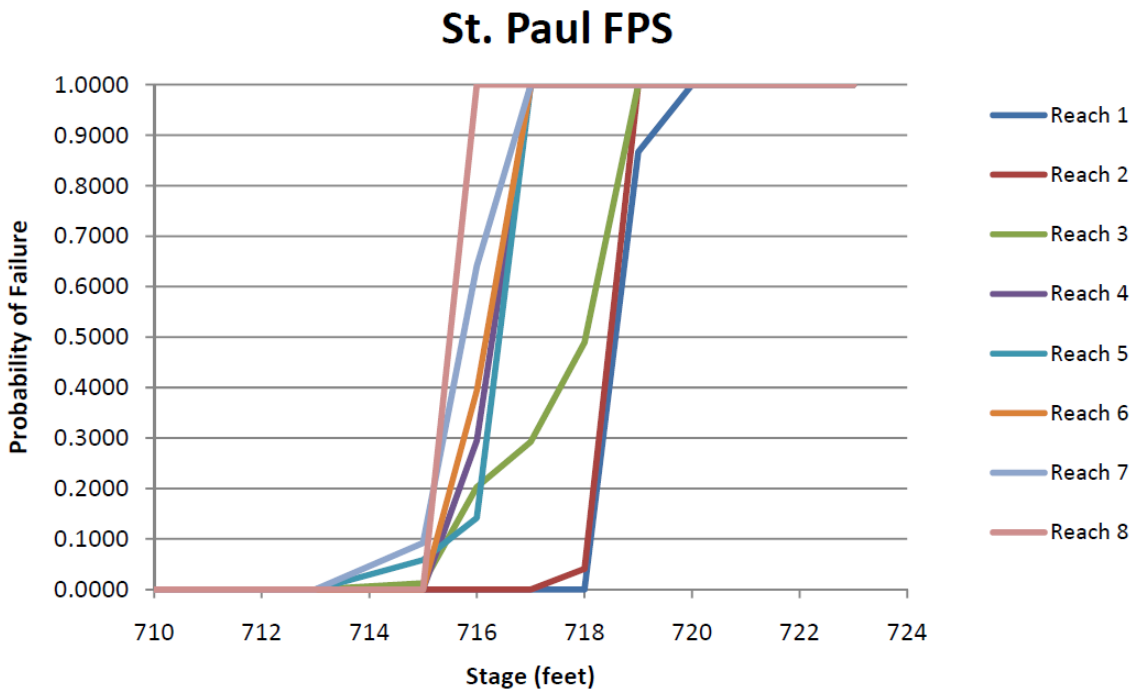

Figure 3.3 Reach Fragilities for St Paul FPS (from USACE 2011)

To assess the likelihood of defence failure, reaches 1, 3 and 8 have been selected to be used within RELIABLE. Table 3.4 shows the assessed failure modes for each reach.

Table 3.4 Assessed failure modes in RELIABLE

Reach	Failure modes
1	Seepage through the embankments leading to piping failure Erosion of embankment surface by overflow Sliding of the embankment
3	Sliding failure of the wall element
8	Erosion of embankment surface by overflow

A number of modelling runs have been undertaken with RELIABLE to establish the fragility curves for reaches 1, 3 and 8. Details of each run are given below.

Reach 1

For Reach 1, a run was undertaken to obtain the fragility curve for the following failure mechanisms (See Figure 3.3):

- Seepage through the embankments leading to piping failure which covers flow through general material or holes. Predominantly sandy or silty fluvial / estuarial dykes, or pre-damaged clay surface layer. Flows / pressures lead to internal erosion and piping (FLOODsite, 2007).

- Erosion of embankment surface by overflow which can lead to the failure of the crest and/or the rear face of the embankment. If the flow velocities are high, grass cover (if exists) can also be damaged, leading to direct erosion of embankment materials.

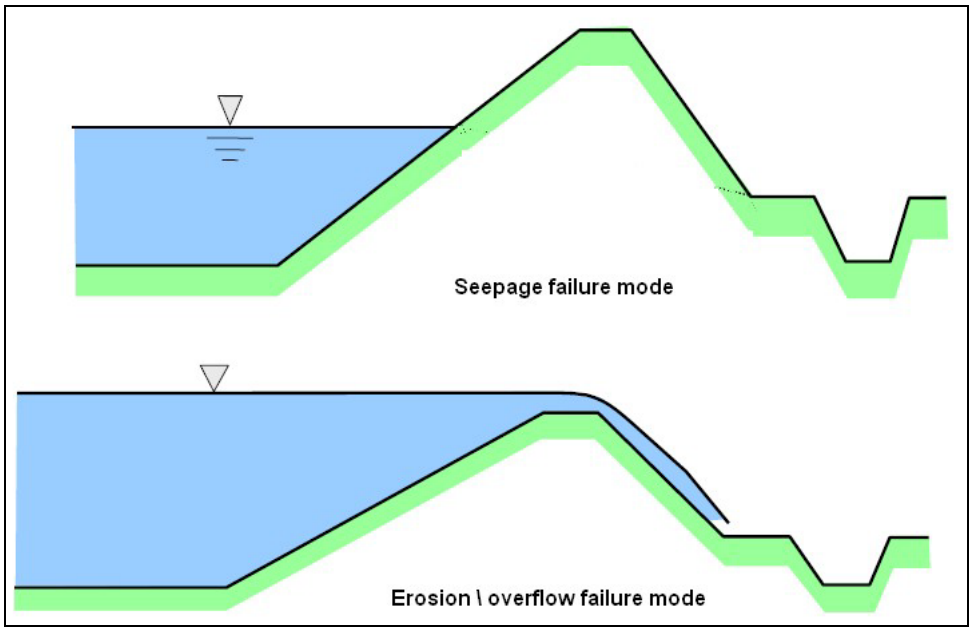

Figure 3.3 Reach 1 failure modes

A combined run for the above two failure modes has been undertaken in RELIABLE. Figure 3.4a shows a comparison between the fragility curve obtained by RELIABLE against that provided by the USACE.

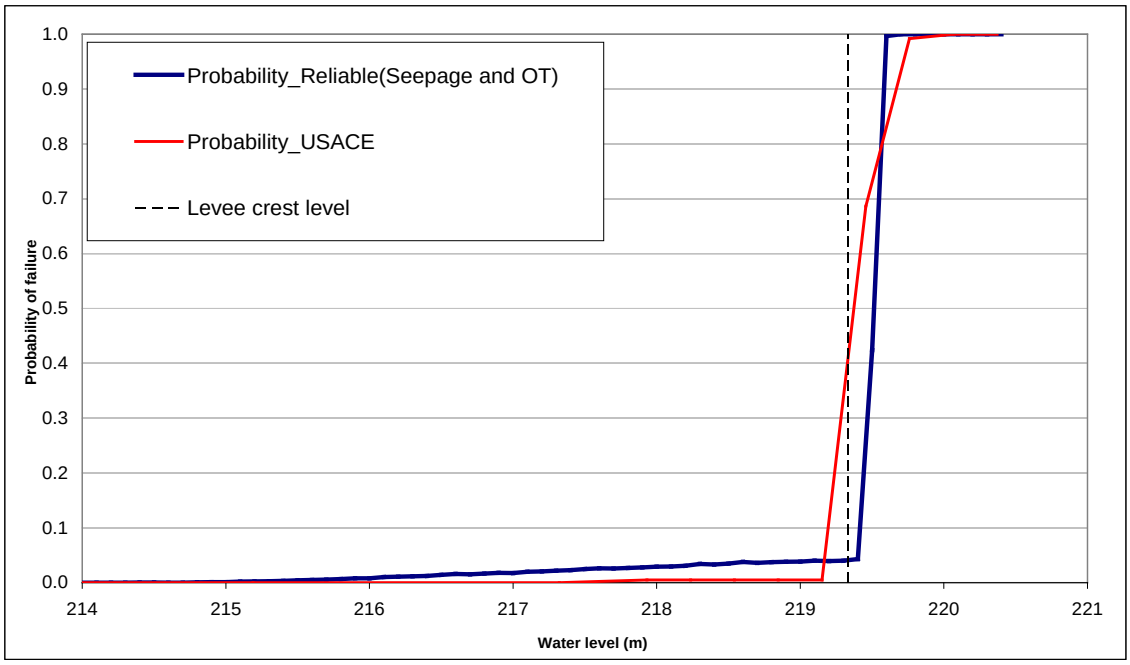

Figure 3.4a Reach 1 Fragility curves from RELIABLE and USACE 2011

For completeness, the RELIABLE and USACE 2011 fragility curves were compared with those that would be used to represent the defence reach in a typical UK high level risk assessment study. Namely, the generalised fragility curves associated with a Defence Class 10 (Narrow, turf covered levee with no crest, front or rear protection).

The generalised curves for this defence class are shown alongside the RELIABLE and the USACE 2011 data in Figure 3.4b

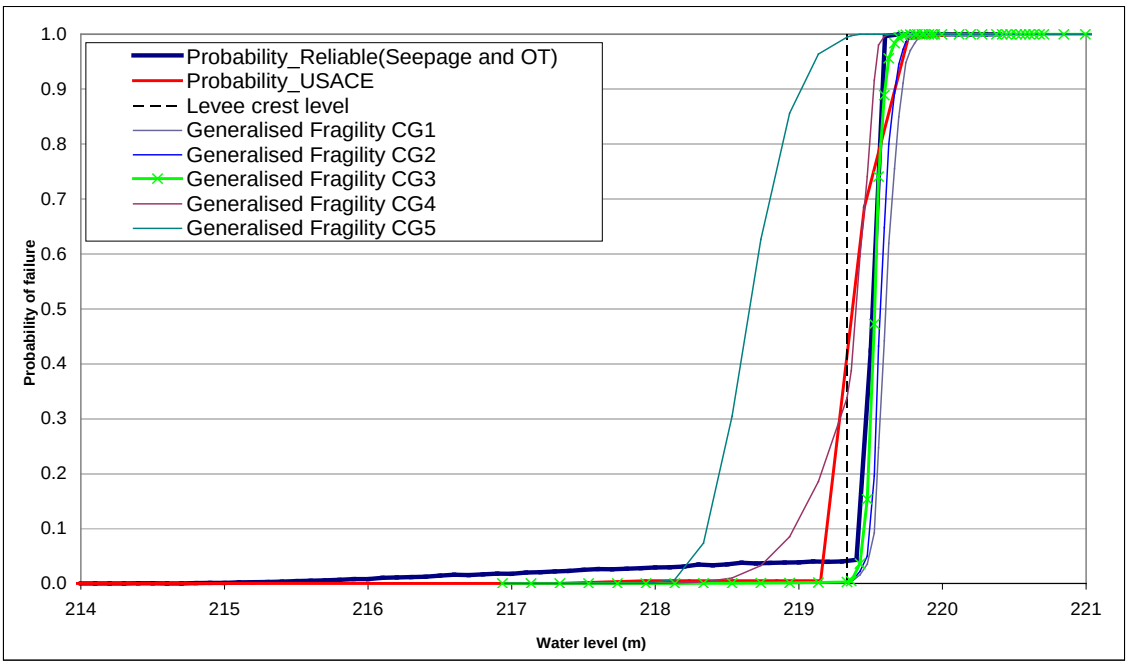

Figure 3.4b Reach 1 fragility curves from RELIABLE, USACE 2011 and UK generalised fragility for Defence Class 10.

From Figure 3.4b it can be seen that the generic fragility curve for condition grade 3 (fair condition) would give a good match for Reach 1. It should be noted that when undertaking high level probabilistic risk assessments in the UK, if a defence's condition is unknown, grade 3 is applied with greater uncertainty. As well as giving a good approximation of the fragility curve without the need to do defence specific reliability analysis, the curves could be used to explore scenarios of investment in maintenance and deterioration by allowing the risk assessment model to use fragility curves which vary through the simulation time from condition grade 1 (very good) through to condition grade 5 (very poor).

Reach 3

For Reach 3 two runs have been undertaken to obtain the fragility curve for the following two failure mechanisms (See Figure 3.5):

- Sliding of an embankment which is a complicated process that typically depends on an adverse combination of several rather than a single factor. The factors that could lead to sliding include (FLOODsite, 2007):
  1- Reduction in deadweight of organic fill material in embankment due to seasonal desiccation.
  2- Increase in hydrostatic horizontal loading due to formation of deep tension cracks.
  3- Increase in uplift pressures beneath embankment in confined founding strata that is in hydraulic continuity with flood water.

- Sliding failure of wall element which is a simple sliding failure of crown wall or similar element driven by static water level differences. Most likely after other effects have reduced soil strength. Failure occurs when

horizontal force from hydrostatic water level difference exceeds net shear strength of wall / foundation junction (FLOODsite, 2007).

Figure 3.6 shows a comparison between the fragility curves obtained by RELIABLE against that provided by the USACE. It can be seen that the USACE 2011 reliability assessment shows a higher likelihood of failure given load than the RELIABLE assessment. Or put another way, for a given probability of failure, the load is typically one foot higher in the RELIABLE assessment than those of the USACE assessment. This may be associated with additional failure mechanisms that may have been simulated with the USACE, 2011 assessment for these particular I-Walls, taking on board the very detailed failure mode assessments that had previously been undertaken.

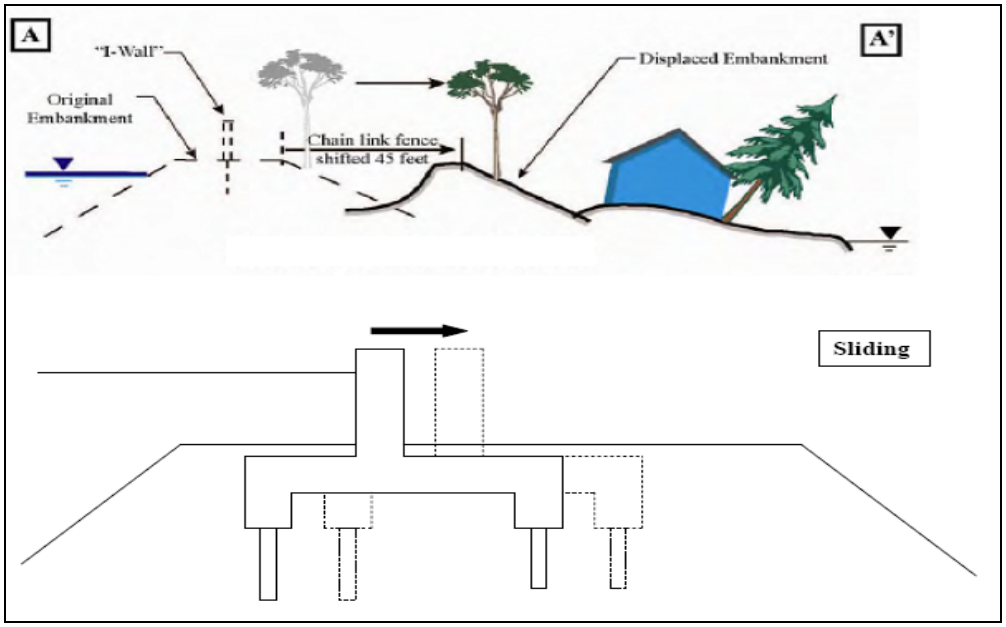

Figure 3.5 Reach 3 failure modes

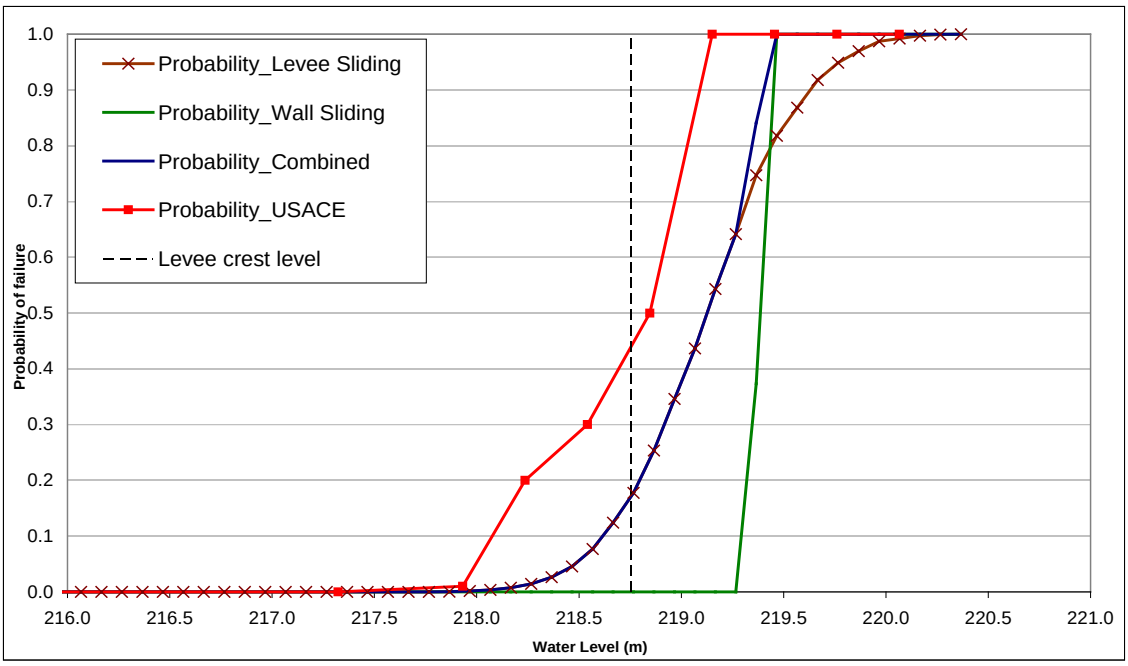

Figure 3.6a Reach 3 fragility curves from RELIABLE and USACE 2011

The RELIABLE and USACE 2011 fragility curves were compared with the UK generalised fragility curves associated with a Defence Class 5 (Narrow, brick and masonry or concrete wall with front and crest protection). The results are shown in Figure 3.6b

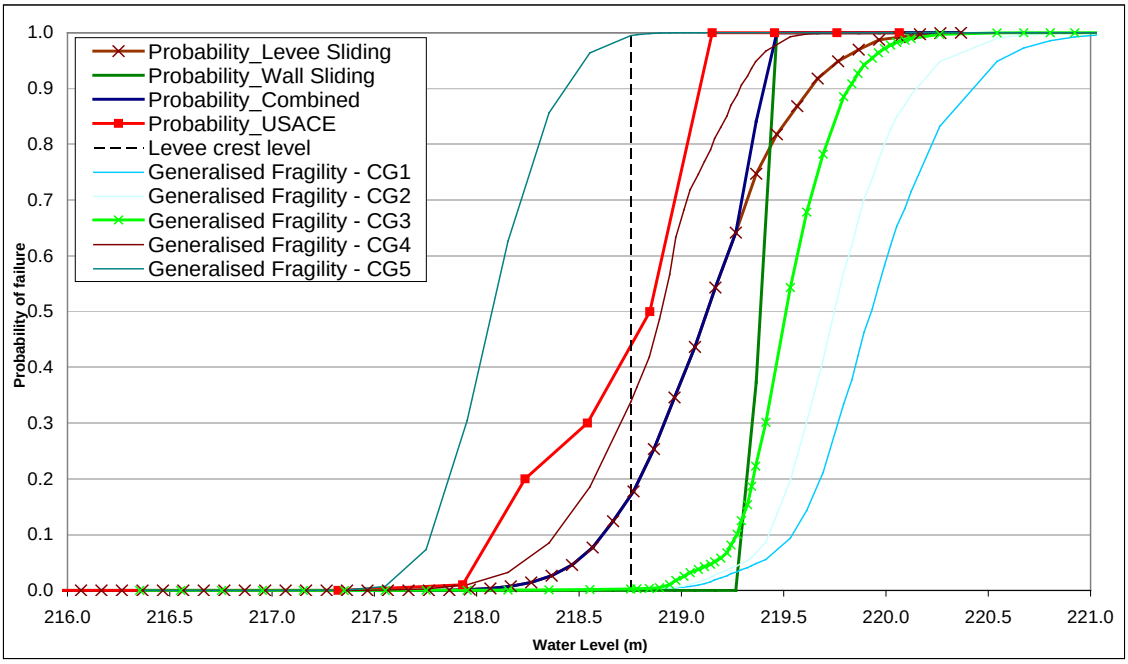

Figure 3.6b Reach 3 fragility curves from RELIABLE, USACE 2011 and UK generalised fragility for Defence Class 5

It can be seen that the generalised fragility curve for 'fair' condition (CG3) overestimates the performance of the structure when compared to the defence specific assessments. This may be a result of the generalised fragility curves being unable to

represent the complex nature of the defence. Of note, the generalised curve for poor condition compares reasonably well with the defence specific assessments.

Reach 8

For Reach 8, one run of RELIABLE has been undertaken to obtain the fragility curve for the erosion of embankment surface by overflow. Figure 3.7a shows a comparison between the fragility curves obtained by RELIABLE against that provided by USACE 2011. Similar to Reach 1, the reliability assessments are in close agreement.

The RELIABLE and USACE 2011 fragility curves were compared with the UK generalised fragility curves associated with a Defence Class 10 (Narrow, turf covered levee with no crest, front or rear protection) and similar to those for Reach 1, a very close match was found between those of the generalised fragility for fair condition and those of the more detailed, defence specific reliability assessments. The results are shown in Figure 3.7b

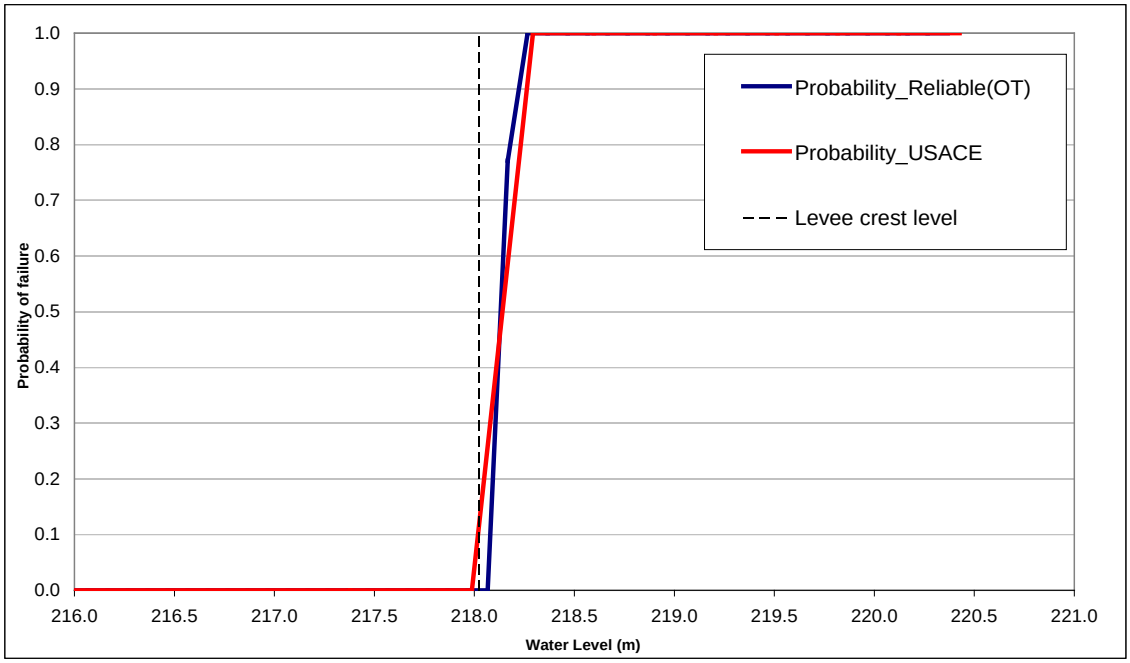

Figure 3.7a Reach 8 fragility curves from RELIABLE and USACE 2011

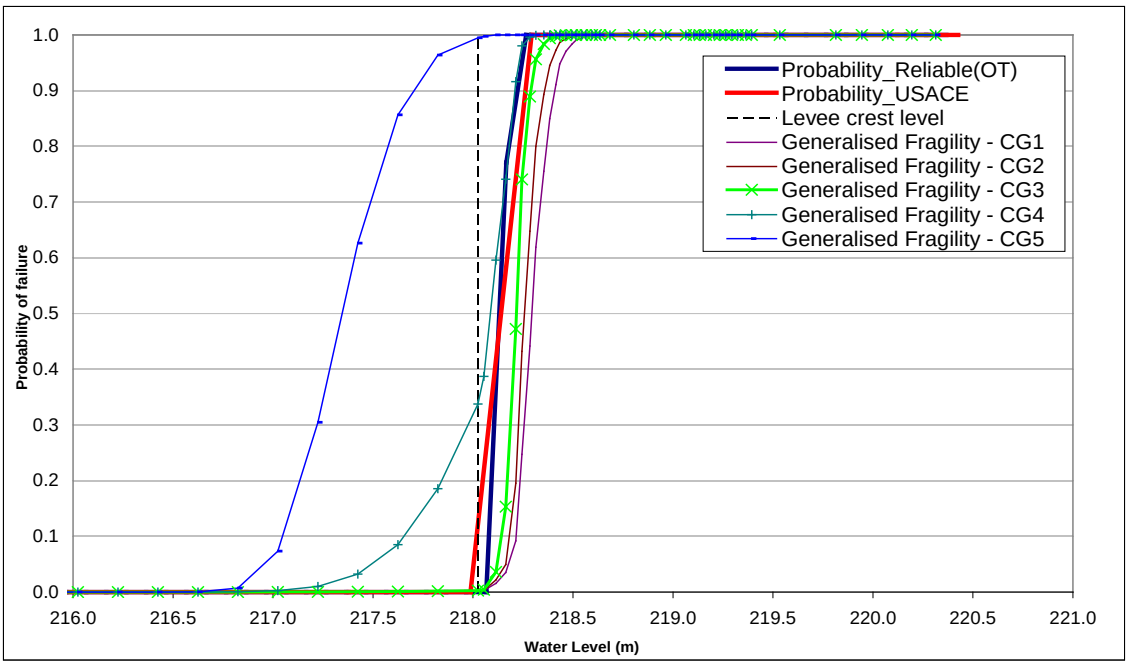

Figure 3.7b Reach 8 fragility curves from RELIABLE, USACE 2011 and UK generalised fragility for Defence Class 10

The following points may be concluded from the reliability modelling work undertaken:

In general terms, the analysis undertaken with RELIABLE yielded similar results to those obtained by the USACE. It is of note that these results were also in broad agreement with those that would be obtained from using the UK generic fragility curves. The differences, in terms of risk, that arise using different fragility curves are explored further below.

3.3 HR BREACH

When undertaking flood hazard or flood risk modelling for locations that are protected by flood defences, it is important to consider the presence and performance of the defences. As discussed in the previous text, the structural reliability of the defences can be represented by fragility curves, which depict the probability of the defence structurally failing when subjected to a given load. It follows that defences can be in one of two system states;

- Failed
- Non-failed

In the non-failed state, the defence remains structurally intact throughout the period of raised water levels. Any flooding that may occur within this system state is a consequence of either water levels exceeding the defence crest level leading to overflow conditions or exposure to waves leading to overtopping. Both of these processes can be estimated using relatively simple relationships.

In the failed state however the water enters the floodplain via a breach in the defence which may begin relatively small but grow over time due to the inflowing water eroding the defence material and causing instability leading to collapse of the exposed faces.

With the breach dimensions varying through time, one needs to consider more than the final breach size to estimate the inflow accurately and the flood hydrograph water level; hence, the evolution of the breach during the flood must be simulated.

To investigate the improvements that could be made to flood estimation in the St Paul area when using a breach simulation rather than assuming a fixed breach condition, simulations of breaching have been undertaken using the numerical model HR Breach, described in Section 2.2.

The breach modelling was undertaken for Reach 1, a large levee constructed of relatively porous sand with grass protection. The principal failure mode for this levee is piping leading to crest lowering and subsequent overflowing and erosion. This is followed by rapid growth of the breach through successive phases of erosion and bulk failure of the exposed breach faces. Figure 3.8 shows the dimensions of the levee as represented in HR Breach.

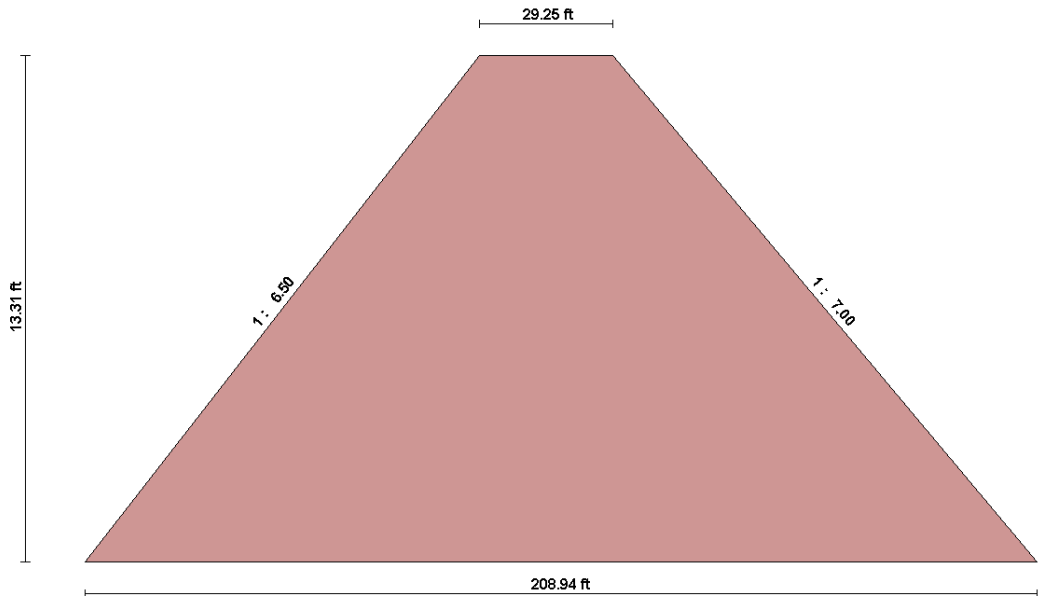

Figure 3.8 HR Breach representation of the Levee cross-section at Reach 1

The modelled flooding conditions simulated were for a 1 in 1000 year extreme flow event as represented by Figure 3.9.

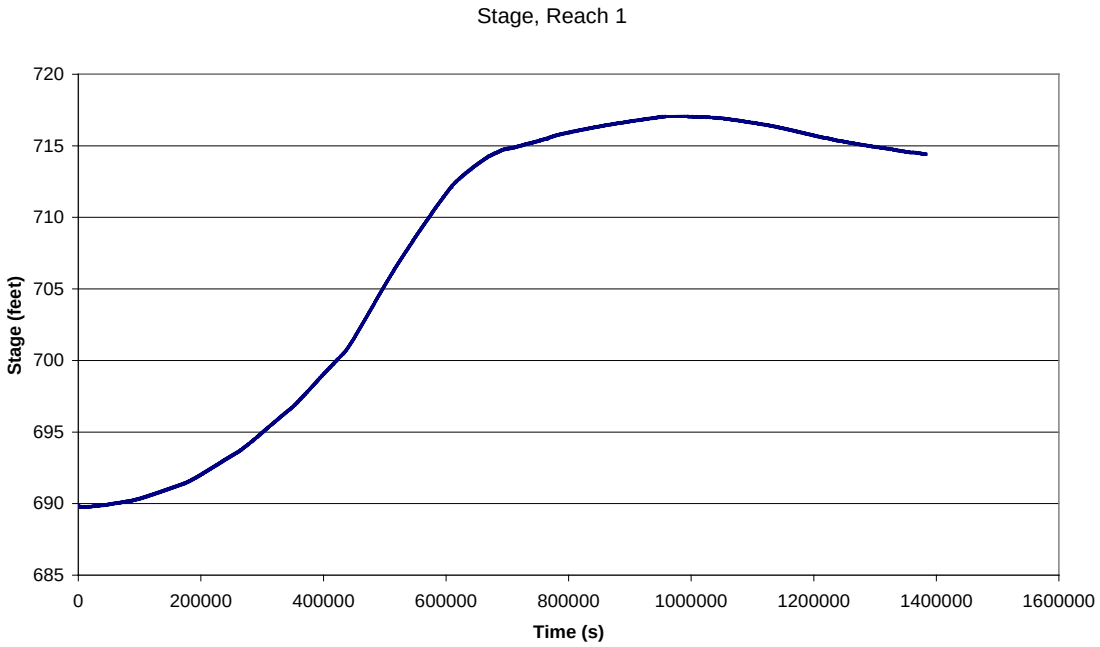

Figure 3.9 1 in 1000 year stage curve for Reach 1.

The first few simulations of breach in Reach 1 revealed a shortfall in the HR Breach functionality which prevented it from accurately representing the St Paul Floodplain; the HR Breach model previously allowed the downstream (landward side) flow conditions to be described by either a cross-section and slope (as found in a river valley below a reservoir), a rating curve or a head versus time curve. The downstream condition influences the inflow hydrograph and thus the breach growth. The St Paul floodplain has a fixed area being completely bound by either the flood defences or rapidly ground along the southern edge of the floodplain.

In order to represent the St Paul assessment better, a new downstream condition was introduced to consider the finite capacity of the St Paul floodplain basin and the associated water levels on the floodplain side of the levee. The model was re-run for a number of different scenarios of piping leading to overtopping and erosion. The results are presented in Figure 3.10. The scenarios modelled were all run with a 1 in 1000 year flood hydrograph and are described as follows;

Scenario 1: A one foot diameter pipe was initiated one foot above the toe of the levee, as the water level reaches the pipe, it grows until instability causes the pipe to collapse and the material above the pipe falls plugging the pipe but lowering the crest of the defence. The levee continues to protect the floodplain until the lower crest is exceeded and overflow commences, eroding the levee material and forming a breach. The breach grows from the crest to the bottom of the levee and grows in width until the water levels in the river fall below the ground level at the levee.

This scenario does not consider the depth of water on the floodplain side of the levee when calculating the evolution of the breach it is inappropriate for modelling the St Paul site. The continued growth of the breach gave a final breach width of 306ft, while the maximum inflow discharge was 20,600cfs.

Scenario 2: The same parameters and chain of events as scenario 1, however this time the new downstream condition is used to simulate the finite capacity of the St Paul flood basin. As the water enters the floodplain through the breach, the water within the floodplain basin rises. This reduces the water level differential at the breach and thus reduces the inflow rate. The new downstream condition allows much better representation of the breach evolution at St Paul. The inflow rate peaked at 3,700cfs and the breach width was 36.4ft.

Scenario 3: The same parameters and chain of events as scenario 2, however this time when the pipe collapses, all of the material above the pipe is washed away, commencing the breach. The inflow rate peaked at 2,200cfs and the breach width was 37.3ft.

Scenario 4: The same parameters and chain of events as scenario 3, however this time the pipe is located three feet below the crest of the levee. The inflow rate peaked at 3,000cfs and the breach width was 33.5ft.

Scenario 5: The same parameters and chain of events as scenario 3, however this time the pipe is located half way up the levee 6.65ft below the crest of the levee. The inflow rate peaked at 2,300cfs and the breach width was 32.9ft.

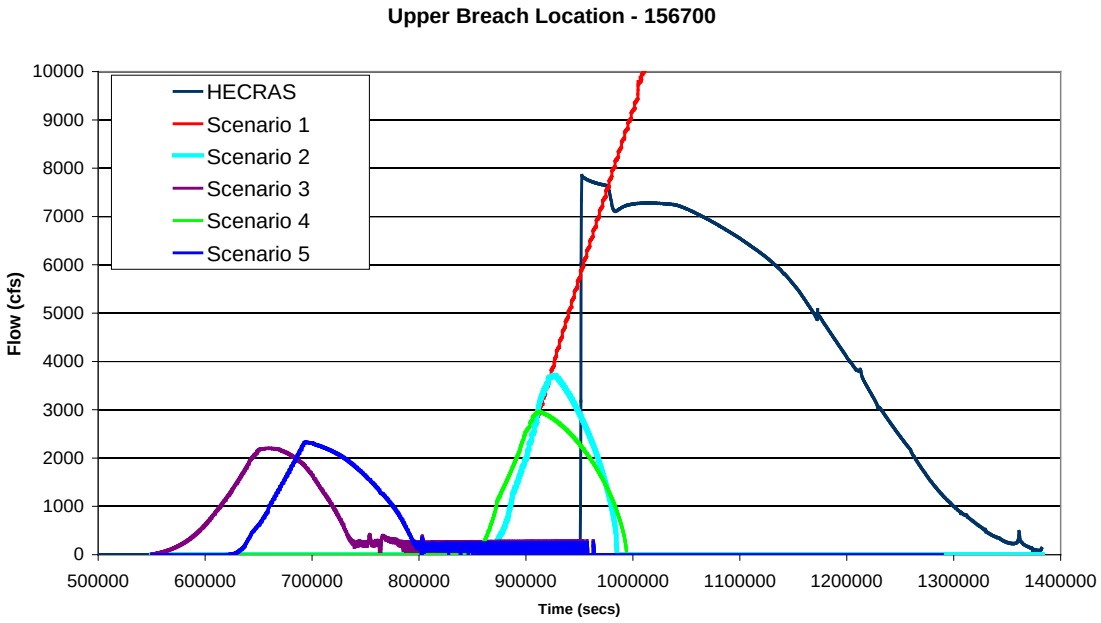

Figure 3.10 Results from the HR Breach simulations of a breach in the levee at Reach 1 compared with those from the USACE's HECRAS breaching simulation.

The analysis has shown that using a dedicated breach model can give significant improvements in the estimation of inflow through a breaching levee than is achieved via simple assumptions on breach width and height. The breach model simulates the growth of the breach through time providing better estimates of breach evolution and dimensions and as a result the inflow rate evolves with the breach. The model allows scenarios of breaching to be explored, enabling the exploration of the impacts that may be expected under different circumstances of breaching. This supports the use of breaching models in flood risk models where uncertainty or variability can be introduced to various parameters such as the geotechnics and breach initiation for example. In summary, the breach modelling has shown that significant improvements

can be obtained by modelling the breach rather than performing the traditional approach of considering a static breach.

3.4 FRE

The USACE provided a range of information that was necessary to set up the FRE Model for St Paul. This included:

- Digital Terrain Model (DTM) of the study area
- Spatial location of buildings
- Hydraulic boundary conditions
- Fragility curves
- Spatial location of levee´s and gates (closures)
- Depth-damage information

The first stage of the analysis involved preparation of the DTM into the mesh that is used by the inundation model (Figures 3.11 and 3.12).

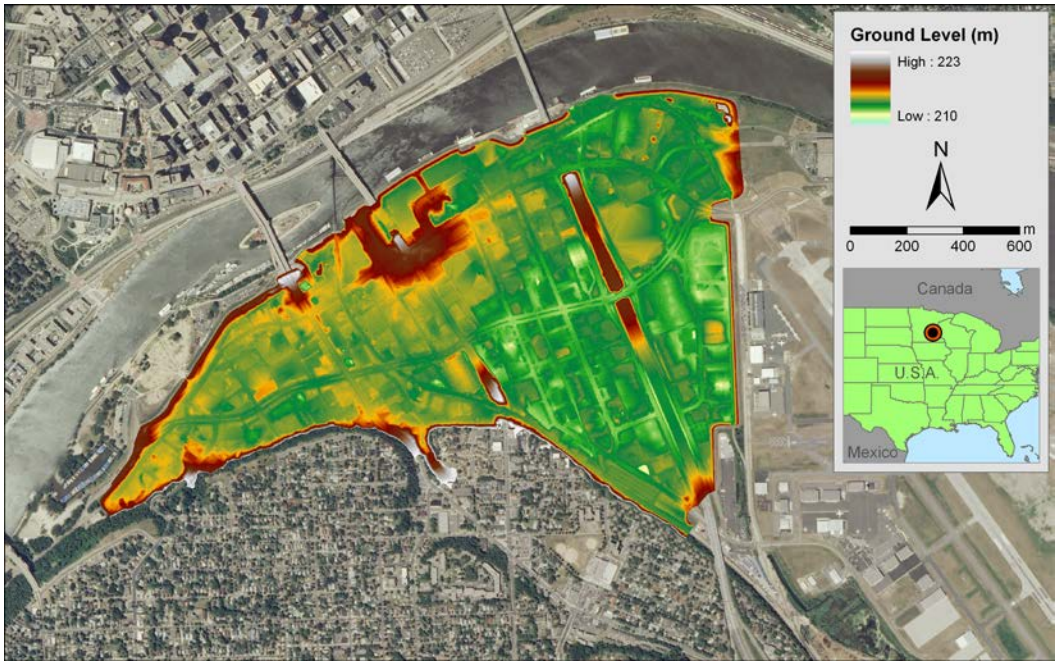

Figure 3.11 DTM Ground model of the St Paul, Minnesota Study Area.

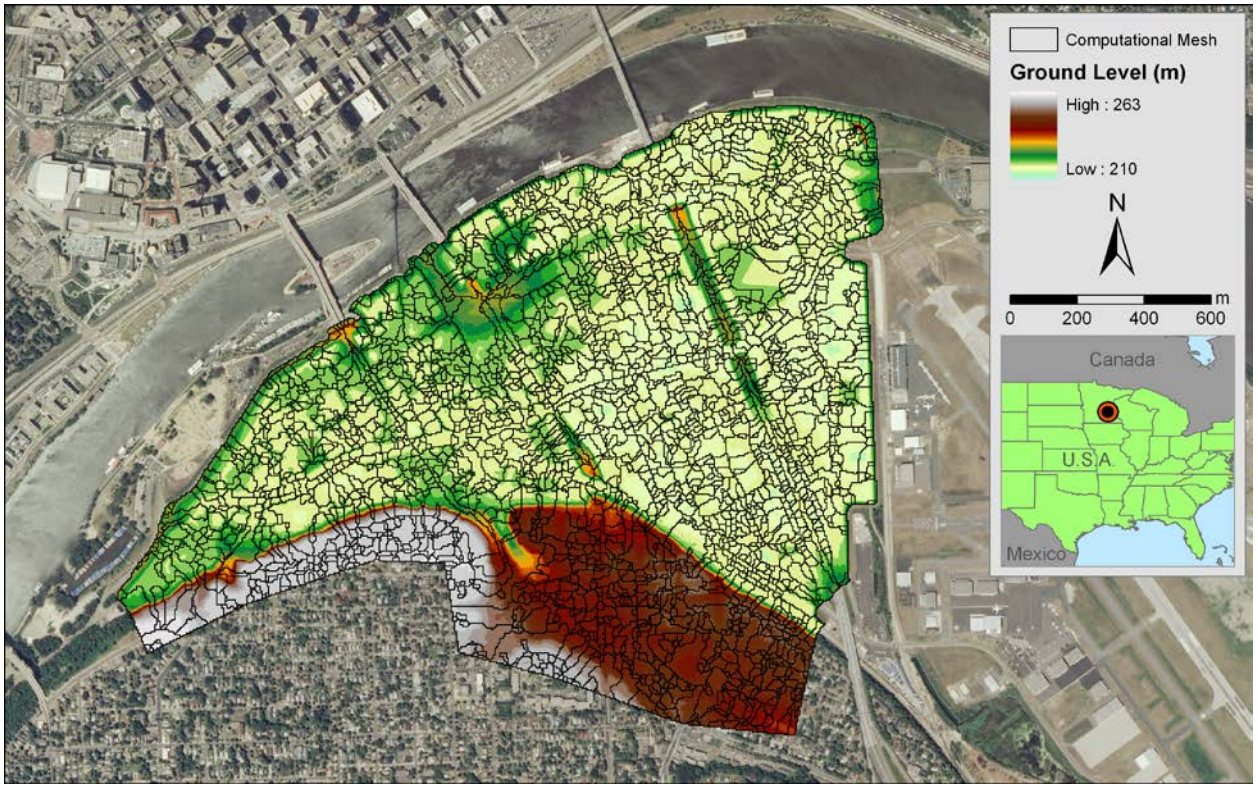

Figure 3.12 Computational mesh of the Inundation model for the study area

The next stage involved preparations of the model databases relating to the fragility of each levee reach and the spatial location of the properties within the floodplain area (Figure 3.13).

Figure 3.13 Spatial location floodplain property

To determine the range of model runs, a series of discussions with USACE staff were held. It was noted that because of the high standard of the defences that the current residual risk was relatively low. Therefore, to obtain results that yielded more insight into the performance of the underlying models, it was agreed to explore the outputs with different assumed crest levels that were lower than reality. Other factors that arose within the context of the discussions related to the difference between the UK generic fragility curves, and the US site specific ones, differences between the UK and US depth damage curves and the resolution of the model, both in terms of number of levee reaches and DTM resolution. In particular it was noted that the pilot site was relatively small scale and that there was a need to run on lager spatial scales and hence coarser resolutions. Hence exploration of these factors was of importance. With regard to the number of levee reaches, further insight provided by USACE identified additional reach lengths that could be defined; sensitivity analysis was therefore undertaken using a finer resolution of reach lengths.

A summary description of the model runs that have been undertaken is provided in Table 3.5. It is of note that once the initial model has been set up, exploration of different scenarios is not an onerous task, generally requiring straightforward modifications to one or more of the database tables. The runtime of the model for this relatively small study area is generally less than 1 min for a single run.

Table 3.5 Summary of risk model runs

Run name	DTM resolution (m)	No. of levee reaches	Fragility	Depth damage functions	Crest levels
Reference	5	8	US	US	existing
CL-1	5	8	US	US	ex. -1m
CL-2	5	8	US	US	ex. -2m
CL-3	5	8	US	US	ex. -3m
UK_fragility	5	8	UK (generic)	US	existing
UK_damage	5	8	US	UK	existing
Levee_resolution	5	54	US	US	existing
Gates_resolution	5	54	US+UK (gates)	US	existing
DTM_resolution	50	8	US	US	existing

A summary of the results of the risk model are provided in Table 3.6. Selected outputs from the model runs are provided in Figures 3.14 to 3.17.

Table 3.6 Summary of results from the risk model runs

Run name	Risk (EAD £k)	Risk (EAD $k)	% change wrt ref.
Reference	25.3	15.9	
CL-1	59	37	+132
CL-2	242	152	+856
CL-3	597	374	+2254
UK_fragility	26.0	16.3	+2
UK_damage	25.1	15.7	-1
Levee_resolution	25.5	16.0	+1
Gates_resolution	24.4	15.3	-4
DTM_resolution	30.1	18.9	+19

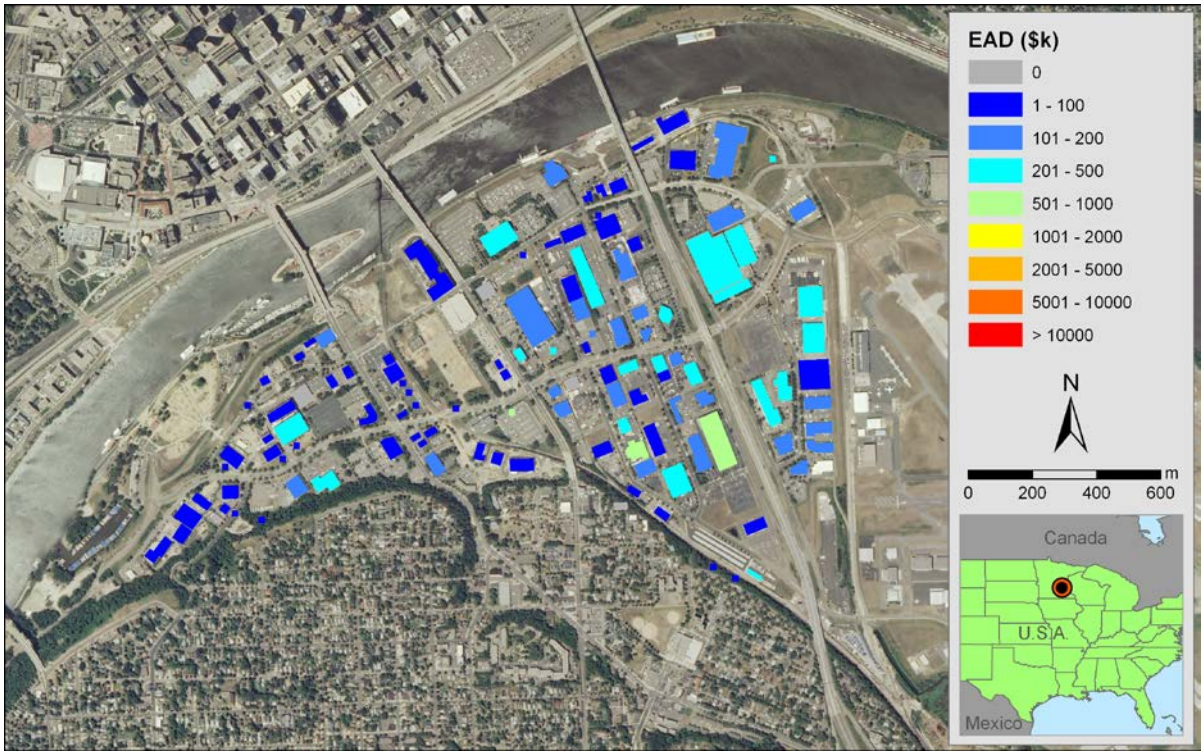

Figure 3.14 Spatial distribution of residual floodplain risk, EAD ($k), reference case (existing situation)

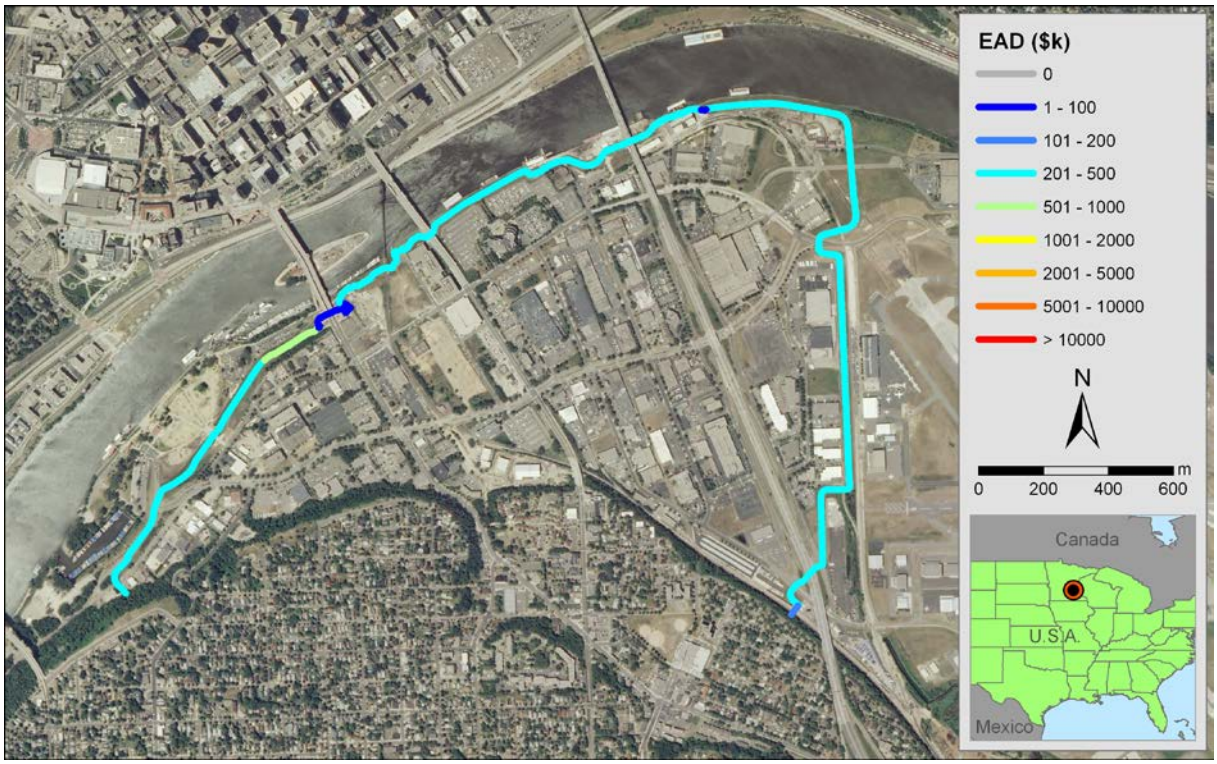

Figure 3.15 Attribution of risk to levee reaches, EAD ($k), reference case (existing situation)

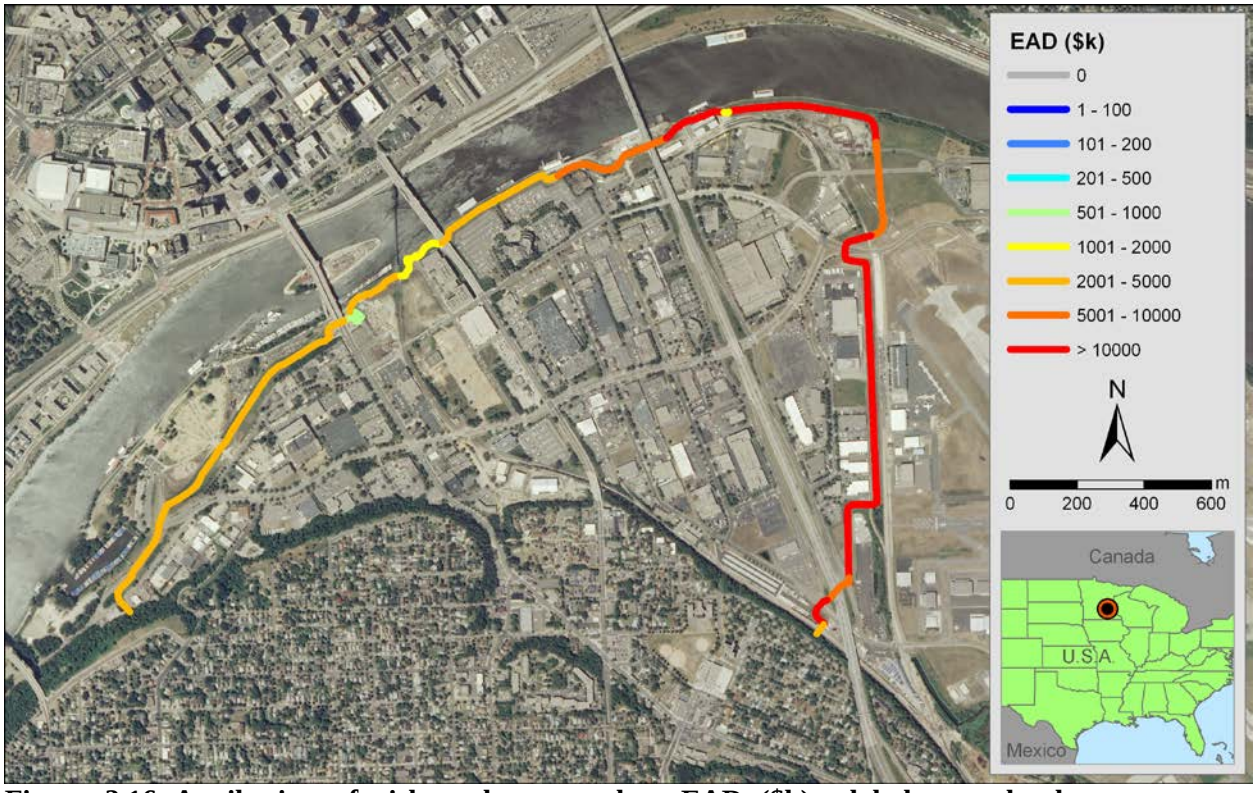

Figure 3.16 Attribution of risk to levee reaches, EAD ($k), global crest level reduction of 3m (CL-3)

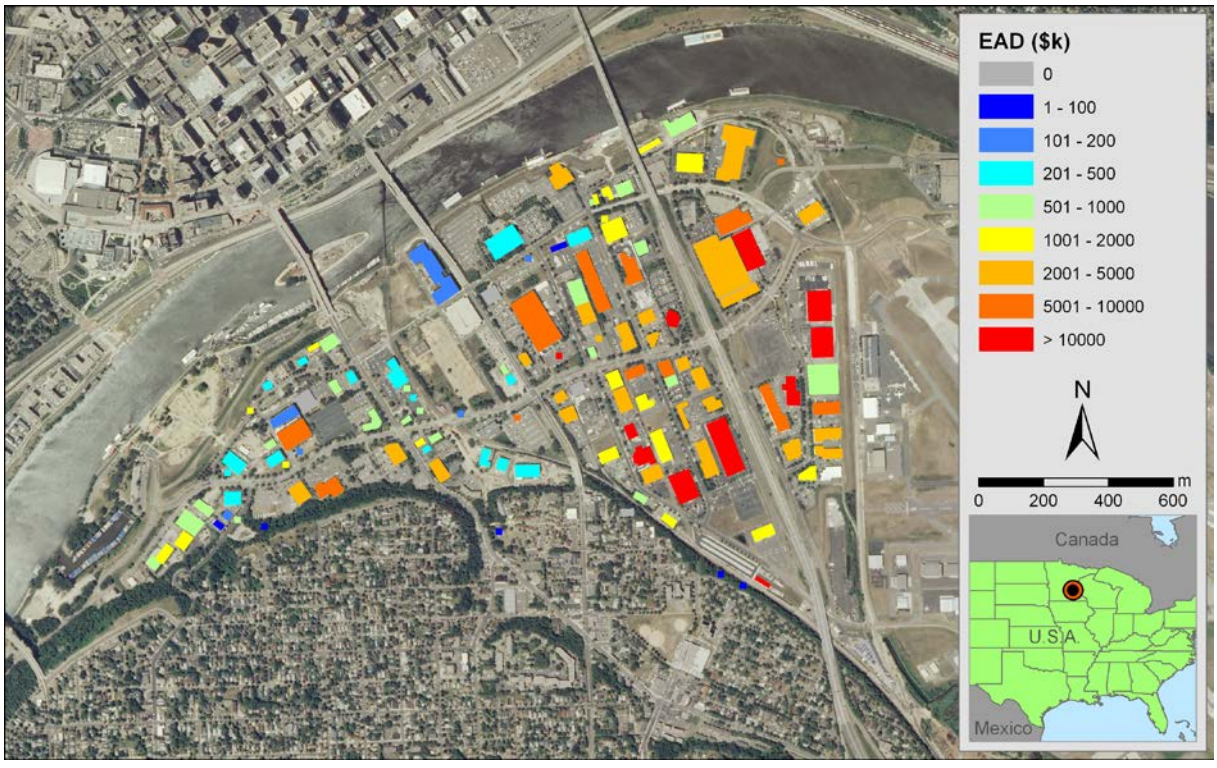

Figure 3.17 Attribution of risk to properties, EAD ($k), global crest level reduction of 3m (CL-3)

The FRE risk analysis model has been run for a range of different scenarios to explore the sensitivity of the model to different inputs and to demonstrate the range of potential outputs. The key points to note are:

- The model is computationally efficient (less than a minute for running a single scenario), this facilitates exploration of a range of different "what if" scenarios.
- The model considers systems of flood defences and the potential consequence of flooding associated with each individual element in the system.
- The model provides a range of outputs that can support risk management decisions, relating to maintenance and refurbishment of existing defences or strategic planning.

The model can be used over broad spatial scales due to its efficient computational runtime. This runtime is achievable as a number of simplifying assumptions are made within the system. These assumptions are:

- Volume based flood spreading algorithm (ie non time-stepping, simplified hydraulics).
- Independence of strength of different levee reaches.
- Dependence of hydraulic load within a flood area
- Hydraulic independence of separate flood areas

Due however, to the simplifying assumptions, it is often beneficial to deploy the model in conjunction with more detailed hydraulic analysis, for example. It can also be deployed in a screening role, to inform further modelling studies or data collation activities. These assumptions do however, impose certain constraints and research initiatives have been undertaken and are currently underway to address these issues. These initiatives are discussed further in Section 4.

4 Gap analysis

4.1 ONGOING RESEARCH INITIATIVES OF RELEVANCE

Generic fragility curve upgrade

Because of the heavy use of generic fragility curves in broad scale flood analysis tools in the UK, HR Wallingford is currently carrying out a project to improve these curves for use in various asset management tools and to fit into a new asset classification being adopted by the Environment Agency. The curves will take account of latest science, balancing accuracy against ease of application within the constraints of existing flood risk management models. The project also links to doctoral research currently underway on sea wall fragility curves.

URBANFLOOD

The UrbanFlood EC FP7 project (http://www.urbanflood.eu/Pages/default.aspx) is creating an Early Warning System framework that can be used to link sensors via the Internet to predictive models and emergency warning systems. The project includes three pilot sites to apply and validate at full scale the technology being developed in the project: Amsterdam (Netherlands), Boston (UK) and Rhine River (Germany). The sensors installed at the various sites include various MEMS modules to measure displacement and pore pressure and fibre optic cables able to detect strains. The gathered data are used for dike stability evaluation with different models and also, combined with an Artificial Intelligence (AI) component, for detection of anomalies in dike behaviour. Detected anomalies trigger assessment of the likelihood of levee breach and the consequences in terms of flood propagation and damage in the defended urban area.

AREBA breach model for system risk analysis

The HR Breach model was developed around a decade ago. This model has been widely used for simulating breaches in dams and embankments. It is however, too computationally demanding for use in system risk analysis models that are applied in practice. A simplified breach model, AREBA, has therefore been developed, Van Damme *et al.* (2012) (reproduced in Appendix 4, for ease of reference). AREBA simulates embankment breach processes that arise as a result of erosion from overflowing water, or internal erosion due to pipes that are formed through the embankment. Discharge through the breach depends on the breach depth and width, or pipe dimensions. AREBA analyses surface erosion failures, headcut erosion failures or piping failures. AREBA has been validated through comparison with the more complex HR BREACH model (Figure 4.1) as well as data from full scale breach experiments. Full details of the model and its validation are provided by Van Damme *et al.* (2012).

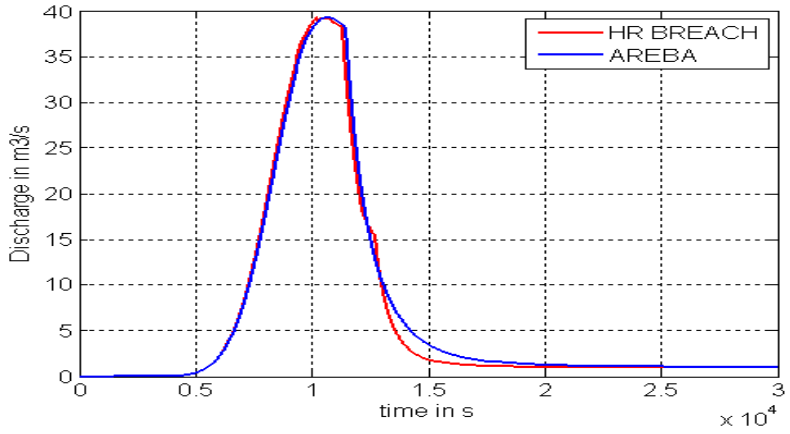

Figure 4.1 Comparison of the outflow discharge from a levee using the AREBA dynamic breach growth model and the well-established HR BREACH Model Van Damme *et al* (2012).

Multivariate extreme value analysis

One of the constraints of the existing FRE methodology is the handling of spatial dependence within the flood risk analysis model. Within the UK there has been a significant amount of research into statistical methods for multivariate extremes, Heffernan and Tawn (2004) and this has been investigated for use within the context of flooding, Environment Agency (2011). HR Wallingford has developed a new version of FRE that builds upon this research, Wyncoll and Gouldby (2012), reproduced in Appendix 5. This new modelling system explicitly captures the spatial dependence in extreme floods enabling the damage associated with widespread areas in a single flood event to be evaluated appropriately, this is particularly important for insurance purposes.

RFSM EDA Inundation model

One of the critical aspects of system flood risk models is the simulation of inundation depths and velocities. The current volume based approach used in FRE, is computationally efficient but uses simplified hydraulics. It is not a time stepping dynamic model and can therefore only output final flood depths. In risk analysis models the inundation component must be computationally efficient because of the many simulations that are often required (100´s, if not 1000´s), this generally exludes models that solve the full shallow water equations. HR Wallingford has therefore developed a time stepping model, RFSM EDA, that is computationally efficient yet sufficiently accurate for flood risk analysis. The model uses a relatively coarse grid for flux computations but utilises the detailed resolution topographic information through a sub-grid process, which ensures it maintains its accuracy. The model has been compared against a range of other inundation models where it has been shown to perform favourably both in terms of accuracy and run time, Jamieson *et al.* (2012).

An example of a comparison between RFSM EDA and a full Shallow Water Equation Model, Infoworks 2D is shown in Figure 4.2 (also see Figure 4.3). Table 4.1 shows a comparison of runtimes of RFSM EDA against other models on a series of benchmark tests (Environment Agency (2010). More information on the performance of RFSM EDA is provided in Appendix 5.

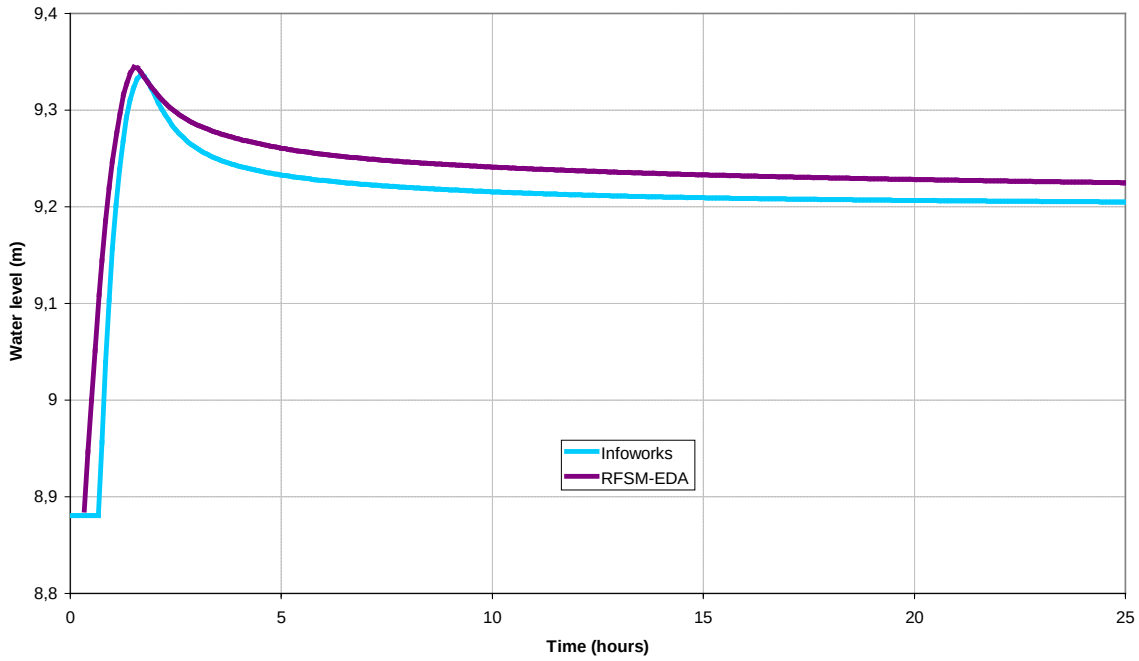

Figure 4.2 level plot for RFSM-EDA and Infoworks 2D

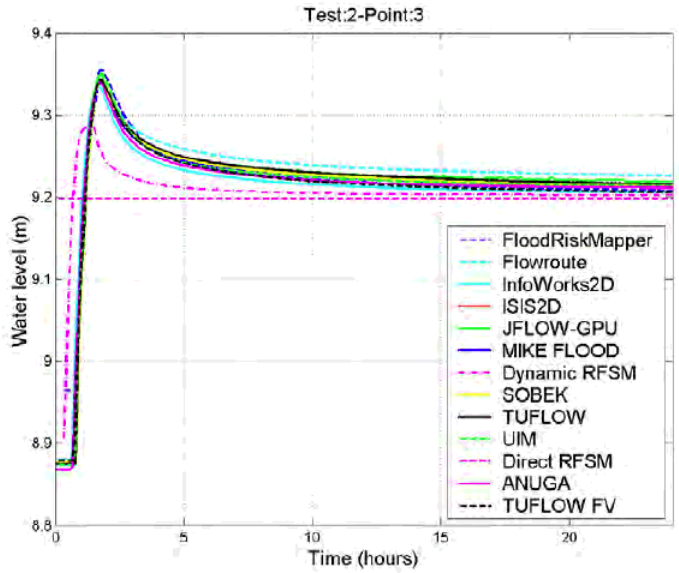

Figure 4.3 Level/time plots for other inundation models for the same test

Table 4.1 Comparison of runtimes, model timesteps and final domain volumes (Jamieson et al (2012)

Model	Computation time in minutes for each test			
	2	4	5	8A
RFSM-EDA (mesh A)	**0.015**	**0.21**	**0.23**	**2.9**
Dynamic RFSM	0.19	5.8	9.8	23.3
TUFLOW FV	2.64	24.5	2.9	72.6
InfoWorks ICM[1]	0.73	6.5	0.7	27.1
JFLOW-GPU	1.83	2.3	10.2	16.2
Lisflood-ACC[2]	n/a	1.97	0.68	n/a
Fastest other[3]	0.4	1.27	0.6	4
Slowest other[3]	130	282.8	350	307.8
Note 1: The runtimes are taken from InfoWorks RS, but the results in this paper are from InfoWorks ICM; little difference is expected. Note 2: Lisflood-ACC runtimes appear in (Neal *et al*., 2011b). Note 3: Fastest and slowest models other than those shown in this paper, but appearing in Wright *et al*. (2012).				

4.2 GAP ANALYSIS AND PROJECT RECCOMMENDATIONS

Throughout the course of the project a wide range of topics have been discussed and potential opportunities for future collaboration have been identified. An initial list is summarised here. This list is however, only intended to initiate discussion at the final workshop and it is anticipated this will be amended and updated following the workshop

Improved RELIABLE model

Fragility is a primary requirement for the FRE model, MDSF2 and HEC FRM and is embedded within the Dutch Reliability model HydraRing and FLORIS. The existing RELIABLE tool is prototype only and further investement is required to create a fully functional and robust tool. The UK Environment Agency have indicated some interest in further development of the tool and given the interest in these approaches from the Netherlands, there maybe an opportunity for a jointly funded project to develop this tool.

Multivariate analysis for HEC FRM

The HEC FRM model requires upstream flows from different river systems as input. It is likely that flows on these different systems will often be partially, not fully, correlated. The Heffernan and Tawn (2004), method can be used to analyse flow records from different gauging stations and extrapolate the joint probability density to extreme values. In principle this can be applied to any number of gauging stations. Samples that form the input to the HEC FRM model can then be generated whilst preserving the appropriate correlation structure, particularly in the extremes. HR Wallingford staff are intimate with the application of the Heffernan and Tawn (2004) methodology in the context of flooding and would welcome the opportunity to work in partnership with counterparts at HEC to implement this system in HEC FRM.

Sub-grid inundation modelling within HEC FRM

Inundation modelling is a particularly computationally intensive aspect of system flood risk models and the computational efficiency of the inundation model can be the governing factor in the overall performance of the system. Both HR Wallingford and

HEC are developing sub-grid inundation models to speed up the computation whilst maintaining accuracy. There may well be merit in a collaboration to share ideas and knowledge with the overall aim being to implement the model within the HEC FRM system.

Defence system state importance sampling within HEC FRM

The total number of simulations required of the inundation model governs the overall time taken to complete the calculation of risk. In order to minimise the model runtime it is therefore desirable to limit the number of simulations to a practical number. Both HEC FRM and FRE, currently utilise a Monte-Carlo sampling method. There are however, potential opportunities to improve the computational efficiency of both methods by implementing Importance sampling (sometimes known as variance reduction) techniques. Rather than sampling at random from the range of defence system states, the samples are stratified and weighted. This can enable a significant reduction in the number of samples that require simulation. Coupling this type of sampling method with an efficient sub-grid computational model is likely to yield a significant increase in the computational efficiency of HEC FRM and FRE.

Dynamic Breach growth modelling

The rate of development and final dimensions of breaches in levee´s can have a critical influence on the final flood extent and depths. The AREBA model is a computationally efficient model that can be used to simulate the development of breaches. Incorporating AREBA within HEC–FRM will enable this process to be accurately represented without adding additional runtime.

5 Conclusions and Recommendations

To be completed post workshop

6 References

Environment Agency (2007) Performance and Reliability of Flood and Coastal Defences R&D Technical Report FD2318/TR1

Environment Agency (2010) Benchmarking of 2D Hydraulic Modelling Packages. SC080035/SR2. Environment Agency, Bristol, UK.

Environment Agency (2011) The risk of widespread flooding – Capturing spatial patterns in flood risk from rivers and coasts, SC060088/R1 Spatial Coherence of Flood Risk – Technical Methodology Report

Gouldby, B., Sayers, P., Mulet-Marti, J., Hassan, M. and Benwell, D. (2008). "A methodology for regional-scale flood risk assessment." Water Management **161**(3): 169 –182.

Hassan M, Morris M and Samuels PG (2002). Improving the Accuracy of Prediction of Breach Formation through Embankment Dams and Flood Embankments. Proc. Int. Conf. Fluvial Hydraulics, Louvain-la-Nueve, Belgium.

Hassan M, Morris M and Samuels PG (2002). Improving the Accuracy of Prediction of Breach Formation through Embankment Dams and Flood Embankments. Proc. Int. Conf. Fluvial Hydraulics, Louvain-la-Nueve, Belgium.

Heffernan, J. E. and Tawn, J. A. (2004). "A conditional approach for multivariate extreme values (with discussion)." Journal of the Royal Statistical Society: Series B (Statistical Methodology) **66**(3): 497-546.

HR Wallingford, 2010, Flood Risk Estimator User Manual, HR Wallingford

Jamieson, S., Lhomme, J., Wright, G. and Gouldby, B. (2012). "Highly efficient 2D inundation modelling with enhanced diffusion-wave and sub-element topography." Proc. Inst. Wat. Man. **in press**.

Schultz, M., Gouldby, B., Simm, J. and Wibowo, J. (2010) Beyond the Factor of Saftey: Developing Fragility Curves to Characterize System Reliability

Simm, J., Gouldby, B., Sayers, P., Flikweert, J., Wersching, S. and Bramley, M. (2009). Representing fragility of flood and coastal defences: Getting into the detail. Flood Risk Management: Research and Practice. P. Samuels, S. Huntington, W. Allsop and J. Harrop, Taylor and Francis Group, London, UK.
USACE (1996) Risk-based Analysis for Flood Damage Reduction studies Engineer Manual EM 1110-2-1619

Van Damme , M., Morris, M. W. and Hassan, M. (2012) A new approach to rapid assessment of breach driven embankment failures w. p. FRMRCII report

Wyncoll, D. and Gouldby, B. (2012). "Application of a multivariate extreme value approach to system flood risk analysis." Journal of flood risk management **in press**.

Appendix 1 Workshop Summaries

Two workshops have been held between representatives of the USACE and HR Wallingford. The first in January 2011, HR Wallingford, the second in July, 2011, (HEC) Davis, California. The workshop agendas and outcomes are summarised below.

HR Wallingford and USACE Workshop :
Flood risk, levee safety and asset management

HR Wallingford, Tuesday 1st February - Thursday 3rd February, 2011

Attendees

USACE
Noah Vroman
David Schaaf
Corby Lewis
Bob Patev
Neil Schwanz
William Lehman
David Margo
Alex Roos
Mitch Laird

HR Wallingford
Ben Gouldby
Caroline McGahey
Mark Morris
Mike Panzeri
Paul Sayers (S&P)
Andy Tagg

Programme

Workshop Objective:
The objectives of the workshop are summarised under two components:

1. Exchange knowledge on levee safety, flood risk and asset management.
2. Develop and define a detailed work-plan (activities and programme) for implementing methods and software tools at agreed locations to produce specific agreed outputs.

These activities are to support USACE in the development of their methodology for prioritisation of maintenance activities for risk reduction.

The knowledge exchange aspects will comprise topics that include, but are not limited to:

- Condition inspection
- Geotechnical stability
- Closure (active) structures
- Fragility/reliability

- Levee deterioration
- Breaching and breach modelling
- Risk, uncertainty and sensitivity analysis
- Economic consequences of flooding
- Loss of life from flooding
- Hydraulic modelling

The development of the work-plan will seek to agree specifics relating to:

- the location of piloting activities,
- the software tools to be deployed at specific locations
- data gathering activities
- site location visits
- further workshop/s

NB - The programme comprises a series of topics for discussion. Presentations/slides will be provided, it is however, envisaged these will be informal round the table discussion format to stimulate debate.

Tuesday 1st February

Morning

9.00 Introductions and workshop overview

Overview of flood risk management in the UK,	(HRW)
Overview of flood risk in the US, current project description	(USACE)
Condition inspection, fragility and asset management in the UK	(HRW)
Levee monitoring and safety in the US	(USACE)

12:30 – 13:15 lunch

13:15 – 14:15 Ship Simulator demonstration

Afternoon

14:15 (Description of Modelling tools) (HRW)
System risk modelling
Inundation modelling
Breach modelling
Consequence modelling
Reliability modelling

17:00 Finish

Evening meal – venue tbc

Wednesday 2nd February

Morning

9:00 (Description of modelling tools) (USACE)
Risk analysis
Hydraulic analysis
Consequence analysis
Reliability modelling
Levee screening approaches

12:30 – 13:15 lunch

13:15 – 14:15 Tour of the physical laboratory

Afternoon14:15 (Case studies)
New Orleans (USACE)
St Paul's Minnesota (USACE)
Thames Estuary (HRW)
Humber Estuary (HRW)

17:00 Finish
Evening meal – venue tbc

Thursday 3rd February
Morning
9:00 Software demonstration (HRW)
Programme development
12:30 – 13:15 lunch

Afternoon
14:15 (Summarising programme development and wrap up) (HRW/USACE)
17:00 Finish
Evening meal – venue tbc

HR Wallingford and USACE Workshop : Flood risk, levee safety and asset management HR Wallingford, Tuesday 1st February - Thursday 3rd February, 2011

Minutes (Final)

Attendees:

USACE	HR Wallingford
Noah Vroman (NV)	Jonathan Simm (JS)
David Schaaf (DS)	Caroline McGahey (CM)
Corby Lewis (CL)	Mark Morris (MM)
Bob Patev (BP)	Mike Panzeri (MP)
Neil Schwanz (NS)	Paul Sayers (PS)
William Lehman (WL)	Andy Tagg (AT)
David Margo (DM)	Ben Gouldby (BG)
Alex Roos (AR)	

Workshop Objective:
The objectives of the workshop are summarised under two components:

- Exchange knowledge on levee safety, flood risk and asset management.
- Develop and define a detailed work-plan (activities and programme) for implementing methods and software tools at agreed locations to produce specific agreed outputs.

These activities are to support USACE in the development of their methodology for prioritisation of maintenance activities for risk reduction. It is currently envisaged the USACE will develop a framework that is not prescriptive with regard to modelling tools and implementation but provides overarching guidance on principles and concepts.

Summary of discussions (Days 1 and 2)
A series of presentations from all parties took place, the topics were wide ranging and included:

- Condition inspection
- Deterioration
- Geotechnical stability
- Closure (active) structures
- Fragility/reliability
- Levee deterioration
- Breaching and breach modelling
- Risk, uncertainty and sensitivity analysis
- Economic consequences of flooding
- Loss of life from flooding
- Hydraulic modelling
- Screening tools
- Optimisation
- Life cycle modelling and continuous simulation

There were many commonalities between the approaches used and in particular common definitions of risk, use of fragility, concepts of screening tools, condition inspection and uncertainty. The differences lay in the specific practical implementation and these were largely a result of different overarching policy and regulation requirements.

Specific actions arising from discussions on Day 1 and 2 are summarised below:
Action DM to provide paper on levee screening approach (and manual?)

Action DS to provide information on unified toolbox for internal erosion and piping

Action BG to provide information on capping of damages

Action BG to provide information on handling of deprivation in consequence analysis, in relation to WL's current research.

Action HRW to circulate draft paper on continuous simulation to WL.

Summary of discussions (Day 3)
During the morning of day 3 software demonstrations took place in particular in relation to the Wallingford risk analysis and decision support tool and the Process based HR Breach model.

In the afternoon, breakout discussions were held to confirm priorities of implementing tools, details of programme of work and points of contact. The outcomes of the discussions are summarised below.

It was agreed that St Paul's would be the focus for the pilot site analysis and trials. It was noted however, that a single site wouldn't cover a full range and provide a full test for the models. An option to overcome this issue was to experiment with different

modifications to the St. Paul's site (eg, modify defence crest levels to facilitate more damage). The primary model applications and outcomes of interest are described below:

Risk analysis model:
As a general principle it was agreed that the main focus of effort should be on implementing the software as is rather than make extensive changes to the Wallingford pre-processing tools for example, to be compatible with USACE data sets.
It was agreed to run the UK risk analysis model on the St Paul's area. The standard outputs the HR Wallingford risk analysis model currently produces are:

- Maps showing EAD over the floodplain area
- Maps showing floodplain EAD attributed to levee sections
- Maps showing annual probability of exceedence over the floodplain area

During the discussions it became apparent that loss of life is a key metric for USACE applications. There was some discussion on whether to include HRW's Dynamic (as opposed to static) Rapid Flood Spreading Model (RFSM) in the risk analysis model. It was felt however, that this may compromise runtimes and that a simple topographically based approach would suffice for the current study. This will mean additional output will become available:

- Expected life loss (ie risk of life loss) over the floodplain area
- Expected life loss attributed to levee sections

Action HRW, to implement simple loss of life approach. WL can provide input and advise on USACE LIFESIM approaches.

To enable comparison with HEC FRM approaches, it was agreed it would be useful to undertake single hydrodynamic simulations for specific realisations (ie single hydrographs and system state combinations). Model cascade could include HEC-RAS, HR BREACH and Dynamic RFSM. **Action HRW** to consider model coupling and advise DM.

It was felt useful to undertake the risk analysis using the UK "generic" fragility curves and compare the results with the site specific fragility curves that have already been derived by USACE. This will provide information that is useful for understanding issues of transferability to other sites (ie, do the generic curves act as a reasonable first pass, without having to undertake detailed reliability analysis for each defence).

Action HRW to set up risk analysis model on the St. Paul's study site and undertake analysis as described above.

Breach process model:
It was felt that it would be of benefit to explore the application of the Breach process model. **Action HRW** to configure breach model for the St Paul study site ready for transfer to USACE.

RELIABLE: It was felt that it would be of benefit to apply the RELIABLE model to compare with fragility curves that have already pr. **Action HRW** to configure RELIABLE model for the St Paul study site.

RAFT: The USACE screening tool is similar to the UK RAFT model. It was felt there would be merit in comparing the two tools in the context of the St Paul's area. Nb: HRW has developed the RAFT tool for the Environment Agency (EA) and its application on St Paul's will require consent from the EA. **Action HRW** to enquire with the EA about use of the tool on St Paul's.

Full uncertainty analysis: Whilst this was an area of interest, this was considered as a lower priority than tasks above and will not be applied as a specific priority at St. Paul's.

Automated intervention optimisation: This current HRW research initiative was of interest, but it was felt this was at a too early stage and of less relevance for the Corp's current project. This will not be implemented at St. Paul's.

Timescales

A number of key milestones were identified together with associated timescales:

1. HRW visit to St Paul's – The primary objectives of this trip are:
    a. HRW site familiarisation
    b. Presentation of initial results
    c. Transfer and training of software

    Date: Provisionally agreed as early May 2011 – **Action BG** to contact DM and confirm dates.

2. USACE visit to HRW– The primary objectives of this trip are:
    a. Familiarisation of approaches for wider group of USACE personnel.
    b. Presentation and discussion of updated results.
    c. Troubleshooting software
    d. Final software transfer

    Date: Provisionally agreed as end June 2011 – **Action**: BG to contact DM and confirm dates.

3 Final USACE reporting: August 2011.

Communication

It was felt most efficient for points of contact (POC) to be identified and direct communications on specific technical issues to occur, keeping BG and DM cc'd. POC's are detailed below:

USACE	
Fragility/reliability/breaching	David Schaaf
Hydraulics and hydrology	Corby Lewis
Consequences	Will Lehman
Data	Andrew Sander

HRW	
Fragility	Jonathan Simm
Breaching	Mark Morris
Risk software	Caroline McGahey
Data/consequences	Mike Panzeri

HR Wallingford and USACE In Progress Review Meeting:
St. Paul Pilot Study
Flood risk, levee safety and asset management
Hosted by USACE, Tue 26th July – Fri 29th July 2011

Programme (Draft)

Meeting Objective:
The objectives of the meeting are summarised under three components:

3. Review application of risk assessment models and tools for the St. Paul Pilot Study
4. Demonstration and handoff of the HRW software tools to USACE for the St. Paul Pilot Study
5. Develop and define a work-plan (activities and programme) for completion of the pilot study including identifying opportunities for further collaboration

These activities are to support USACE in the development of their methodology for prioritisation of activities for risk reduction.

The review of risk assessment models will comprise topics that include, but are not limited to:

- Data and inputs
- Methodology and computations
- Outputs and conclusions
- Comparison of methodologies (USACE, HRW, WAT/FRM)

The demonstration and handoff of software tools will include

- Hands on use of the tools by USACE
- Handoff of the software tools and input/output files

The development of the work-plan will seek to agree specifics relating to:

- List of action items required to complete the pilot study
- Further meetings

The programme comprises a series of topics for discussion. Presentations/slides will be provided, it is however, envisaged these will be informal round the table discussion format to stimulate debate.

Tuesday, 26th July

9.15	Depart Hallmark Inn for HEC Office	
9.30	Arrival at HEC Office Overview and Introductions	(Shewbridge)
9.35	Overview of Sacrament River Flood Risk Management System	(Tibbits)
10.30	Overview of RD1000 Levee System	(Tibbits)

11.30 Q&A

12.00 Depart HEC Office for RD1000 Levee System
Stop for Lunch En Route

13.30 Tour of RD1000 Levee System

17.00 Finish
Depart for Hallmark Inn

Happy Hour at Hallmark Inn
Dinner (venue tbd)

Wednesday, 27th July

08.30	Data, Model Inputs, and Risk Assessment Framework	(HRW)
09.00	Discussion	
09.30	Preliminary Model Results	(HRW)
10.00	Discussion	
10.30	Break	
10.45	Reliability Modeling Condition Grade Methodology Reliable Methodology	(HRW)
11.30	Discussion	
12.30	Lunch	
13.30	Breach Modeling HR Breach	(HRW)
14.00	Discussion	
15.00	Break	
15.15	Model Variations and Sensitivities Overtopping Risks and Breach Risks Levee Crest Elevation Model Resolution USACE Fragility and HRW Fragility	(HRW)
16.00	Discussion	
17.00	Finish	

Happy Hour at Hallmark Inn

Dinner (venue tbd)

Thursday, 28th July

08.30	Software Demonstration	(HRW)
09.30	USACE Trial Use of Software	
12.00	Lunch	
13.00	Overview of USACE Risk Assessment for St. Paul	(Hauck/Schwanz)
15.00	Break	
15.15	Comparison of USACE and HRW methods and tools	
17.00	Finish Depart for Sacramento for tour	
18.00	Start tour	
19.30	Diner (venue tbd)	

Friday, 29th July

08.30	HEC Mission and Current Activities	(Harris)
09.30	HEC WAT/FRM Application for St. Paul	(Baker)
10.30	Break	
10.45	Discussion	
12.00	Lunch	
13.00	Develop Work Plan	
15.00	Finish	

List of HRW Attendees
Gouldby, Ben
McGahey, Caroline
Panzeri, Michael

List of USACE Attendees
Baker, Penni
Empson, Bill
Harris, Jeff
Hauck, Kari
Lehman, Will

Lewis, Corby
Margo, David
Needham, Jason
Patev, Bob
Roos, Alex
Sander, Andrew
Schaaf, David
Schwanz, Neil
Shewbridge, Scott
Terry, Tom

Appendix 2 RELIABLE

RELIABLE

1 Introduction

The RELIABLE model has been developed on the EU funded FLOODsite Project. The prototype software is captured in four main components:

- Structure specific fault trees – constructed externally by the user within OpenFTA software.
- Limit State Equations (LSEs) – comprised within one or more Dynamic Link Library (DLL) constructed from Fortran subroutines, and based upon the Task 4 failure mode report. The software does however, provide the opportunity to extend the library of LSE's if this is a requirement.
- Uncertainties on the input parameters of the LSEs– input through a spreadsheet interface.
- Numerical integration – Monte-Carlo simulation implemented through c# code behind a Microsoft Excel spreadsheet interface.

These components are captured in Figure 1.1. The primary outputs of the software are a fragility curve for a specific structure or the annual probability of failure.

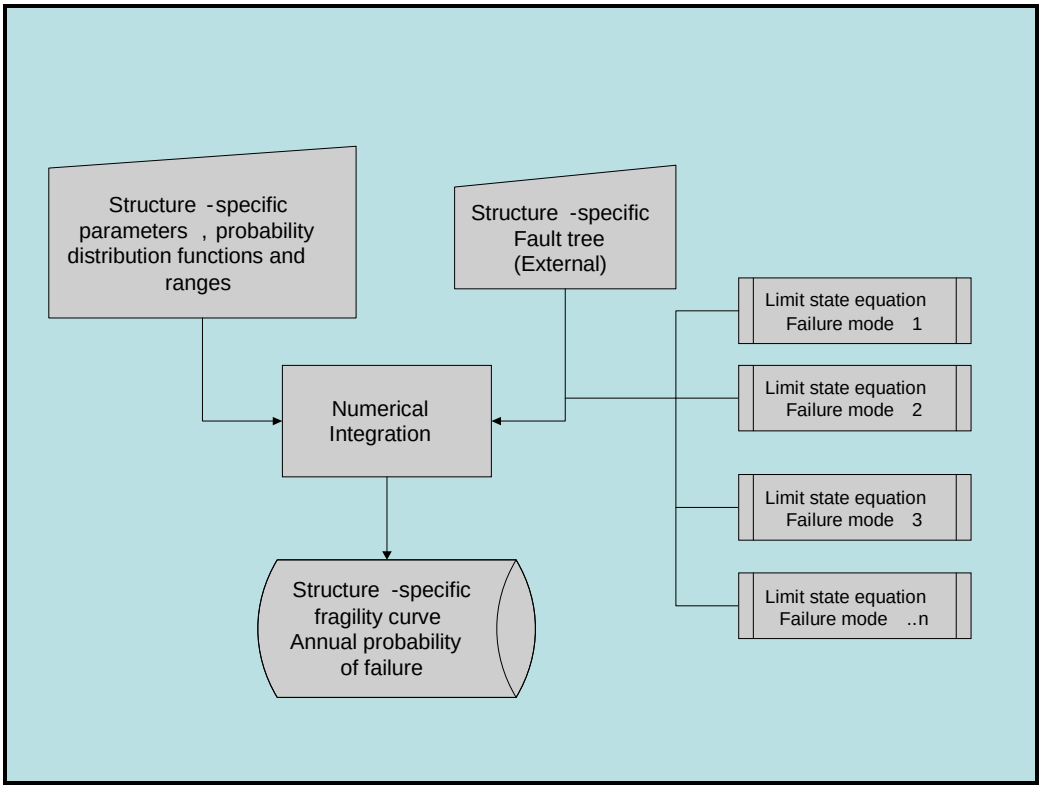

Figure 1.1 Components of the Reliability calculator software

1.1 System requirements

To operate effectively, the reliability calculator requires:

- Windows XP or later
- Microsoft Excel 2003 (earlier versions may be acceptable but have not been tested).
- Microsoft .NET Framework 2.0 (may be downloaded free of charge from http://www.microsoft.com/downloads/details.aspx?FamilyID=0856eacb-4362-4b0d-8edd-aab15c5e04f5&DisplayLang=en
- Local Administrator rights for one or two steps of the installation process.
- A folder C:\TEMP with write access.

2. Description of the system components

2.1 Limit state equations

The calculator uses a DLL that is constructed from a library of LSEs (each LSE is a separate FORTRAN subroutine (Figure 2.). The calculator comes provided with a DLL (Task7_LSEs.dll) built from over 60 LSEs based on the FLOODsite Task 4 report (Allsop et al, 2007). An example FLOODsite Task 4 template is shown in below.

Ba1.5aiii Uplifting of impermeable layers behind earth embankment

Summary: Uplifting behind embankments occurs if the difference between the local water level h, and the water level "inside", h_b is larger than the critical water level h_c

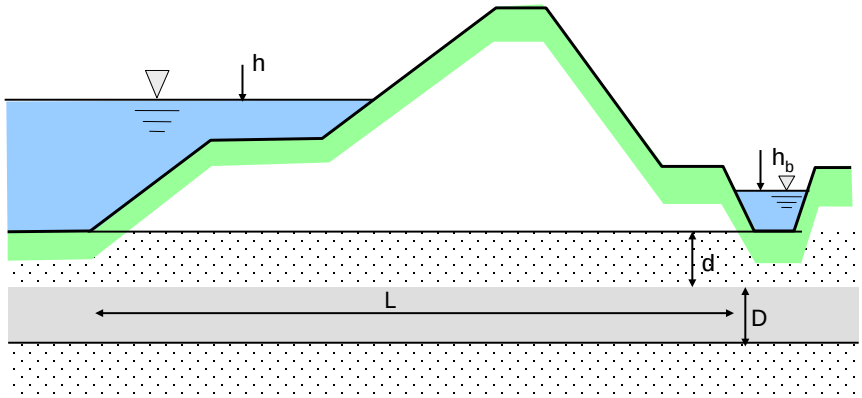

Reliability equation:
The reliability function is expressed by:

$$z = m_0 \cdot h_c - m_h \cdot \Delta h$$

where:

h_c	=	critical water level [m]
Δh	=	difference between local water depth in front of dike and water level in the floodplain [m]
m_o	=	model uncertainty factor [-]
m_h	=	model uncertainty factor for damping[-]

Loading equations:

$$\Delta h = h - h_b$$

Resistance (strength) equations:

$$h_c = \frac{\gamma_{wet} - \gamma_w}{\gamma_w} d$$

Parameter definitions:

γ_{wet}	=	saturated volumetric weight of the impermeable soil layers
γ_w	=	volumetric weight of the water
d	=	thickness of the impermeable layers
h	=	water level on the river [m]
h_b	=	water level in the floodplain [m]

Sources of failure mechanism equations / methods:
Vrouwenvelder et al. (2001)

Sources of uncertainties in failure equations / input parameters:
Vrouwenvelder et al. (2001)

Remarks:

```
REAL FUNCTION LSEBA1_5AIII(VALUES,VALUESCOUNT,ERRORNO,ERRORMSG)
USE LSESupport

       !Standard Arguments for an LSE Function
       INTEGER, INTENT(IN) :: VALUESCOUNT
       REAL, INTENT(IN), DIMENSION(VALUESCOUNT) :: VALUES
       INTEGER, INTENT(INOUT) :: ERRORNO
       CHARACTER(256), INTENT(INOUT) :: ERRORMSG

!Variables to hold our Parameter values
REAL WaterL,Hb,CritWLev,delta_h,hc,GammaS,GammaW,Dimp,MBA1_5AIIIR,MBA1_5AIIIS

!Variables to hold the indexes of our parameters
INTEGER
IX_WaterL,IX_Hb,IX_CritWLev,IX_GammaS,IX_GammaW,IX_Dimp,IX_MBA1_5AIIIR,IX_MBA1_5AIIIS

!WARNING - Parameter names below may change
IX_WaterL=IndexOf('WaterL')
IX_Hb=IndexOf('Hb')
IX_CritWLev=IndexOf('CritWLev')
IX_GammaS=IndexOf('GammaS')
IX_GammaW=IndexOf('GammaW')
IX_Dimp=IndexOf('Dimp')
IX_MBA1_5AIIIR=IndexOf('MBA1_5AIIIR')
IX_MBA1_5AIIIS=IndexOf('MBA1_5AIIIS')

!Check that all our Parameter Names have been recognised
IF(IX_WaterL<0.OR.IX_Hb<0.OR.IX_CritWLev<0.OR.IX_GammaS<0.OR.&
       IX_GammaW<0.OR.IX_Dimp<0.OR.IX_MBA1_5AIIIR<0.OR.IX_MBA1_5AIIIS<0)THEN
       ERRORNO=1
       ERRORMSG="One or more Parameter names unrecognised"
       LSEBA1_5AIII=0.0
       RETURN
END IF

!Get the parameter values that we need
WaterL=VALUES(IX_WaterL)
Hb=VALUES(IX_Hb)
CritWLev=VALUES(IX_CritWLev)
GammaS=VALUES(IX_GammaS)
GammaW=VALUES(IX_GammaW)
Dimp=VALUES(IX_Dimp)
MBA1_5AIIIR=VALUES(IX_MBA1_5AIIIR)
MBA1_5AIIIS=VALUES(IX_MBA1_5AIIIS)

hc=(GammaS-GammaW)/GammaW*Dimp
delta_h=WaterL-Hb
LSEBA1_5AIII=MBA1_5AIIIR*hc-MBA1_5AIIIS*delta_h

END FUNCTION LSEBA1_5AIII
```

Figure 2.3 An example FORTRAN subroutine for a soil uplifting LSE is provided above

It is anticipated that users will add additional LSEs. Instructions for adding additional LSEs are provided in Appendix 3.

2.2 LSE parameters and uncertainties

Each LSE has a number of different parameters associated with it, and most parameters are required within more than one LSE. HR Wallingford (2008) provides details a list and description of parameters associated with the FLOODsite Task 4 report (Allsop et al, 2007) that are included in the pre-coded LSEs supplied with the software. HR Wallingford (2009) also provides details which parameters are used by which LSE (this information is contained within the *FailureModeParam.csv* file which is available from the RELIABLE package).

The user is required to specify a statistical distribution function and its associated parameter values for each variable within each LSE used in the construction of the fault tree. Distributions supported by the software are:

- Normal
- Lognormal
- Gamma
- Rayleigh
- Weibull
- Bivariate gamma

It is also possible to specify constant parameter values by omitting any distribution information (i.e. only a single value is entered).

Whilst the user is required to specify the distributions, example information on distributions is stored within the excel spreadsheet. It is important to note that the information on distribution functions and parameter values should not be considered "default settings" and the user is encouraged to gather evidence for the structure under investigation, to support the selection of distribution function and parameters.

2.3 Fault Trees

The reliability calculator requires the user the opportunity to define a fault tree that shows the logical links between the LSEs for the specific structure under investigation. Construction of fault trees is undertaken in freely available software OpenFTA (http://www.openfta.com/). This software outputs a text file (with .fta extension) which is read in by the reliability calculator. Example output from OpenFTA is shown below (Figure 2.3). An example of the fault tree construction within the OpenFTA environment is shown in Figure 2.4.

```
FailureMode.ped
S NULL 0
0
0
M NULL 1
6 Breach
O NULL 3
M NULL 1
33 Instability due to anchor failure
H NULL 2
N Cb1.2d 0
M NULL 1
```

Figure 2.3 Text file output from OPENFTA

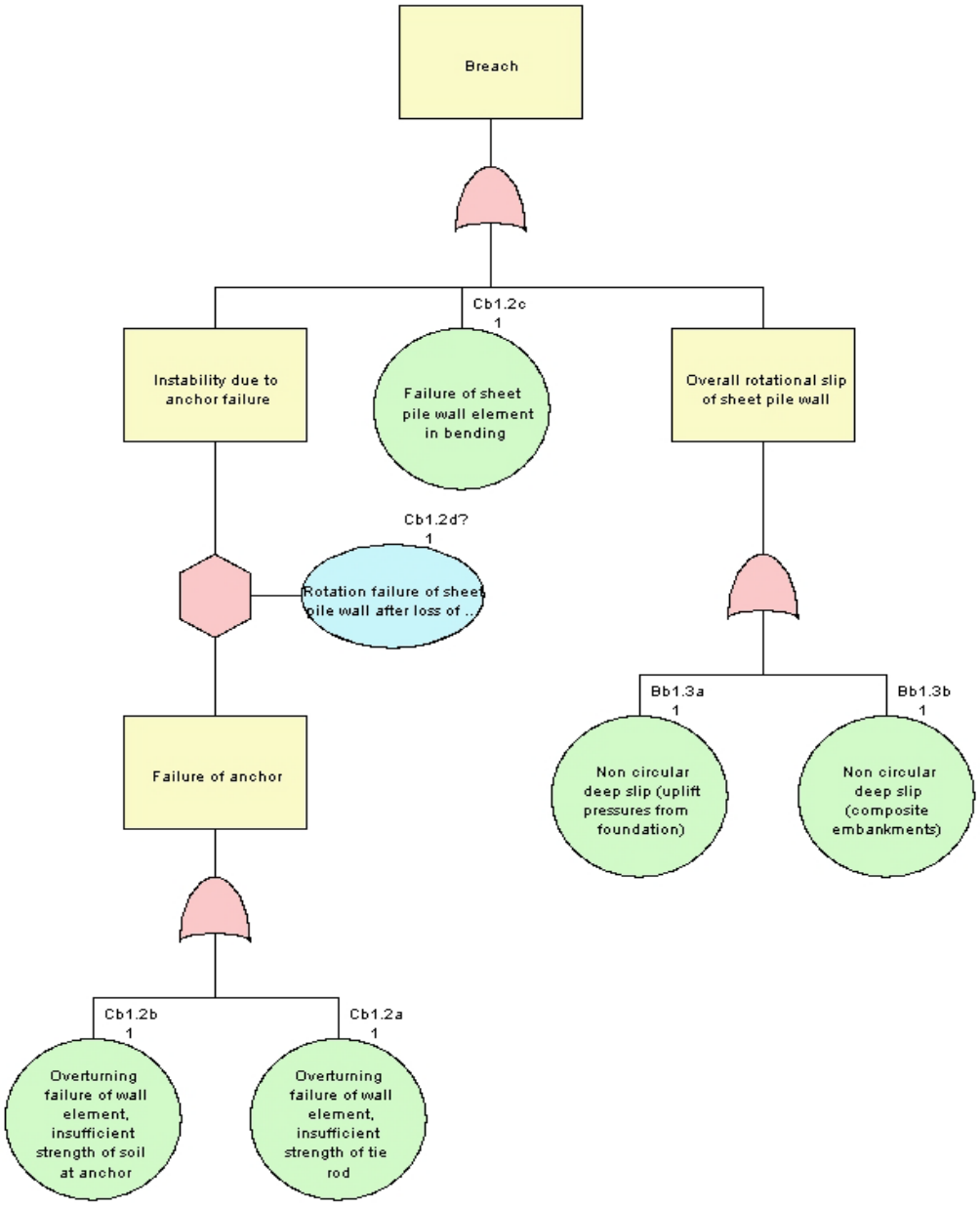

Figure 2.4 Example fault tree for sheet pile wall analysis

An OpenFTA database file (FailureMode.ped) that stores the list of (FLOODsite Task 4) failure modes that have already been coded is provided with the reliability calculator, to facilitate construction of fault trees that are compatible with the reliability calculator.

2.4 Interface

The reliability calculator interface is shown in Figure 2.5.

RELIABLE

Version 1.0
01-Jul-08

Job n:	TE2100
User:	BPG
Date:	26-Jun-08

HR Wallingford *Working with water* · TUDelft · FLOODsite · flood risk management research consortium · FRMRC

INPUTS

Structure Name EXBX8 Calculate Reset

Parameters

Name	Distribution	Distribution Parameters		
CrestH	F (Fixed)	7.5		
DissCoeff	F (Fixed)	1		
GrassRevQ	N (Normal)	1.05	0.07	
Grav	F (Fixed)	9.81		
InsSlopeAng	F (Fixed)	17.49		
KdKf	N (Normal)	0.4	0.03	
Mannings	F (Fixed)	1		
MBA1_1R	F (Fixed)	1		
MBA1_1S	F (Fixed)	1		
OverPercen	F (Fixed)	1		
StormD	N (Normal)	3	0.65	
WaterL	V (Variable)	7.5	0.01	8

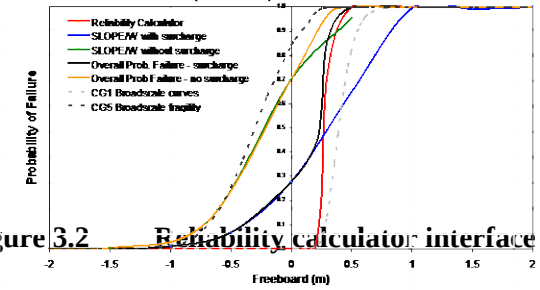

Figure 3.2 Reliability calculator interface

OUTPUTS

Results

Annual Reliability	1
Annual Probability of Failure	0
Converged	YES
Convergence Factor	0
Samples	2200
Time Taken (seconds)	0

Convergence control

Min Samples	2000
Max Samples	100000
Interval	200
Convergence Factor	0.001
Successive Intervals	1

Control

Events Per year	1
Optimise	YES
Log each Sample	NO
Log each LSE call	NO
Failure Mode Summary	Yes

FRAGILITY CURVE

WaterL	Probability

Failure Mode Summary

Name	Calls	Fail Ratio

This interface is used to input information relating to:

- The name of the structure (determined from a drop down list which uses information from OpenFTA files with the pre-constructed fault tree.
- Distribution functions for each parameter
- Parameters for the distribution functions
- The number of samples required for the Monte-Carlo simulation
- The required accuracy of the calculation (convergence)

More detailed information on using the interface and relating to these inputs are provided in Appendix 5. Information on extension of the tool to include additional structure fault trees and failure modes is provided in Appendix 3.

3. Potential improvements

Potential refinements to the software include those identified in Table 3.1

Table 3.1 Potential refinements to RELIABLE

Reliability tool component	**Improvement**
User interface	Provide a more robust user interface
Failure mechanisms and dependencies	▪ Link hydrodynamic models (through emulators) ▪ Link to Finite element geotechnical failure mechanisms (through emulators)
Fault tree	▪ Build in capability rather than external software
Statistical models	▪ Include correlation and extreme values in the hydraulic boundary conditions ▪ Extend the range of distribution functions ▪ Include correlations between other random variables ▪ Include Autocorrelations and system effects
Numerical integration	▪ Extend to include FORM/SORM for example
Sensitvity analysis	▪ Variance decomposion

References

Allsop, N.W.H.; Buijs, F.; Morris, M.W.; Hassan, R.; Young, M.J.; Doorn, N.; Van der Meer, J.W.; Kortenhaus, A.; Van Gelder, P.H.A.J.M.; Dyer, M.; Redaelli, M.; Visser, P.J.; Bettess, R.; Lesniewska, D. 2006. Failure mechanisms for flood defence structures. FLOODsite - Integrated Flood Risk Assessment and Management Methodologies, T04-05-01, Task 4, 150 p.

HR Wallingford (2009) Flood defence reliability calculator: RELIABLE User Manual, Floodsite Report Number T07-10-08

Kortenhaus, A.; Lambrecht, H.-J. 2006. Preliminary reliability analysis of flood defences in the pilot site ‚German Bight Coast'. FLOODsite - Integrated Flood Risk Assessment and Management Methodologies, T07-06-01, Task 7, Braunschweig, Germany, 26 p.

Van Gelder, P.H.A.J.M.; Buijs, F.; Van, C.M.; ter Horst, W.L.A.; Kanning, W.; Nejad, M.; Gupta, S.; Shams, R.; Van Erp, N.; Gouldby, B.; Kingston, G.; Sayers, P.B.; Wills, M.;

Kortenhaus, A.; Lambrecht, H.-J. 2008. Reliability analysis of flood sea defence structures and systems. FLOODsite Report T07-08-01, 118 p.

Appendix 3 HR BREACH (Hassan et al (2003))

Improving the Accuracy of Prediction of Breach Formation through Embankment Dams and Flood Embankments

M. A. A. Mohamed, Dr P. G. Samuels & M. W. Morris
HR Wallingford, Wallingford, UK.

Dr G. S. Ghataora
University of Birmingham, Birmingham, UK.

ABSTRACT: Embankments are constructed for the retention of water for irrigation and supply, and for protecting people, land, and property from flooding. Failure of any embankment poses risks to people and property nearby and the services provided by the embankment. The review of breaching of embankments in this paper identifies significant issues in the parameterisation of the processes in existing models and the data used for calibration. This paper describes the development of a new model the failure of an embankment that can simulate breach formation, and hence consequent risks, more reliably than existing models. The model uses the standard principles of hydraulics, sediment transport and soil mechanics and introduces a new methodology to model the lateral growth of the breach based upon a combination of continuous erosion and mass instability. The model can simulate the failure of different embankments, either homogeneous or composite, by overtopping or piping, and includes a probabilistic distribution for simulating embankment condition and soil parameters. The model has been tested using both experimental and real failure data, with modelling results showing reasonable agreement with observed values for a range of different scenarios.

1 INTRODUCTION

Embankments are constructed for the retention of water for irrigation and supply, and the protection of people, land, and property from flooding. Failure of any embankment poses risks to people and property nearby and the services provided by the embankment. The ability to maintain assets, and provide an acceptable standard of service for water supply and flood defence therefore depends on understanding and predicting performance of the embankments under all conditions. Tools currently available for simulating embankment failure are not very accurate (e.g. Mohamed *et al*, 2001) and can only be used for indicative assessments. Consequently, the prediction of flood risk from embankment breach may be similarly inaccurate. This applies particularly in the critical zone close to the dam or embankment where the risk to life is greatest. Flooding from the failure of the Teton dam in 1976, and from the Mississippi and Missouri rivers, in 1993, and more recently, the Yangtze River in China during1998, are examples of these hazards.

The prediction of potential breaches and the consequent flooding are thus important steps in managing the risk from potential embankment failure. However, breach simulation and breach parameter prediction are considered to contain the greatest uncertainty of all aspects of dam break flood forecasting (Wurbs, 1987, Singh, 1996, and Morris, 2000).

A research project to investigate breach formation through embankments has been undertaken at HR Wallingford, with the following objectives:

1 To review existing methodologies for modelling embankment breaching processes.
2 To identify any weaknesses within these methodologies and determine gaps in current knowledge and understanding.
3 To develop a new methodology that improved the accuracy of prediction of breach formation through embankment dams and flood embankments.

This paper presents an overview of the project giving a summary of weaknesses identified in current methodologies, an overview of a new methodology for predicting breach formation, and an assessment of model performance against a variety of test cases.

2 STATE-OF-THE-ART AND LIMITATIONS

In the last forty years, many models have been developed to simulate the embankment breaching process. In spite of this, the current state-of-the-art for predicting the breaching process still has many uncertainties. A detailed review of existing models

(Mohamed, 2002) has revealed the several weaknesses and gaps within the modelling process, which are discussed in the sections below.

2.1 *Breach Initiation*

Little quantitative information is known about the breach initiation processes for overtopping or piping failure. Determining how the breach initiates will help in reliably determining how long it takes for a breach to develop to a critical point. This in turn can help emergency planners in establishing flood risk and potential warning times for areas downstream of an embankment.

2.2 *Breach Location*

All of the models reviewed (Mohamed, 2002) assumed a breach located centrally within a dam or embankment. However, some failure cases showed that breaching might occur near an abutment rather than in the middle of a dam. Examples include the failures of Teton Dam (Jansen, 1980), Baldwin Hills Dam (Hamilton *et al*, 1971), La-Josefina (Abril, 2001), and the Euclides da Cunha failure (Hughes, 1981). The breach growth and hence outflow from a centrally located breach is likely to be different from a 'side' breach in terms of time to peak discharge, peak value, and hydrograph shape.

2.3 *Data For Calibration and Verification*

Most existing models were calibrated or verified using either or both data sets from the Teton Dam failure or the Huaccoto landslide in Peru. The documented data for these two events is not very detailed. For instance, estimated peak outflow from the Teton Dam failure ranged from 45,000 to 80,000 m^3/s. It was also noticeable that some authors verified their models with data from the piping failure of the Teton Dam in spite of developing their models to only simulate an overtopping failure. Some also calibrated their 'central' breach models (i.e. unrestricted breach growth) with side breach failure data (i.e. erosion was restricted on one side by rock abutments). These wide ranging inconsistencies support the need for good quality data sets (such as large-scale experimental data) for the calibration and verification of breach models.

2.4 *Breach Morphology*

Two common assumptions in many of the existing models are a constant shape (e.g. rectangular, trapezoidal, or parabolic) of the breach and the uniform erosion of the breach section during the formation process. These assumptions simplify the equation(s) used to update the breach section at each time step, but they seem to be physically unrealistic. Assuming uniform erosion throughout the section means that the part of the breach above the water surface will erode at the same rate as that submerged, which is obviously incorrect. It also means that the sides of the breach below the water surface will also erode at the same rate as the breach base, which is inconsistent with the flow stress distribution along the breach sides. Longitudinal growth of the breach was assumed to be parallel to the downstream face in some of the models (BREACH (Fread, 1988), BRES (Vissser, 1998) models). This representation is not compatible with the assumptions of continuity for sediment transport (Mohamed, 2002). For example, the BREACH model computes the flow depth and velocity along the downstream face of the embankment using the steady uniform flow equation. This flow condition, if combined with the sediment continuity equation, will not give parallel retreat of the downstream face.

2.5 *Hydraulics of the Flow over the Embankment*

Most existing breach models use two techniques to simulate flow over the crest and on the downstream face of the embankment. These are:

- the broad crested weir equation and
- the 1-D Saint Venant equations (a simplification)

The Saint Venant equations incorporate the following assumptions (Cunge *et al*, 1980):

- The flow is one-dimensional.
- The water pressure is hydrostatic.
- Boundary friction and turbulence effects can be accounted by steady state flow resistance laws.
- The average channel bed slope is small.

It is clear that the second and fourth assumptions may not be applicable for breaching of embankments. Since the streamline curvature is not small, vertical acceleration may not be negligible. Also, the downstream face of the embankment may be considered as steep in hydraulic terms. In the derivation of the broad crested weir formula, the curvature of the flow is taken into consideration. The weir formula is thus often used to calculate the flow over the crest since it accounts for the acceleration of the flow to the critical point on the crest.

The steady non-uniform flow equations have also been used to compute the water depths, velocities, and energy slope on the downstream slope due to the short reach of the breach channel and its steep slope and their relatively simpler computations compared to the Saint Venant equations.

2.6 *Sediment Transport Equations*

The selection of a sediment transport equation to be used in any mobile bed problem is difficult and is typically based on professional judgement, previous experience, or even personal preference. When con-

sidering the breaching process, the problem becomes even more difficult. Most existing sediment transport equations were derived for steady state subcritical flow conditions, for specific types of sediment, and for a certain range of sediment diameters. These conditions are likely to be violated during the breaching process since conditions are typically unsteady, supercritical flow, and with a wide variety of soil types used for embankment construction. Research in the area of the unsteady non-uniform sediment transport is still in its early stages and more work is required in order to achieve reliable results that could be used for simulation of problems such as breach formation. However, in the absence of any other method to predict the sediment transport, careful selection from the existing sediment transport formulae might be undertaken. On selection of these formulae, the following might be taken into consideration:

- Their applicability to flow on steep slopes and for supercritical flow.
- Their derivation (e.g. based on dam breach experimental data?).

2.7 *Geo-Mechanics of the breach*

In all of the breaching experiments that were reviewed by the authors during this research, instability of the breach sides was observed during the breaching process. Most existing models do not consider this process which means that they neglect a process that is likely to be vital, and thus the calibration and validation of these models must be questioned. The models that consider this process use very simplified assumptions e.g. BREACH (Fread, 1988) and BEED (Singh, 1997). Assuming constant breach shape and uniform erosion of this section also affects the accuracy of the slope stability calculations since lateral erosion will tend to steepen the banks and the breach side slope will get steeper and steeper as water flows through the breach (Osman et al, 1988). This means that the side slope of the breach changes throughout the simulation and hence its shape.

2.8 *Modelling Composite Embankments and Surface Protection Layers:*

Despite that composite embankments represent a significant percentage of real embankments around the world, the majority of existing models were developed to simulate failure of homogeneous embankments. The failure of composite embankments might involve other processes such as core wall instability and mixed sediment transport in addition to the processes encountered with homogeneous embankments. Moreover, many man made embankments have surface protection to prevent erosion of the embankment faces (Singh, 1996). The effect of surface protection was either neglected or oversimplified in many of the existing models (BREACH (Fread, 1988)).

2.9 *Key issues for the research*

It is clear that there are many gaps in our knowledge for reliably predicting breach growth and location and the research has focused on the following issues:

1 A realistic representation of breach development during the breaching process.
2 A more accurate analysis of the breach side slope instability process and the transport of this material after the instability.
3 A methodology to model the failure of composite embankments, including the effect of embankment protection layers on breach development.

3 DESCRIPTION OF A NEW METHODOLOGY FOR BREACH SIMULATION

3.1 *Overtopping of Homogeneous Embankments*

Adjusting the breach shape is a crucial process in any embankment-breach model. Several methods have been used in existing models that simulate breach top width adjustments. A new method is proposed to predict top width adjustment. The process assumes a rectangular initial shape of the breach, as water flows into the breach its shape and side slope will change as shown in Figure 1(B). The bottom width and the breach depth will increase as the water erodes the section sides and bottom. The top width will not change significantly and can be assumed constant until slope instability is encountered.

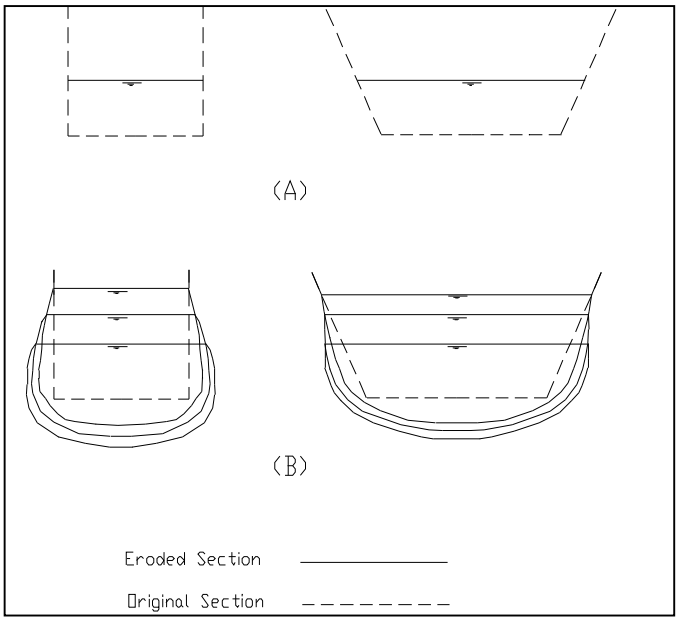

Figure 1: (A) initial breach shape (B) Hypothetical breach shape after three successive time steps.

The process is a combination of continuous erosion and discrete mass failures due to side slope instability. Continuous erosion is calculated by using a sediment transport formula to quantify the volume of the sediment transported. Then by analysing the effective shear stress distribution[1] for the breach section the new breach shape can be obtained, as erosion can be assumed to be proportional to the effective shear stress. The new shape of the breach may be approximated as shown in Figure 2.

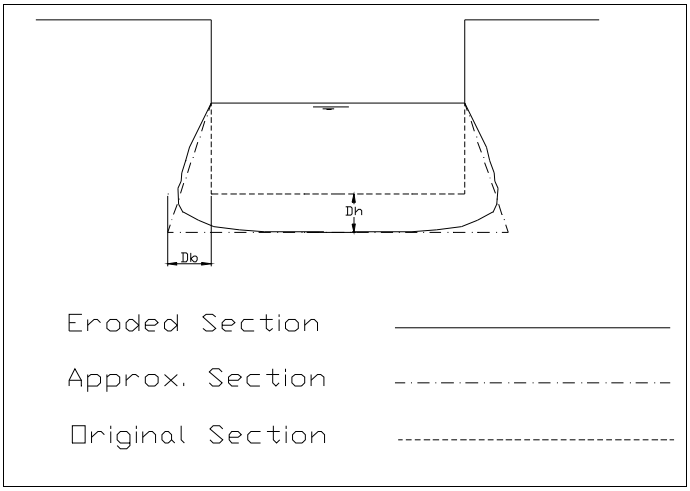

Figure 2: Approximated shape of the breach

The breach section is updated at each time step assuming that maximum lateral erosion (Db) is equal to the vertical erosion (Dh) and it is assumed to occur very near to the bottom level of the breach. The top width is kept constant until slope instability is encountered. The stability of the breach side slope is analysed by taking into consideration the forces acting on the slope, and variation of the soil density. A factor of stability (FOS) is obtained using the following equation:

$$FOS = (\text{Stabilising Forces} / \text{Destabilising Forces}) \quad (1)$$

Where:

The stabilising forces are:

- Water pressure forces in the breach channel.
- Friction forces.
- Cohesion forces (if any).

The destabilising forces are:

- Gravity forces.
- Pore water pressure forces in the embankment.

The nearly vertical sides of the breach (as observed in both lab experiments and real failures) suggest that slope instability failure modes might be either through shear or bending failure (Mohamed, 2002). Both these modes of failure can lead to a near vertical failure plane. In the following two sections, a description of each failure mode is given.

3.1.1 *Bending Failure*

An initial rectangular notch is assumed on the crest and the downstream face of the embankment. Water flows through the initial notch. Flowing water erodes the breach sides below the water surface and the bottom of the notch and undermines the slope. The erosion process continues until slope instability is encountered. A tension crack develops progressively as the actual tension stress exceeds the soil tension strength. The soil block rotates and falls into the flowing water. Water erodes the slumped material and the process continues until the reservoir is depleted or the breach reaches its maximum dimensions. This mode of failure is likely to occur in cohesive embankments.

The following assumptions have been made in developing the analysis below (Figure 3):

- Suction is neglected in the zone above the water level within the embankment. This zone is considered dry.
- Changes in water level inside the embankment during the embankment failure time are small and can be neglected.

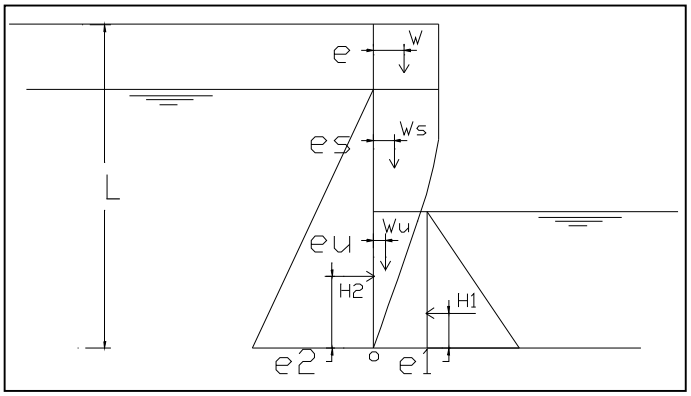

Figure 3: Moments for bending failure

$$\text{Moment}(M_o) = W.e + W_s.e_s + W_u.e_u + H_2.e_2 - H_1.e_1 \quad (2)$$

Where:

W	: Weight of dry block of the soil.
W_s	: Weight of saturated block of the soil.
W_u	: Weight of submerged block of the soil.
H_1	: Hydrostatic pressure force in the breach channel
H_2	: Hydrostatic pressure force inside the embankment.
e, e_s,e_u	: Weight forces eccentricities.
e_1, e_2	: Hydrostatic pressure forces eccentricities.
L	: Length of the failure plane.

1 Effective shear stress equals the difference between the total shear stress and the critical shear stress.

Based on the above analysis, the maximum actual tensile stress ($\sigma_{t(actual)}$) on the plane of failure can be computed as follows:

$$\sigma_{t(actual)} = (H_2 - H_1)/L + 6M_0/L^2 \quad (3)$$

Assuming that the allowable soil tensile strength ($\sigma_{t(soil)}$) is known, then $\sigma_{t(actual)}$ is compared with $\sigma_{t(soil)}$ and if ($\sigma_{t(actual)} > \sigma_{t(soil)}$) then failure occurs.

3.1.2 *Shear Failure*

A similar process to that explained above occurs for this failure mode, however the slope fails due to exceeding the shear strength of the soil (Figure 4). This mode of failure is likely to occur in a non-cohesive embankment.

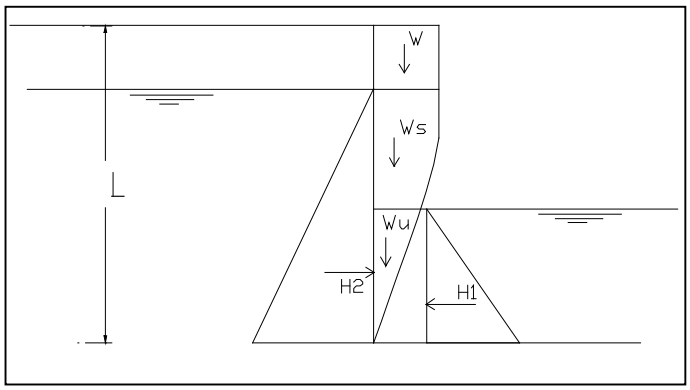

Figure 4: Forces for shear failure.

Making similar assumptions to the bending failure analysis above:

$$FOS = \frac{c * L + H_1 \tan \phi}{W + W_s + W_u + H_2 \tan \phi} \quad (4)$$

Where:

c : Soil cohesion.

ϕ : Soil angle of friction.

3.1.3 *Dealing with uncertainty in soil properties and construction quality*

A probabilistic approach is used to take into account uncertainties in soil properties and the quality of construction. A Sigmoid function has been used to represent a probability distribution for the factor of safety. This was selected since it allows both extremes of 100% and 0% to be represented along with various ranges of distribution in between:

$$f(m) = \frac{1}{1 + e^{a(m-1)}} \quad (5)$$

The value of m represents the factor of safety. The uncertainty coefficient, a, controls the probability distribution and may represent the quality or knowledge of materials within and construction of the embankment (e.g. very good, good or poor material and construction). Three different uncertainty distributions (Figure 5) were used to represent the quality of materials and construction, however, other distributions may also be used to represent varying conditions and uncertainty.

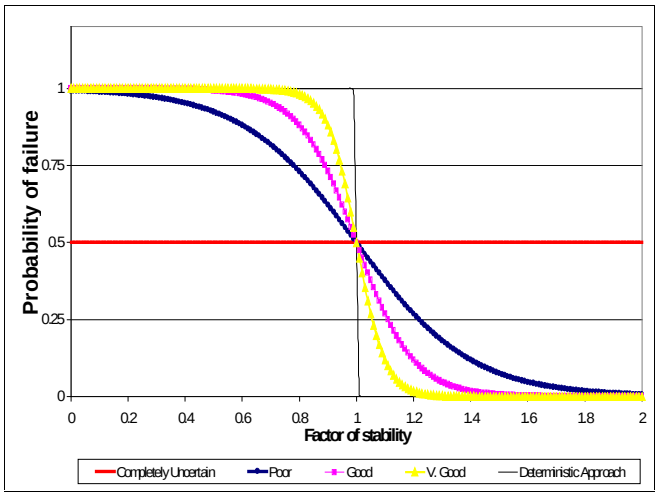

Figure 5: Probability distribution functions for the slope stability factor of safety

3.1.4 *Cohesive Embankments:*

The methodology discussed so far is mainly for non-cohesive embankments with some apparent or conventional cohesion. For cohesive embankments, the failure process might be different. Hughes (1981), Al-Qaser (1991), and Hanson (2000) conducted laboratory and field experiments to determine the failure process of cohesive embankments due to overtopping. They observed the formation of an over fall or steps that progressively advanced towards the upstream face (Figure 6). Hanson (2000) concluded that the erosion process and soil type have a significant effect on the timing and rate of discharge during overtopping events. The observed processes were described as follows:

- Initial downstream surface erosion.
- This initial erosion progresses into stair-stepped multiple over falls.
- Over falls then merge into a single upstream migrating head cut.
- The head cut then migrates upstream, lowering the crest by advancing into the upstream embankment face.

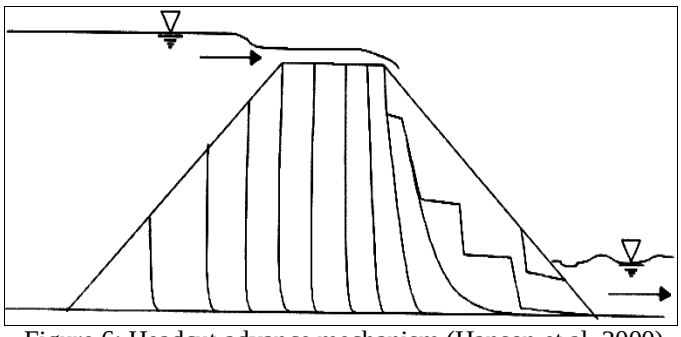

Figure 6: Headcut advance mechanism (Hanson et al, 2000)

Of all the models reviewed within this research, only the SITES model (Wahl, 1998) simulates the

first three processes described above. It does not, however, model the fourth process, which is critical for predicting the flow of water from a breach.

3.2 *Overtopping of Composite Embankments*

The failure of composite embankments differs from that of homogeneous embankments, because of the existence of less erosive layers (such as a clay core) within the dam body. The erosion of the material behind the core may affect the stability of the core and could eventually lead to its failure. The likely failure mechanisms of the core wall of a composite embankment dam, assuming that a large part of the downstream face has been eroded, are:

- Sliding of the clay core wall.
- Overturning of the clay core wall.
- Bending of the core wall.

In the following sections a description of the possible modes of failure of the core are presented.

3.2.1 *Sliding Failure:*

Figure 7 shows the forces acting on the core after a large amount of the downstream body material has been eroded. These forces include:

- Active soil earth pressure forces from the material behind the core (F1).
- Water pressure forces (F2).
- Weight of the clay core material above the failure plane (F3).
- Weight of the material above the upstream face of the clay core and the failure plane (F4).
- Weight of the water above the core (F5).
- Earth pressure forces on the core sides (F6).

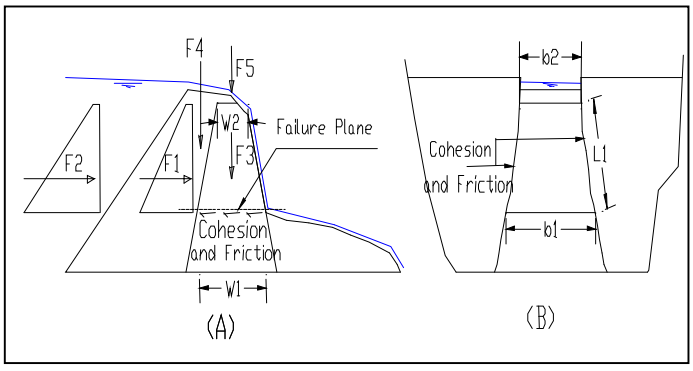

Figure 7: Forces acting on the clay core wall.

The failure plane is assumed to be (as shown in Figure 7) just above the non-eroded material of the downstream face. Forces (F1) and (F2) are the destabilising forces, while the forces (F3), (F4), (F5), and (F6) are stabilising forces. The latter forces mobilise the friction on the bottom and the sides of the failure plane. The cohesion on the right, left, and bottom sides of the failure plane will also resist the destabilising forces. The ratio of the stabilising to the destabilising forces is calculated and if it is less than unity the core is considered to have failed.

3.2.2 *Overturning Failure:*

A similar analysis to that for sliding failure is used here. However, the stabilising and destabilising moments are compared. If the ratio between them is less than unity the core is considered to fail by overturning.

3.2.3 *Bending Failure:*

Hughes (1981) showed that the core failure mechanism could be as shown in Figure 8. He supported this by the observations of Jayasinghe (1978) who noticed similar cracks to those shown in Figure 8 before failure of the core wall.

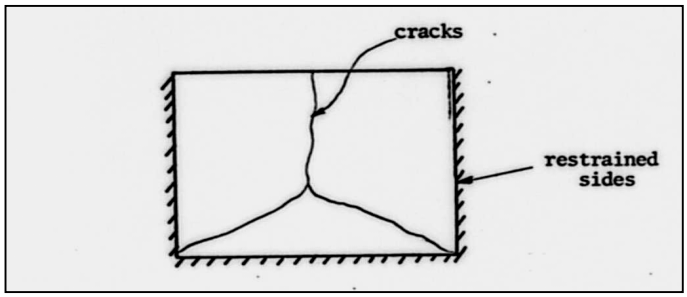

Figure 8: Typical cracking of a clay core restrained on three edges and subject to overtopping (Hughes (1981)).

Analysis of this failure mechanism is difficult because:

1. The geometry of the core and the variation of forces with the height of the core wall.
2. The difficulty in defining the support type on the sides and the bottom of the core wall (hinged, fixed, or something in between).
3. The difficulty in computing the load distribution factors of the core sides and bottom.

The following simplified analysis is proposed for this problem. The clay core might fail by a bending failure as shown in Figure 9 if the left, right, bottom sides can be considered as hinges. Figure 9 (A) shows the failure plane in that case. Figure 9 (B) shows an assumed failure plane neglecting the hinge at the bottom side. This assumption can be justified since the breach depth is likely to be greater than the breach width at that stage of the embankment failure so the effect of the hinge at bottom can be neglected.

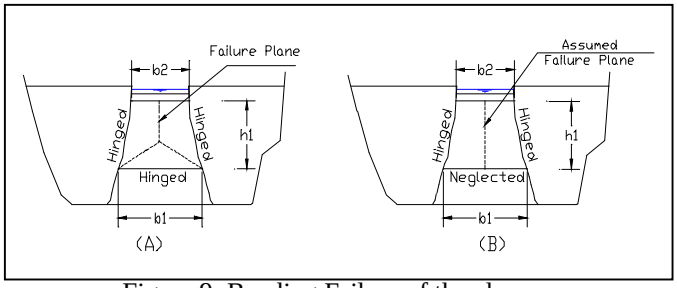

Figure 9: Bending Failure of the clay core

Figure 10 shows the forces acting on the clay core in the case of bending failure after a large part of the downstream face material has been eroded, namely:

– Active earth pressure from the material behind the core (F1).
– Water pressure forces (F2).

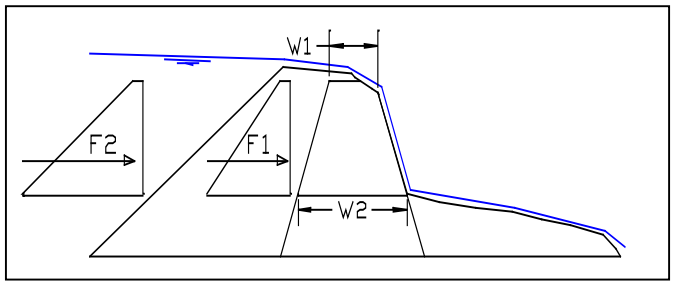

Figure 10: Forces acting on the core wall in bending failure.

The core is assumed to be as a simple beam and the max bending moment and stress is computed. The bending stress can be compared to the tension strength of the clay core material. If the bending stress exceeds the tension strength of the core material then failure will take place.

3.3 *Piping of Embankments*

Piping starts when water flows through an embankment body via cracks, cavities, weak layers etc. As flow increases, the water starts to remove soil particles until a pipe (tunnel) is formed through the body of the embankment (
Figure 11 (A)).

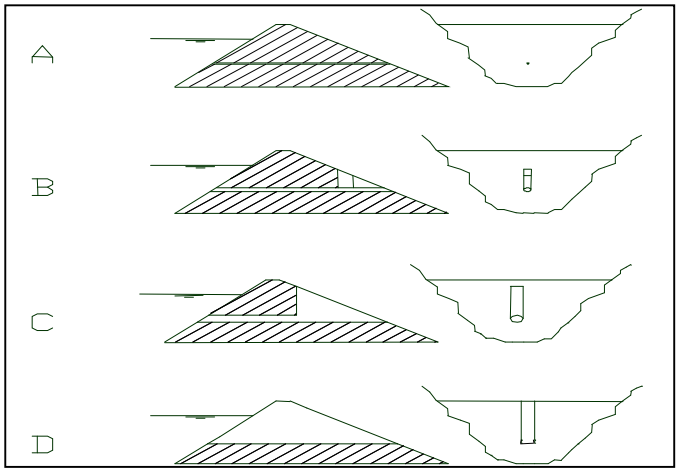

Figure 11: Piping failure in embankments.

After the formation of a pipe inside an embankment, the failure process can be divided into the following processes:
– Erosion of material in the pipe.
– Slumping of the downstream face above the pipe (Figure 11 (B and C)).
– Collapse of the embankment crest, under its own weight or by water pressure Figure 11 ((D)).
– Erosion of the embankment body in a similar manner to that for overtopping breach formation (Sections 3.1 and 3.2).
– In the following sections a description of the modelling procedure for each process is given.

3.3.1 *Erosion of the material in the pipe.*

Figure 12 shows a typical hydrograph for the piping failure of an embankment. It can be noted that different time scales are associated with each process. For the Teton Dam these times were approximately as follows:
– The initiation stage was at least 2 days.
– Erosion of the pipe stage until the collapse of the top of the dam was about 4 hours.
– Emptying of the reservoir was about 2 hours.

The initiation stage was not studied in this research but attention was focussed on growth of an initial pipe.

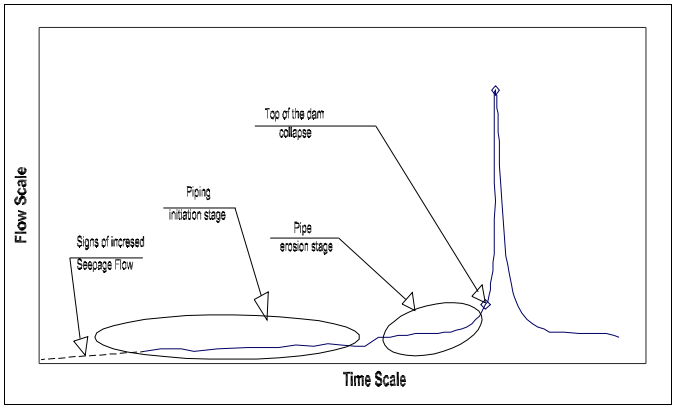

Figure 12: Time scales for piping processes

An initial pipe is assumed to establish within the dam body at the start of the simulation. The flow through the pipe is calculated using the orifice flow equation as follows:

$$Q_b = A\sqrt{2g(H - H_p)/h_L} \qquad (6)$$

Where:
Q_b : Flow through the pipe.
g : Acceleration due to gravity.
A : Pipe cross section area.
H : Water level in the dam.
H_p : Pipe centre line elevation.
h_L : Losses due to friction and contraction.

$$h_L = (0.05 + \frac{fL}{D}) \qquad (7)$$

Where:
f : Friction coefficient determined as function of D_{50}.
L : Pipe Length.
D : Pipe Diameter.

The factor (0.05) in the above equation represents the coefficient of the contraction losses. The enlargement of the pipe was modelled using the simplified procedure used by Fread (1988) and Paquier et al (1998). The pipe is enlarged uniformly along its length based on the volume of sediment eroded

(V_s) within a specified time step. V_s can be computed as shown below:

$$V_s = Q_s \Delta t \quad (8)$$

Where:

Q_s : Sediment transport rate.

Δt : Time step.

It should be noted that this procedure has been used in the absence of any more detailed approaches. This highlights the need for research on the initiation of piping. This simplified procedure can be used for homogeneous and composite embankment dams.

3.3.2 *Slumping of downstream face material above the pipe*

As the pipe develops, material from the downstream face falls into the pipe and is swept away in the flow. This mechanism was observed during the piping failure of the Teton dam in 1976. Justin *et al* (1945) and Hagerty (1991) also reported this process. It is anticipated that the material falls under its own weight. The vertical failure planes observed during the Teton Dam failure and reported by Hagerty (1991) suggest that this is likely to be a shear failure. The ratio between the weight of the material of the wedge and the soil strength is computed. If its value is below unity then the wedge of soil above the top of the pipe is assumed to be unstable.

3.3.3 *The collapse of the top part of the dam, above the pipe.*

As material from the downstream face slumps into the pipe, the width of material above the pipe reduces. If water forces are high enough to exceed the shear strength of the embankment material above the pipe, then this 'wedge' of material may fail. The 'wedge' may also collapse under it is own weight. This mechanism was observed during failure of the Teton Dam. For more information about these failure mechanisms, the reader is referred to Mohamed (2002).

3.3.4 *Erosion of the dam body.*

The process here is similar to that described in Sections 3.1 and 3.2 of this paper, which is a combination of erosion and slumping of material.

4 MODEL PERFORMANCE:

Three sets of data were selected to test different aspects of the proposed new modelling methodology. A detailed description of each case is given in Mohamed (2002) these are briefly summarised below. The test data was obtained from:

– CADAM project Munich proceedings (1998).

– The Teton Dam failure (Fread (1988), and Jansen (1980)).

4.1 *Case 1*

To check the model performance for modelling the overtopping failure of homogeneous embankments, a set of data was used from a series of laboratory experiments that were carried out at the Federal Armed Forces University in Munich (Bechteler et al, 1998) to explore the 3D-development of a dam breach.

Figure 13 shows the results of test case 1. Three simulations have been carried out using different sediment transport equations (Visser (1998), Yang (1979), and Chen and Anderson (1986)). The available measured outflow hydrograph was compared against the corresponding simulation results. For Visser's and Yang's equations, it can be seen that the model results are reasonably in agreement with the measured results in terms of peak outflow value and timing. Chen's sediment transport equation gave poorer results than the other two. The jagged nature of the plots arises from breach growth through bank instability.

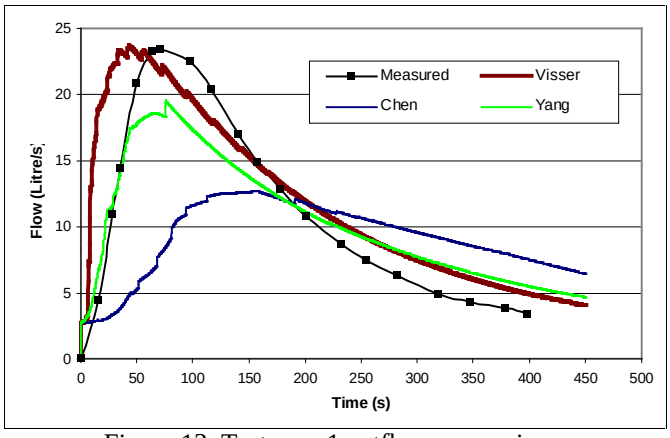

Figure 13: Test case 1 outflow comparison.

Within the CADAM project, several models were tested against the data. A comparison between these models and the developed model is shown in Figure 14 below.

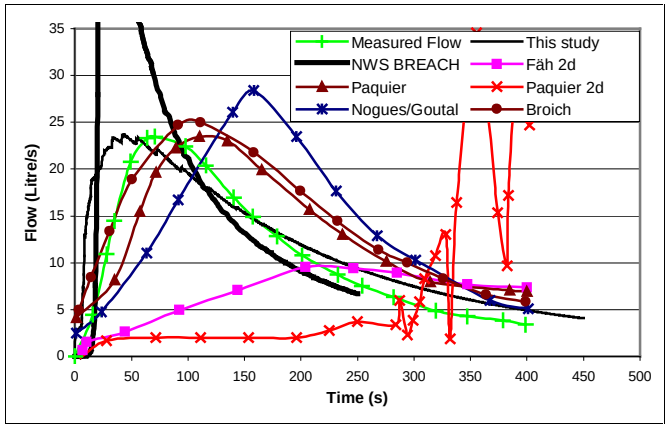

Figure 14: Model comparison (Test case 1).

Apart from the results of Broich's model (which

was calibrated against the test case data) the model performance is generally better than the other models in terms of predicted peak outflow time and value.

4.2 *Case 2*

To check the model performance in modelling the overtopping failure of composite embankments, the data was used from a fuse plug breach test that was conducted in 1982 in the spillway chute of the Yahekou Dam in China. The fuse plug embankment was made of sand fill with a clay core, 5.6 m high and 41 m long at the top and 31 m long at the bottom, with a crest width of 4m, creating a reservoir with a capacity of 46,000 m³.

Two simulations were undertaken using this test case data to investigate the effect of core failure mechanisms. The first considered only sliding and overturning failure modes (A) whilst the second included the bending failure mode (B) as well. This was undertaken to see whether the bending failure mechanism is a critical mode of failure or not, since modelling this failure was based on a simplification of the real processes (See Figure 15).

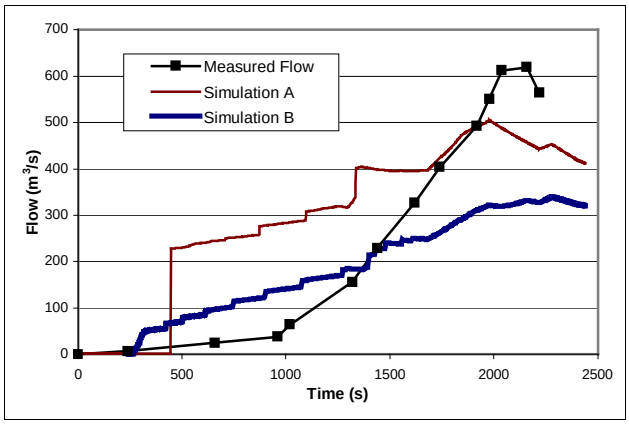

Figure 15: Test case 4 outflow comparison.

The predicted peak flow and its time for simulation A was closer to the measured value than those predicted in simulation B. However, the predicted time of the first failure of the core was earlier than what was observed during the experiment for the two simulations. For simulation A, the magnitude of the flow at the first core failure was significantly higher than the measured value. Whilst, for simulation B, it was slightly higher than the measured value. The results obtained here showed that further investigations and tests are needed to check the performance of the model of the composite embankments.

4.3 *Case 3*

The data of Teton dam failure was used to test the model performance in modelling piping failure of embankments. The Teton dam failed on the 6th of June 1976. The dam was a 91.45 m high earth dam with a 914.5 m crest length, 10.65 m crest width, and 79.85 m depth storing about 307 million m^3 of water at the time of failure (Fread, 1988). Failure occurred close to the right rock abutment, which potentially restricted lateral growth of the breach.

Modelling the piping failure was undertaken assuming a small initial pipe within the dam, and then a central breach or a side breach after the top of the dam collapses. Figure 16 shows the results obtained from both simulations using Yang's equation. It can be seen that the central breach simulation gave a higher peak outflow value than the side breach case. The results of the central and side breach simulations highlight the importance that the breach location and the valley shape might have on the peak outflow value. This also raises questions as to the validity of models (such as BREACH, BEED) which were calibrated using the Teton dam failure data yet only assumed a centrally located breach.

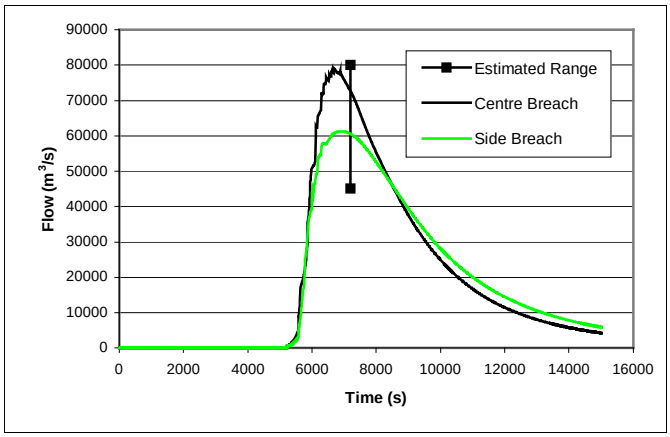

Figure 16: Test case 3 outflow comparison.

To test the effect of using different sediment transport equations on the model results, the Visser, Yang, and Chen and Anderson equations were also used assuming a side breach failure. Figure 17 shows the results obtained using these three equations.

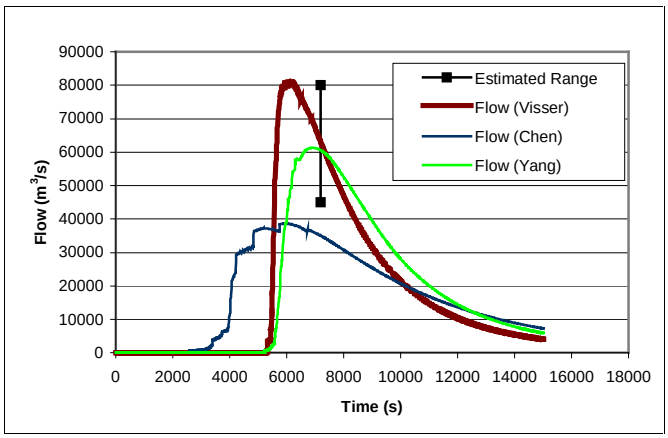

Figure 17: Test case 5 outflow comparison using different sediment equations.

The peak outflow values obtained using Visser and Yang equations were within the estimated range

of the peak outflow value. However the predicted value using Yang's equation was less than that obtained using Visser's equation. The value obtained using Chen and Anderson's equation was below the estimated range. It can also be seen that the time to peak obtained using each equation varied significantly. This variation highlights the importance of selecting a sediment transport equation in dam breach problem and their effect on the results.

5 CONCLUSIONS:

There are several weaknesses in the commonly-used methods for simulating breaching of embankments. These arise from what now appear to be unrealistic simplifications of the breach growth processes and from using as calibration data information from past failures where the valley topography or failure mode were different from those included in the model. Thus the situation is that there remains a high degree of uncertainty on the assessed outflow hydrograph of the water impounded behind an embankment during a failure. This has important social and economic impacts, particularly for risk management and emergency planning.

A new methodology has been put forward in this paper based upon well-established principles of soil and fluid mechanics, although uncertainty still remains in some aspects of the parameterisation of the model. The evidence from the documentation of actual failures is that the failure of an embankment progresses through general erosion of the embankment material and mass failures caused by soil slope instability. The novelties in the model described in this paper includes updating the shape of the eroding part of the breach at each time step rather than assuming a fixed shape and allowing for uncertainty in the knowledge of soil properties through a probabilistic approach. The model has not been calibrated on a particular data set but has been shown to perform well on a range of data obtained from laboratory investigation, field scale measurements and historic failures.

Whilst the model presented here represents and advance on other available methods, several issues remain for further research including:

- the failure processes of embankments with substantial flow parallel to the crest
- the initiation of piping failures
- fracturing mechanisms of exposed clay cores
- the influence of downstream topography on the failure process
- the sediment transport rates for highly unsteady, non-uniform flows, and
- sediment transport for natural mixtures arising from landslide dams.

REFERENCES

Abril, B. 2001. Hipótesis de un Nuevo Deslizamiento del Cerro Tamuga en la Zone de la Josefina Anzlizada Mediante un Modelo Numérico para Rotura de Presas. *1st International symposium on Masses movement*. Cuenca, Ecuador.

Al-Qaser, G. & Ruff, J. F. 1993. Progressive Failure of an Overtopped Embankment. *Hyd. Eng. Proc. of the 1993 National Conf. on Hyd. Eng. San Francisco*. California, USA.

Bechteler, W., & Kulisch, H. , 1998, Description of Test Case No. 1 on Dam Erosion, *Concerted Action on Dam-Break Modelling Proceedings, Munich Meeting*.

Alcrudo, F., Morris, M. & Fabbri, K. 1998, proceedings of the 2nd CADAM workshop, Munich, Germany: Office for official publication of the European Communities.

Chen, Y. H. & Anderson B. A. 1986. Development of a Methodology for Estimating Embankment Damage Due to Flood overtopping. *US Federal Highway Administration Report* No (FHWA/RD-86/126). Fort Collins, Colorado, USA.

Fäh, R., 1996, Erosion-based dambreak simulation, Proc. Of the Second Int. Conference on Hydroinformatics , Zurich.

Fletcher, B. 1992. Center Hill Fuseplug spillway Caney fork River, Tennessee. Hydraulics Laboratory, US Army Crops of Engineers. Technical Report HL-92-15.

Fread, D. L. 1988. *BREACH: an Erosion Model for Earthen Dam Failures. Model description and User Manual*, US National Weather Service.

Hagerty, D. J. 1991. Piping / Sapping Erosion I. Basic Considerations. *Journal of Hyd. Eng.*, Vol. (117), No. (8).

Hamilton, D. H.& Meehan, R. L. 1971. Ground Rupture In The Baldwin Hills. *Science*, Vol. (172), No. (3981), 333-344.

Hanson, G. J. 2000. Preliminary Results of Earthen Embankment Breach Tests. *ASAE Annual international Meeting*, July, Paper No. (002007).

Hughes, A. K. 1981. *The Erosion Resistance of Compacted Clay Fill in Relation to Embankment Overtopping*. Vol.(I) PhD Thesis, The University of Newcastle Upon Tyne.

Jansen, R. B. 1980. *Dams and Public Safety*. The US Department of the Interior, Water and Power Resources Services (Now the Bureau of Reclamation).

Justin, J. D., Hinds, J. & Creager, W. P. 1945. *Engineering for Dams Volume III: Earth, Rock-Fill, Steel, and Timber Dams*. New York.: John Wiley & Sons INC.

Mohamed M. , 2001, Uncertainties in Dam Failure Modelling using the US NWS BREACH model, *Proc. of the Conf. River Basin Management*, Ed Falconer & Blain, WIT press

Mohamed, M. 2002. *Embankment Breach Formation and Modelling Methods*. PhD. Thesis. (To be Published).

Morris, M. W. 2000. CADAM: A European Concerted Action Project on Dam Break Modelling. *Biennial Conference Proceedings, British Dam Society*. Thomas Telford.

Osman, A. M. 1988. River Bank Stability Analysis. I: Theory. *Journal of Hyd. Eng.*, Vol. (114), No. (2), 134 -150.

Paquier, A., Nogues, P. & Herledan, R. 1998. Model of Piping in order to Compute Dam-break Wave. *CADAM Proc., Munich Meeting*, Germany.

Singh, V. P. 1996. *Dam Breach Modelling Technology*, Dordrecht, Boston, London.: Kluwer Academic.

Visser, P. J. 1998. Breach Growth in Sand-Dikes. *Communication on Hyd. and Geotech. Eng.*, TU Delft, Report no. 98-1.

Wahl, T. L. 1998. *Prediction of Embankment Dam Breach Parameters - Literature Review and Needs Assessment*. U.S. Bureau of Reclamation.

Wurbs, R. A. 1987. Dam-Breach Flood Wave Models. *Journal of Hyd. Eng.*, Vol. (113), No. (1), 29-46.

Yang, C. T. 1979. Unit Stream Power Equation for total load. *Journal of Hydrology*, Vol. (40), 123-138.

Appendix 4 AREBA (Van Damme et al (2012))

Rapid embankment breach modelling

M. van Damme
University of Oxford, United Kingdom

M.W. Morris
HR Wallingford / Samui France

A.G.L. Borthwick
University College Cork, Ireland

M.A.A.M Hassan
HR Wallingford, United Kingdom

This paper describes a rapid embankment breach modelling method that has been developed as part of the FRMRC2 programme to improve current methods for predicting breach outflow volumes and hence to improve the accuracy of flood risk assessments. Application of the method led to the development of a fast model called AREBA which rapidly predicts the breach hydrograph of homogeneous embankment failures whereby discharge through the breach is controlled by the breach dimensions. AREBA's surface erosion failure mode, and piping failure mode have been validated against the IMPACT project data (www.impact-project.net), and benchmarked against HR BREACH model version 4.1. Validation showed that AREBA is able to predict the breach hydrograph within the bounds of uncertainty that originate from uncertainty in the model input parameters.

1 INTRODUCTION

System risk models for assessing flood risk at a catchment or larger scale are used to determine how investment in flood control measures might be optimised. The system risk approach requires a rapid and accurate method of assessing the impact of a possible flood event on a given system of flood protection. One part of that process is the prediction of a flood volume through an embankment breach. The AREBA model, developed as part of the FRMRC2 programme, rapidly predicts a breach hydrograph, final breach width and final breach depth for grass covered embankments that fail due to overflow or piping. Within the overflow failures, surface erosion failures and headcut erosion failures are distinguished. The AREBA model is limited to predicting failures of homogeneous, trapezoidal shaped flood embankments and requires soil parameters, an embankment geometry, and upstream and downstream boundary conditions, as input. A box shaped reservoir with an inflow and outflow is assumed to allow the use of a triangular or trapezoidal hydrograph as the upstream boundary condition for the breach model. The downstream boundary condition consists of a user-defined flood area which for simplicity has been assumed constant over the height of the embankment. AREBA can however be easily adapted to deal with more complicated boundary conditions like stage-area curves or specific river hydrographs. This paper addresses the constitutive equations and validation of the surface erosion and piping failure modes and shortly considers the headcut failure mode. The paper also discusses the accuracy of AREBA with respect to the assumptions made. Section 2 focuses on the simplifications made with respect to the breach physics to obtain a fast model. The test results of AREBA are presented in Section 3 and discussed in Section 4.

2 MODELLING METHODOLOGY

2.1 *Overflow failures*

In the case of overflow failure the overall erosion behaviour is a balance between the rate at which the crest erodes downward due to flow over the crest, and the rate with which the landside slope erodes towards the waterside slope due to the flow over the landside slope. Within overflow failures AREBA distinguishes

between headcut erosion and surface erosion (see figure 1). In the case of headcut erosion, the downward

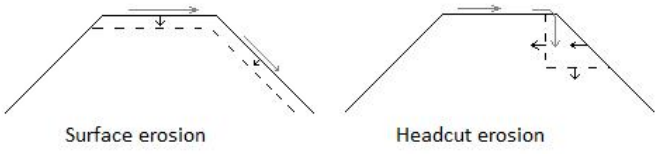

Figure 1: Illustration of surface and headcut erosion

erosion rate of the crest is negligible with respect to the rate at which the landside slope retreats towards the waterside slope (Temple et al., 2005). In the case of surface erosion, both processes play an equally important role. In AREBA, the choice of failure mode is user defined. A broad assumption would be to assume headcut failure for a strong erosion resistant soil such as a strong clay, and surface erosion for a weaker, more erodible soil with higher sand or gravel content. However the point of transition between these two processes as a function of soil erodibility is unclear, hence where uncertain, both failure modes may be considered. As a starting point to calculating the erosion rates, AREBA calculates the discharge over the crest using the following broad crested weir equation to account for the effects of non-hydrostatic pressures over the crest due to flow contraction.

$$Q_b = c_w b h_2 \sqrt{2g(H - h_2)}, \qquad (1)$$

where Q_b is the discharge over the crest in m^3/s, c_w the weir coefficient, $H - h_2$ (m) is the difference in water level in the reservoir H and the waterlevel over the hydraulic control h_2, and b is the flow width which is assumed to be spatially constant (Nortier and De Koning, 1991). The hydraulic control is assumed to be located where the crest meets the waterside slope. The water depth d over the crest is expected to be equal to $2/3H$. h_2 is assumed to be equal to the depth d, for non-drowned weir flow, and equal to the downstream water level for a drowned weir flow. Every time step, the upstream and downstream water levels are updated assuming an equal drop or rise in water level everywhere in the reservoir or flood plain. The weir coefficient c_w is a combination of three coefficients. Before the landside slope has reached the waterside slope $c_w = c_{w1}$ whereby c_{w1} accounts for the effects of vertical flow contraction. When the landside slope reaches the waterside slope, the rate of lowering of the invert level increases rapidly and the effects of horizontal flow contraction, represented by c_{w2} are assumed to become important. c_w is now equal to the product of c_{w1} and c_{w2}. The third weir coefficient, c_{w3}, replaces the first two once the vertical erosion process has stopped and purely represents the effects of the horizontal contraction at the final breach stage.

2.1.1 *Surface erosion*

When surface erosion drives the breach process, the crest lowers while the landside slope retreats towards the waterside slope. The flow along the landside slope accelerates and reaches maximum velocity at the bottom of the landside slope. With the increase in flow velocity, the bed shear stresses, and corresponding erosion rates, also increase. One would expect this to lead to an increasingly steepening slope. However, this appears not to be the case. It has therefore been assumed that either live-bed scour effects, or geotechnical failures prevent the slope from steepening and smooth out differences in the erosion rates along the landside slope. In AREBA this has been represented by assuming that the landside slope gradient remains equal to its initial value. The overall erosion is assumed to be a combination of the downward erosion of the crest and the retreat of the landside slope towards the waterside slope. The breach invert level controls the discharge through the breach. Initially the breach invert level is solely influenced by the downward erosion of the crest. However when the erosion of the landside slope reaches the waterside slope, the rate at which the breach invert level drops increases with increase of the flow velocities. The downward and lateral erosion rates are quadratically dependent on the flow velocity. Once the water level in the breach falls below the crest level the breach grows laterally as the flow undercuts the breach sides and undermines the embankment causing the soil above the undercut sections to become unstable and collapse. Most breach models deal with the breach evolution process by assuming a predefined breach shape which is rectangular, triangular, trapezoidal, or parabolic. The eventual breach geometry then follows from the breach depth, and pre-defined breach shape (Morris et al., 2009). The majority of other models that differentiate between the breach erosion and breach side slope stability processes deal with the latter using a simplified approach. The slope angles on both sides of the breach are usually found to be steeper than the corresponding repose angle angle of the embankment soil. This is because the shear failure strength of soils is related to the amount of water in the pores. Richards (1931) found a relationship between soil pore pressure and moisture content. When a soil dries out, the matric suction increases. As the pore pressure becomes progressively negative with a decrease in moisture content the soil stability is eventually affected. The shear strength of the soil depends on the scale of matric suction. In AREBA, the effects of the matric suction on the side slope instability have been accounted for by assuming vertical breach sides. AREBA requires a user-defined initial breach depth and width. Flow over the intact landside slope is assumed to be bounded by the same rectangular pro-

file as the breach. Hence, the flow is assumed not to spread along the landside slope. The breach width is assumed as spatially constant, and the lateral and downward erosion rates are assumed to depend solely on the mean flow velocities. The lateral erosion rate has been expressed as a function of the downward erosion rate. For simplicity the foundation of the embankment is assumed to be non-erodible. The validity of this assumption is questionable though erosion below the bed level of the reservoir has a negligible effect on the discharge and hence the shape of the breach hydrograph. Once the vertical erosion reaches to the foundation level and stops, the lateral erosion rate is assumed to be a function of the breach bed shear stress. In AREBA, the downward erosion rate of the crest follows from

$$E_d = K\left(\rho u^2 \frac{n^2 g}{d^{\frac{1}{3}}} - \tau_c\right), \tag{2}$$

where E_d is the downward erosion rate in m/s, K is the soil erodibility coefficient in m^3/Ns, ρ is the density of water in kg/m^3, n the Manning coefficient in $s/m^{1/3}$, g the acceleration due to gravity in m/s^2, and d the water depth over the crest in m. The downward crest erosion of the assumed trapezoidal shaped embankment leads the crest width to increase with a rate equal to the downward erosion rate multiplied with factor S which follows from

$$S = \frac{1}{i_{bi}} + \frac{1}{i_{bo}}. \tag{3}$$

where i_{bo} and i_{bi} represent the waterside and landside slope gradients. Recall the assumptions that the landside slope remains straight and equal to its initial value, and that no spreading of the flow occurs along the landside slope. Using these assumptions and the Bélanger equations, the shear stress has been expressed as a function of the distance along the landside slope. With the flow depth assumed equal to the critical depth d_c at the top of the landside slope and approaching the normal depth d_n further down the landside slope, the erosion rate perpendicular to the slope E_s becomes

$$E_s = K\rho\left(\frac{1}{\left(-ae^{\frac{x-x_0}{L}} + a + e^{\frac{x-x_0}{L}}\right)^2}\right) u_c^2 \frac{n^2 g}{d_n^{1/3}} \tag{4}$$

where d_n (m) replaces the value of the hydraulic radius. L is the length in (m) over which a change in the normal depth Δd varies with a factor e, and u_c (m/s), is the velocity corresponding to the critical depth d_c (m) that follows from

$$d_c = \left(\frac{q^2}{g}\right)^{\frac{1}{3}} \tag{5}$$

where q is the width averaged discharge in m^2/s, and g the gravitational constant. a follows from

$$a = \frac{g^{1/3} n^{2/3}}{d^{1/9} i_{bi}^{1/3}} \tag{6}$$

The erosion perpendicular to the landside reduces the crest width, the rate R_c of which follows from

$$R_c = \overline{E_s}\sqrt{\left(\frac{1}{i_{bi}}\right)^2 + 1} \tag{7}$$

where $\overline{E_s}$ is the numerical averaged mean erosion rate along the landside slope, and i_{bi} is the landside slope gradient. From the moment the landside slope reaches the waterside slope the rate at which the hydraulic control lowers is given by

$$E_d = \frac{1}{i_{bi}^{-1} + i_{bo}^{-1}} \overline{E_s}\sqrt{\frac{1}{i_{bi}}^2 + 1} \tag{8}$$

where i_{bo} is the outward slope gradient. The calculation of the total breach widening rate has been adopted from HR BREACH and is assumed to be proportional to 1.4 times the rate at which the crest lowers (Mohamed, 2002). Once the crest height equals the foundation level of the embankment no further vertical erosion is assumed to occur. The breach widening rate now follows from

$$E_w = 1.4K\left(\frac{\rho g n^2 u^2}{h_2^{1/3}} - \tau_c\right) \tag{9}$$

where E_w is the rate of breach, or hydraulic control, widens. The breach stops growing when the shear stresses exerted by the breach flow become lower than the critical shear stress.

2.1.2 *Headcut erosion*

Headcut erosion is often taken to be the driving breach formation process for an embankment composed of cohesive soil. Irregularities along the landside slope initiate a cascade formation that defines the headcut erosion process. The cohesive properties of the soil prevent geotechnical failures from occurring and instead allow small cascades to initiate and grow in step size. Where the cascade flow impacts on the embankment surface the flow disperses and undercuts the embankment. The local erosion rate depends upon the energy with which the flow hits the soil and therefore on the height of the cascades. At the point when erosion causes the cascades to reach the waterside slope, the flow rate increases rapidly due to the lowering of the crest (i.e. hydraulic control) and an increase in the horizontal contraction of the flow. Whilst the increase in flow leads to an increase in the energy with which

the flow hits the soil, the reduction in crest height also reduces the height over which the flow drops before hitting the soil and therefore reduces the flow energy. Zhu et al. (2008) mention the growth of headcuts due to an increase in flow velocity. From field observations, Temple et al. (2005) assumed that the downward erosion of the crest is negligible during the retreat of the headcut through the soil. In AREBA, headcut failure is modelled using the method described by Temple et al. (2005). This method is based on observations of large scale breach experiments of cohesive clay embankments. The following assumptions made by Temple et al. (2005) regarding the overall erosion process have been adopted for the development of AREBA.

1. The crest level does not lower before the headcut has reached the upstream slope.

2. The cross sectional breach shape is rectangular.

3. The foundation of the embankment is not erodible

4. Headcut initiates at the top of the landside slope.

The first assumption is in conflict with the physical process as described by Zhu et al. (2008) who mention that headcuts grow due to an increasing flow velocity caused by downward erosion of the crest. However as mentioned above, Temple et al. (2005) assumed (based on field observations) that the downward erosion of the crest is negligible during the retreat of the headcut through the soil. This can be explained by the positive effect of cohesion on the critical erosion shear stress of the soil. It should be noted that the first assumption may limit the validity range of the model. For example, just below the threshold between headcut and surface erosion the critical shear stress may be relatively low. Hence the assumption of no vertical crest erosion may cause an error in the predicted hydrograph. The second and third assumption have been discussed under the header of surface erosion. With regard to the fourth assumption, the relatively sharp transition in slope angle from the horizontal crest to the landside slope would explain a separation of the flow at this stage that initiates the headcut erosion process. However the irregularities, which are often present along the landside slope could initiate the headcut failure process anywhere along the landside slope and the sharp transition at the toe of the slope often provides a focal point for erosion. The constitutive equations for the modelling of the headcut erosion process can be found in the paper by Temple et al. (2005) and will not be further addressed here.

2.2 *Piping*

Piping is defined here as the internal erosion of embankment material by seepage flow. Sellmeijer (1988) reports that piping may stop once some erosion has taken place due to the larger permeability of the embankment where the soil has eroded, compared with the permeability of the surrounding soil. The increase in permeability reduces the hydraulic gradient that initiates the piping process. Piping failure is modelled using the method proposed by Mohamed (2002) and applied in the HR BREACH model whereby an initial open pipe connection has been assumed between both sides of the embankment. The erosion along the perimeter of the pipe causes the pipe diameter to increase to the point that the soil above the pipe fails and slumps downs into the pipe. Depending upon the flow velocities through the pipe and the volume of soil slumping down, the slumped material could either be transported almost instantaneously or could cause the pipe flow to stop and the embankment crest to lower after which an overflow failure could initiate. In AREBA the latter of the two is assumed to occur. Soil properties like cohesion, matric suction and internal friction angle determine when the material above the pipe fails. Positive arching of the soil above the pipe, whereby part of the load above the pipe is transferred to other soil prisms, reduces the load on the pipe. The effects of soil parameters are difficult to predict using rapid methods. For that reason AREBA assumes that soil cohesion and arching solely affect the instant at which slumping occurs. It should be noted that though this is quite a coarse assumption, its effects are expected to lie within the bounds of uncertainly associated with the soil parameters themselves since the properties of soils in embankments can be quite uncertain. The pipe is assumed to grow at an equal rate along its perimeter and to maintain its circular cross-sectional shape. The pipe cannot grow below the foundation level of the embankment or above the water level upstream, in which the shape takes the form of a segment. The soil immediately above the pipe is assumed to fail once its weight exceeds the stabilising forces along the sides of the soil mass. The steady pipe flow rate is calculated using Bernouilli's energy equation (Nortier and De Koning, 1991)

$$Q_b = A\frac{2g\Delta H}{h_f} \tag{10}$$

where A is the wet cross sectional area of the pipe in m^2, ΔH is the head difference over the pipe in m, and h_f is a head loss factor representing contraction and friction losses. In AREBA the head loss factor is given by

$$h_f = 1.05 + \frac{fL}{D_p} \tag{11}$$

where L is the pipe length in m, and D_p is the pipe diameter in m. f is a friction coefficient determined from

$$f = 0.2165 \left(\frac{D_{50}}{D_p} \right)^{1/6} \tag{12}$$

where D_{50} , is the grain diameter in m exceeded by 50% of the soil mass. Due to the long straight pipe geometry, the energy losses are dominated by the wall friction and hence the losses due to outflow from the pipe are neglected. The cross sectional area of the pipe A is calculated assuming a circular shaped pipe that does not grow beyond the embankment's foundation level. Once the pipe bottom reaches the embankment's foundation, the pipe shape becomes that of a truncated circle. The surface area of the pipe then follows from

$$A = \frac{1}{4}\pi D_p^2 - \frac{\alpha}{4} D_p^2 + h_p^2 tan\alpha \tag{13}$$

in which

$$\alpha = \frac{arccos\left(2h_p\right)}{D_p} \tag{14}$$

where h_p is the distance between the centreline of the pipe and the foundation level of the embankment. The pipe is assumed to grow uniformly along its length according to

$$E = 2K\left(\rho h R i_w - \tau_c\right) \tag{15}$$

where R is the hydraulic radius of the pipe, which for a submerged circular pipe is equal to $D_p/4$, with D_p representing the pipe diameter. i_w is the gradient in water level over the pipe and follows from

$$i_w = f \frac{u^2}{2gD_p} \tag{16}$$

In AREBA the assumption has been adopted from Mohamed (2002) that the soil mass, above the pipe fails when the weight of the soil above the pipe exceeds the friction at its sides. Mohamed gives the following relationship for the factor of safety (FOS)

$$FOS = \frac{cA_s}{W} \tag{17}$$

where c is the cohesion of the soil in N/m^2, A_s is the cross-sectional area of the embankment in m^2 above the centreline of the pipe. For simplicity the weight of the soil W in N is purely determined for the soil above the top of the pipe from.

$$W = f_a \rho g D_p A_s \tag{18}$$

where A_s is the surface area of the sides of the soil wedge calculated from the top of the pipe upwards, Mohamed gives the following relationship for f_a which is an empirically based reduction factor representing the arching of the soil.

$$f_a = 9.860 \times 10^{-5} r^2 - 2.918 \times 10^{-4} r + 3.757 \times 10^{-4} \tag{19}$$

where r represents the ratio of the distance between the top of the pipe and the crest, and the pipe diameter. The ratio r has a minimum value of 0.1 and a maximum value of 1.6. For $FOS < 1$, the pipe collapses, and the embankment crest is assumed to lower a distance equal to the height needed to fill the volume of the pipe. From this time onwards the embankment's failure mechanism transfers to that of a surface erosion process.

3 VERIFICATION AND VALIDATION

The results from AREBA presented and discussed in this Section were obtained with model run speeds of less than one second per run. This makes AREBA suitable for use within system risk models where many hundreds or thousands of simulations may be necessary to calculate the overall system flood risk. As a benchmark for the modelling accuracy, AREBA has been tested against the HR BREACH model, which, together with the SIMBA model, was selected by the Dam Safety Interest Group (DSIG) breach modelling project as models with the potential for further development for industry use (Wahl, 2007). HR BREACH version 4.1 contains the headcut failure mode from SIMBA, and so is used for benchmarking.

Validation of HR BREACH against different datasets led to the incorporation of an empirical coefficient of 1.6 for the downward erosion rate. This factor was based on model performance for a range of material and structure types. To enable proper comparison between AREBA and HR BREACH the same coefficient has been adopted in AREBA. Table 1 lists the input parameters that were kept constant for all verification runs with HR BREACH, and Table 2 gives the input parameters that were varied. h_{crest} refers to the crest height, and $Slope$ refers to both the landside as the waterside slope gradient. A box shaped reservoir with continuous constant inflow was chosen for the upstream boundary condition. An infinitely large floodplain was chosen for the downstream boundary condition to facilitate a clear comparison between the two models. In AREBA's surface erosion mode the landside slope gradient is assumed to remain equal to its initial value when the landside slope retreats towards the waterside slope. In HR BREACH unrealistic landside slope gradients are prevented from occurring by averaging the erosion rates at the top of the landside slope and downstream side of the crest, and averaging the erosion rate at the toe of the landside slope and the foundation level. Figures 2, and 3 show respectively the results of Run 1 and Run 2. whereby the steepness of the slope was

Table 1: Fixed input parameters HR BREACH validation runs

Parameter	Value	Unit
Initial water level reservoir	$h_{crest} - 0.3$ *	m
Crest width	6	m
Discharge into reservoir	1	m^3/s
Surface area reservoir	30000	m^2
Initial breach depth	0.25	m
Crest length	200	m
Soil cohesion	1×10^{-5}	kN/m^2
Soil tension strength	1×10^{-5}	kN/m^2
Friction angle	30	degrees
Porosity	0.2	-
Dry unit weight	16.8	kN/m^3
Critical shear stress	1×10^{-5}	N/m^2
Manning coefficient	0.035	s/m^3
Weir coefficient	1	-

* h_{crest} = crest height

Table 2: Variable input parameters HR BREACH validation runs

Run no.	Erodibility coefficient (m^3/Ns)	crest height (m)	Slope m/m
1	5×10^{-6}	12	1/3
2	5×10^{-6}	6	1/3
3	5×10^{-6}	9	1/6
4	5×10^{-6}	9	1/2

kept constant. Differences in approaches to limit the

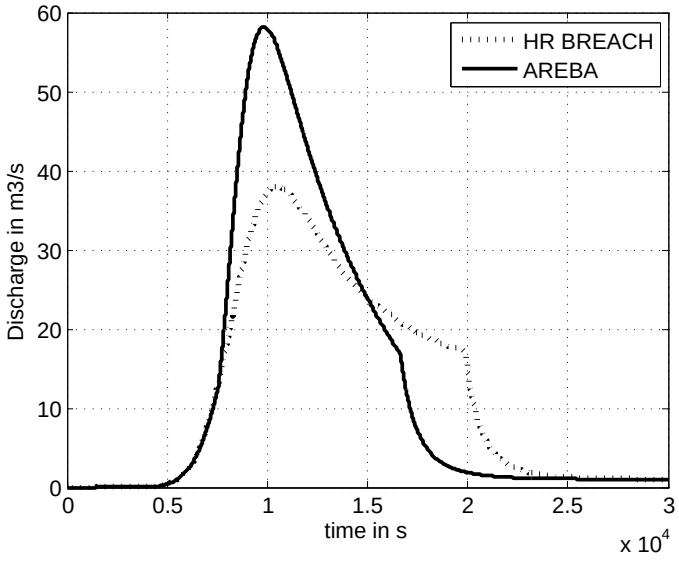

Figure 2: Hydrograph output HR BREACH and AREBA: Run 1

steepness of the landside slope lead to differences in model outcomes, which are evident by comparing the results from Runs 3 and 4 which only differ in the steepness of the landside slope (see Figures 4 and 5).

To get a better estimate of the impact of the assumptions, AREBA has been validated against the EU IMPACT project experiments for the surface erosion failure and piping failure (IMPACT, 2005).

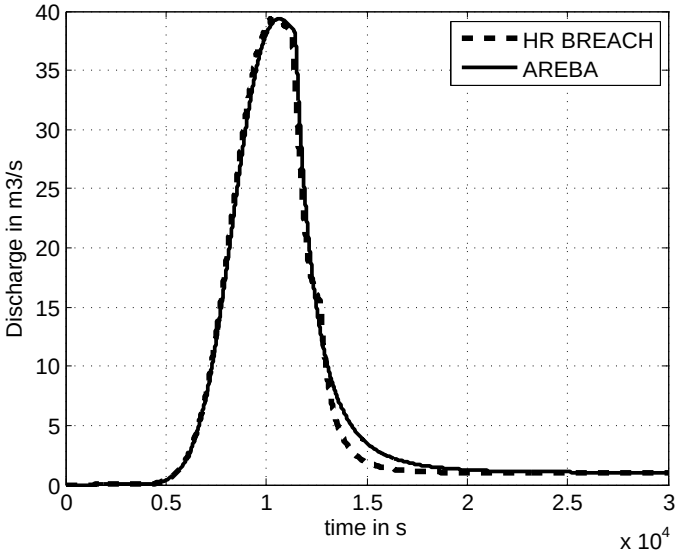

Figure 3: Hydrograph output HR BREACH and AREBA: Run 2

3.1 *Validation*

For proper validation against the EU IMPACT experiments AREBA was adapted to use a hydrograph, and stage-area curve as boundary conditions. Hassan and Morris studied the accuracy of the input and output values of the IMPACT project experiments (Hassan and Morris, 2009). Besides being uncertain about the exact values to use as input, some of the model input parameters were undefined and needed to be estimated. The problem with the uncertainty of the input parameters is that more unknowns exist than there are validation tests available. Several combinations of input parameters can therefore be found that all give a near perfect match with the validation data. This does not however mean that the model represents the physical processes correctly. Therefore instead of calibrating the unknown model parameters to fit the experimental data, upper and lower limits have been estimated for the input parameters based on the data, reports, and empirical relationships. These limits formed the boundaries of the uniform distribution from which input values were drawn. By running AREBA 500 times for different combinations of input parameters an envelop was obtained between which the experimental results are expected to lie. After having obtained the outer envelop, the same process was repeated for half the range of input values while maintaining the same mean value in order to study the impact on the bounds of not knowing the input values. Table 3 shows the upper and lower limits and the mean values used for validation of AREBA's surface erosion mode, where n is the Manning coefficient, τ_c is the critical shear stress, K is the erodibility of the embankment soil, c_{w1} and c_{w2} are respectively the first

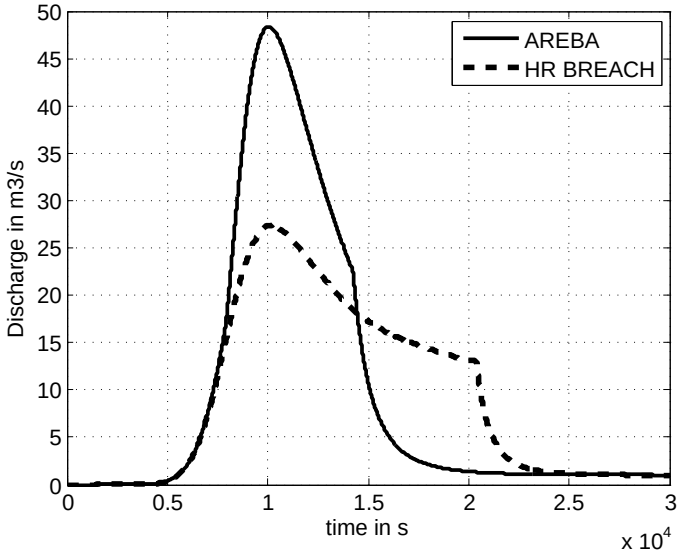

Figure 4: Hydrograph output HR BREACH and AREBA: Run 3

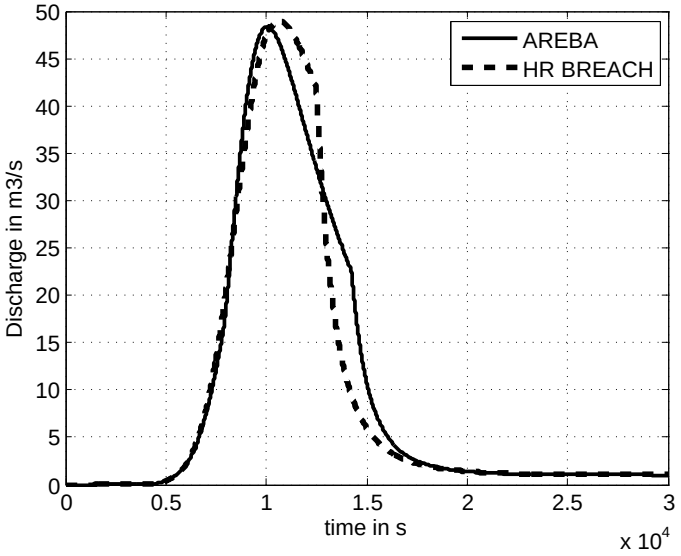

Figure 5: Hydrograph output HR BREACH and AREBA: Run 4

Table 3: Range of input parameters AREBA for IMPACT surface erosion validation

Symbol	Lower bound	Mean	Upper bound
n	0.025	0.035	0.045
τ_c	1.8	4.2	7.1
K	1.8×10^{-7}	9×10^{-6}	1.8×10^{-5}
c_{w1}	0.9	1	1.1
c_{w2}	1	1.2	1.4
S_w	$1/1.7$	$1/1.8$	$1/1.9$
S_l	$1/1.6$	$1/1.65$	$1/1.7$
h_{br}	0.1	0.105	0.12

and second discharge coefficient, S_w and S_l are respectively the waterside and landside slope gradient, and h_{br} the initial breach depth. The third weir coefficient c_{w3} was set to be 1. Figure 6 displays the maximum and minimum values of the discharge found per run. Figure 7 shows the breach width development.

The term large range mentioned in the figures represents the results found by applying the Lower and Upper bound as bounds for the uniform distribution. The term small range refers to the outcome obtained when using the average of the mean and the lower bound, and the average of the mean and upper bound as respectively the lower and upper bound values. The final breach width measured during the IMPACT experiment was $10m$ which falls between the upper envelopes given by AREBA for the large range and the small range. The lower envelopes found with AREBA coincide with the time-axes in Figures 6 and 7 and therefore have not been plotted.

The technical report describing the IMPACT piping experiment mentions a rapid pipe failure after approximately 20 minutes. The moment of opening the pipe was estimated from the field data and was expected to coincide with a sudden drop in water level (see Figure 8). The exact moment at which the pipe was opened, relative to the start time of the given inflow hydrograph, is however unknown. Before the drop in water level, the reservoir was filled slowly. During the experiment it was attempted to keep the upstream water level constant irrespective of the outflow. The ability to control the upstream water level by accounting for the effects of the outflow from the pipe had strongly been underestimated and caused for a rapid increase of inflow into the reservoir. Validation of AREBA against the IMPACT field data was complicated due to the unknown opening time of the pipe relative to the given inflow hydrograph, the unknown discharge into the reservoir before opening the pipe, and the sudden increase in discharge into the reservoir just after opening the pipe. Treating the relative opening time of the pipe as a statistical variable in the analysis resulted in a very large uncertainty bound since the sudden increase in discharge just after opening the pipe resulted in widely varying outcomes for different initiation times. A similar problem was encountered with specifying a wide range for the erodibility. The range for the erodibility was therefore limited. The inflow before the pipe was opened, and the time at which the pipe opened were obtained by fitting the data slightly to the found outcome and were respectively estimated at $0.6m^3/s$ and $13450s$. The range of each of the input parameters is given in Table 4. The model outcomes are presented by Figures 9 and 8. Due to the small statistical range of the variables the piping case was only run for the wide range in data.

4 DISCUSSION

The accuracy with which AREBA predicts a flood hydrograph is directly related to how well the underlying

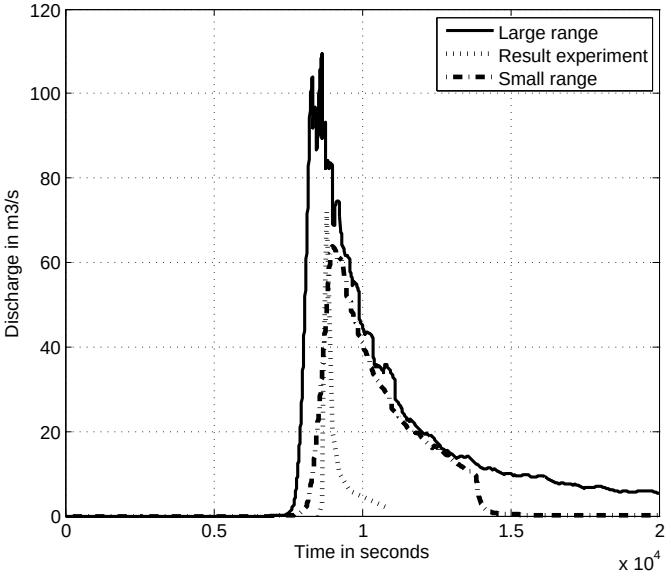

Figure 6: Maximum and minimum discharge (per time step) predicted by AREBA for 500 runs, compared against the IMPACT field data

Table 4: Range of input parameters AREBA for IMPACT piping validation case

Symbol	Lower bound	Mean	Upper bound
n	0.025	0.035	0.045
c	18	20	22
ρ	2000	2100	2200
τ_c	0	5	10
K	$9e-6$	$1e-5$	$1.1e-5$
c_{w1}	0.9	1	1.1
c_{w2}	1	1.2	1.4
S_w	$1/1.3$	$1/1.35$	$1/1.4$
S_l	$1/1.3$	$1/1.35$	$1/1.4$
h_p	0.29	0.3	0.31
h_{crest}	4.3	4.4	4.5
W_{crest}*	2.8	2.9	3

* W_{crest} = crest width

assumptions represent the physics of the breach formation. The impact of the error made assuming one-dimensional flow behaviour, for example, is quadratically amplified when calculating the erosion rate due to the quadratic dependence of the shear stress on the mean flow velocity. The assumptions that influence the accuracy of the hydrograph prediction are

- Negligible flow accelerations perpendicular to the main flow direction
- Horizontal flow contraction commences only when the landside slope retreat has reached the waterside slope
- Flow velocities in the reservoir are negligible
- The breach width is spatially constant.

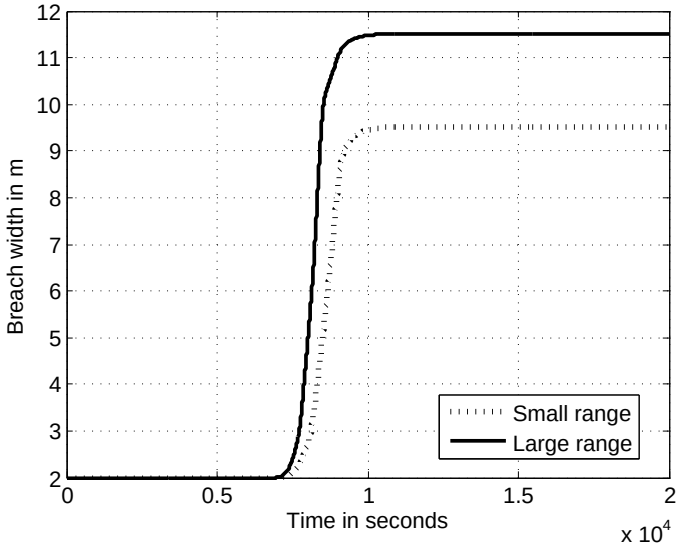

Figure 7: Maximum and minimum breach width (per time step) predicted by AREBA for 500 runs compared against the IMPACT field data

- The flow depth on top of the landside slope is equal to the critical depth
- The bed roughness is spatially constant
- The critical shear stress is spatially constant

These assumptions originate from the objective to have a high computational speed but limit the ability of AREBA to simulate the physics accurately. The physics behind breaching is in itself still relatively inadequatly understood. The question as to how to change the assumptions for a more accurate description of the breach formation, while maintaining a fast model, is difficult to answer. For example, the Manning coefficient is known to vary along the breach, but it is unknown where and by how much it varies, and is consequently assumed as constant.

Verification of AREBA against HR BREACH indicated a very close agreement between the models for Run 2 (Figure 3). The input of Run 2 differs from that of Run 1 (Figure (2) in the ratio of the crest height over the crest width. In AREBA, the crest is assumed to erode downwards while the landside slope retreats towards the waterside slope. For relatively high ratios of the crest width to the crest height, or relatively high values for the erodibility, the crest will already have eroded down to the foundation level before the retreat of the landside slope reaches the waterside slope. Figure 5 shows a nice fit is obtained between both model outcomes for a landside slope of 1:2. To the contrary Figure 4 shows less agreement for a landside slope of 1:6. It should be noted that the model outcomes of AREBA are identical for the two landside slope gradients because the downward crest erosion has already reached the embankment's foundation before the landside slope retreat

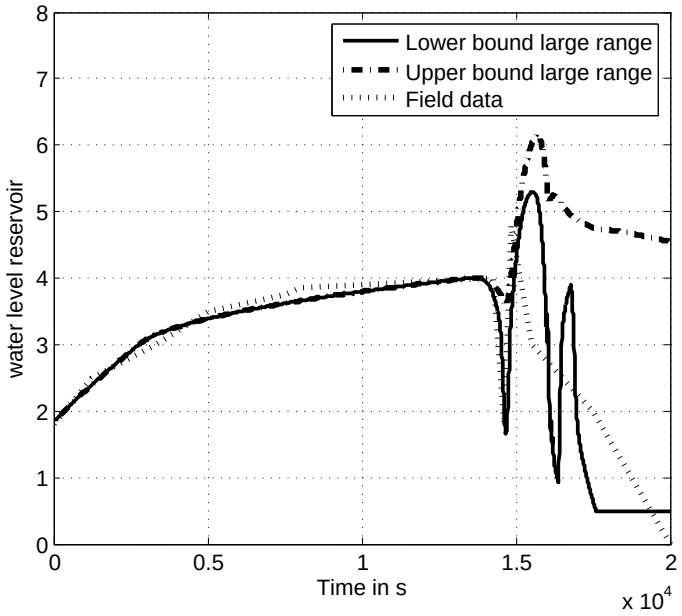

Figure 8: Maximum and minimum breach width (per time step) predicted by AREBA for 500 runs compared against the IMPACT field data

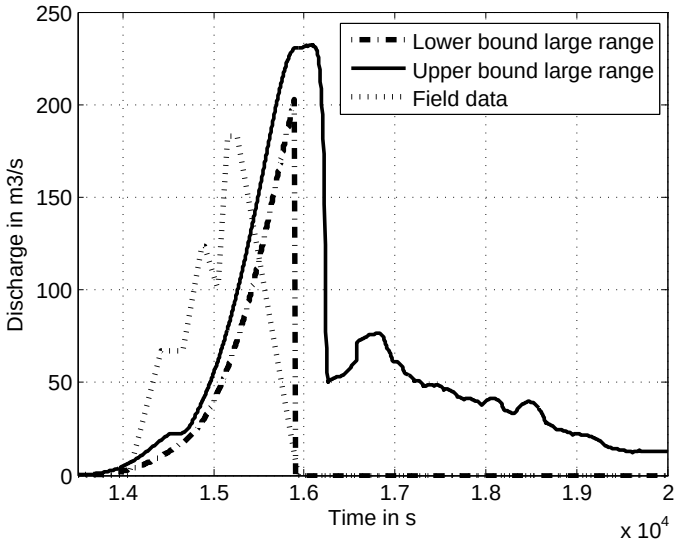

Figure 9: Maximum and minimum discharge (per time step) predicted by AREBA for 500 runs, compared against the IMPACT field data

has reached the waterside slope. Despite the fact that AREBA and HR BREACH disagree in the value for the peak discharge, they do agree on the overall shape of the hydrograph and the time of the peak discharge. Both assumptions for the prevention of unrealistic steep slopes are empirical. Without modelling all the physics involved it is not possible to state which assumption has the greater effect on the accuracy to which the physical process is represented.

To validate AREBA, the influence of the uncertainties in the input parameters was assumed to outweigh the effects of simplifying the physics in the constitutive equations. AREBA was validated against field data using a range of input parameters. Figures 6 and 7 show that for the surface erosion case, the hydrograph and final breach widths obtained from field measurements lay within the envelopes found by AREBA for the large range, and close to envelopes found for the small range. Since the model is volume conservative the model is capable of reproducing the outcome of the field data. However, it is unknown if the close match is only found by using values for the Manning coefficient and erodibility coefficient that do not represent the actual situation, and hence it is unknown to what accuracy AREBA is able to simulate the physical breach processes. Similar to other breach models the low quality of the limited amount of datasets available makes it difficult to make a statement regarding the capability of the AREBA model to simulate the physical processes of an embankment failure correctly.

The nature of the EU IMPACT piping experiment did not permit validation based on a large range of input parameters. The sudden increase in discharge into the reservoir combined with an unknown time at which the pipe was opened resulted in model conditions that caused the model to be highly sensitive for the input parameters. For example, an under-predicted Manning coefficient or erosion coefficient leads to a smaller growth in pipe diameter and a smaller outflow. A sudden increase in inflow in the reservoir then results in unrealistic high water levels in the reservoir, which at the instant the pipe would fail would cause for unrealistic outcomes when the model changes to surface erosion mode. Both Figures 9 and 8 show a second spike in the model outcomes which results from the assumption that when the pipe fails the body of soil above the pipe fills up the volume of the pipe. During the experiment the soil that slumped in the pipe was washed away instantly. However since the instantaneous removal of slumped material is case dependent, the description of the physics by the model has not been changed.

As shown by the dataset used for validation the soil parameters are often poorly known or unknown. In some cases even the type of construction material is unknown. The contribution of modelling the influence of soil parameters on the breach process of an embankment is therefore variable. Even if the soil parameters were known, it is still poorly understood as to how these interact with the hydrological aspects. The assumptions used in AREBA are crude and do affect the ability of the model to simulate a breach correctly though the limited amount of input data available make the use of highly sophisticated models over the simplified ones questionable.

5 CONCLUSIONS

AREBA is able to rapidly predict a flood hydrograph, breach width, and breach depth development for surface, headcut, and piping failures for trapezoidal shaped homogeneous embankments. The speed at which the AREBA model runs (less than 1s) makes it suitable for an application in system risk models. The time of occurrence of the peak discharge corresponds closely with those found by HR BREACH. Any difference in the prediction of the peak discharge was found to originate from assumptions with respect to preventing unrealistic values for the steepness of the landside slope. However, in order to better assess the accuracy, and validity of the underlying assumptions of AREBA and other breach models, more accurate, large scale experiments are required. At this point it is possible to state, based on the validation of AREBA against the IMPACT experiments that AREBA is able to reproduce the shape of the breach hydrograph for input values that lie within the range of uncertainty. In comparison to the use of existing simple breach assumptions within system risk models, or even the use of regression equations that predict the potential peak discharge from a breach, the AREBA model should provide a more accurate answer and in doing so, also provides an estimate of the breach flood hydrograph shape.

REFERENCES

Hassan, M. and M. Morris (2009, Feb). Impact project field tests data analysis. Technical Report T04-08-04, Floodsite.

IMPACT (2005). Investigation of extreme flood processes & uncertainty (impact), breach formation (wp2), technical report: Section 4. Technical report, HR-Wallingford.

Mohamed, M. A. A. (2002). *Embankment Breach Formation an Modelling Methods*. Ph. D. thesis, Open University, UK.

Morris, M., M. Hassan, A. Kortenhaus, and P. Visser (2009, Mar). Breaching processes, a state of the art review. Technical Report T06-06-03, HR-Wallingford.

Nortier, I. W. and P. De Koning (1991). *Toegepaste Vloeistofmechanics, hydraulica voor waterbouwkundigen, (Dutch)*. Stam Techniek.

Richards, L. A. (1931). Capillary conduction of liquids through porous mediums. *Journal of Physics 1*, 318–333.

Sellmeijer, J. B. (1988, Oct). *On the mechanism of piping under impervious structures*. Ph. D. thesis, Delft University of Technology.

Temple, D. M., G. J. Hanson, M. L. Nielsen, and K. R. Cook (2005, Jun). Simplified breach analysis model for homogeneous embankments: part 1, background and model components. In *Technologies to Enhance Dam Safety and the Environment*, pp. 151–161.

Wahl, T. L. (2007). Laboratory investigation of embankment dam erosion and breach processes.

Zhu, Y.-H., P. J. Visser, and J. K. Vrijling (2008). Soil headcut erosion: process and mathematical modeling. In *Sediment and Ecohydraulics: INTERCOH 2005*, pp. 125–137.

Appendix 5 Multivariate extreme and flood risk (Wyncoll and Gouldby (2012))

Integrating a multivariate extreme value method within a system flood risk analysis model

Wyncoll D[1]
Gouldby B[1]

1 Flood Management Group, HR Wallingford

Corresponding author: Dr. David Wyncoll
Email: d.wyncoll@hrwallingford.com
Tel: 01491 822425
HR Wallingford
Howbery Park
Wallingford
Oxfordshire
OX10 8BA

2nd author: Mr Ben Gouldby
b.gouldby@hrwallingford.com

Abstract

Effective management of flooding requires models that are capable of quantifying flood risk. Quantification of flood risk involves both the quantification of probabilities of flooding and the associated consequences. Modern flood risk models account for the probabilities of extreme hydraulic loading events and also include a probabilistic representation of the performance of flood defence infrastructure and its associated reliability. The spatial and temporal variability of flood events makes probabilistic representation of the hydraulic loading conditions on the flood defences complex. In the system method used widely within England and Wales, simplifying assumptions relating to the spatial dependence of flood events are made. Recent research has shown the benefits of using improved multivariate extreme value methods to define the hydraulic loading conditions for flood risk assessment. This paper describes the development of a new modelling system that improves the systems based risk analysis model currently applied in practice, through the incorporation of a multivariate extreme value model. The new system has been presented on a case study site in the North West of England.

Keywords
Flood risk analysis, Spatial dependence, Multivariate extremes, Systems modelling, Flood defence failure, Reliability analysis

Introduction

Flooding is a global problem with extreme flood events having major consequences recorded at different locations relatively frequently. It has long been recognised that risk management approaches offer a number of benefits over more traditional deterministic design event based approaches, USACE (1996), Sayers *et al.* (2002), for example. A primary component of successful flood risk management is the ability to quantify flood risk and to simulate the risk reduction that results from introducing different mitigation measures.

Flood risk is generally regarded as a function of probability and consequence and quantifying flood risk can be complex. Extreme flood events at any particular spatial location occur, by definition, rarely and there is limited data with which to verify models. The temporal variability of flooding can also be complex. Some flash flood events last for a short period of time, a day, for example, whilst others can last for many weeks. Flooding can be localised in terms of its impact or can effect large spatial scales. Within the UK for example, the flooding of the village of Boscastle (August, 2004), that took place over a day, Roca-Collel and Davison (2010), can be contrasted with the summer floods of 2007, Marsh and Hannaford (2007), that lasted for a period of six weeks and affected most of England and parts of Wales. Flooding can arise from different sources; pluvial, fluvial, waves and surges for example. These different sources can often interact to exacerbate the impact of the flood event.

As risk is a function of probability, establishing the joint probability of different combinations of flood inducing events arising has been the subject of much research. Examples include extreme, fluvial flows at confluences, estuarine water levels, astronomical tides and metrological surges, waves and sea levels, see for example, Tawn and Vassie (1989), Acreman (1994), Bruun and Tawn (1998), Hawkes *et al.* (2002), Cai *et al.* (2008), Wahl *et al.* (2012). These approaches have, in the past, tended to have been restricted in terms of the number of variables that have been considered and the spatial extents that are covered. The reasons for this primarily relate to constraints placed by the statistical models that have been used. In particular, traditional multivariate extreme value statistical models have constraints relating to the handling of the dependence structure. These constraints make extensions to large spatial scales, where the degree of dependence between extremes of a given variable can cover a wide range, impractical to implement. Recent developments in multivariate extreme value methods, Heffernan and Tawn (2004), have however, removed some of these constraints and opened opportunities for improving flood risk analysis methods.

Risk analysis models of flooding systems that incorporate the likelihood of flood defence failure are now recognised as an effective means of supporting the flood risk management process. These models have been applied at national and regional scales for supporting decisions relating to long term climate change adaptation, strategic planning and asset management prioritisation purposes, see USACE (1996),Hall *et al.* (2006) , Evans *et al.* (2006), Apel *et al.* (2004), Gouldby *et al.* (2008b) and Vorogushyn *et al.* (2010), Woodward *et al.* (2011), Woodward *et al.* (2012), for example. Within England and Wales, the Environment Agency has been utilising these flood defence systems based models for around a decade, Environment Agency

(2003), Hall *et al.* (2003), Gouldby *et al.* (2008a). The latter methodology has now been implemented within the Environment Agency´s flood risk modelling decision support system (MDSF2), Environment Agency (2011a), where it is being routinely applied for systems based flood risk analysis. One of the limitations of this current method however, relates to the handling of dependencies of flood events over large spatial scales. To address this problem the Environment Agency commissioned a research project to further explore aspects of spatial dependence in relation to flood risk analysis. More specifically, the application of the multivariate extreme value statistical model of Heffernan and Tawn (2004) was explored in the context of flood risk analysis. The findings of this research project have been published in a series of reports, Environment Agency (2011b), Environment Agency (2011c), Environment Agency (2011d), and also by Lamb *et al.* (2010).

Lamb *et al.* (2010) and Environment Agency (2011b) note the potential for integrating the statistical method of Heffernan and Tawn (2004) with the system-based risk model used by the Environment Agency, and provide a thorough discussion of the issues. This paper forms the natural extension of this discussion. The Heffernan and Tawn (2004), multivariate extreme value method, refined by Keef *et al.* (2009), has been used to generate boundary conditions for the system risk model, described by Gouldby *et al.* (2008a). The new modelling system has been applied on a case study in the North West of England, with the results described below.

Background to system flood risk analysis

System risk models that are currently applied in practice typically define risk through consideration of the aleatory uncertainty associated with the random nature of extreme flood events and the epistemic uncertainty associated with the potential for flood defence infrastructure to suffer failure. Whilst there are many other sources of uncertainty, Hall and Solomatine (2008), approaches to quantify these, Merz and Thieken (2009b), Gouldby *et al.* (2010), for example, are not commonly applied in practice, primarily due to the computational burden associated with the implementation of the methods. The primary components of the risk models are: hydraulic loads, described by extreme value distributions, flood defence infrastructure (dykes, levees or embankments for example), defined by fragility curves, flood inundation simulation representation and functions that relate the simulated floods to consequences. The flood defences are typically defined as discrete lengths with a specific fragility curve prescribed for each length. The models that are applied in practice within England and Wales assume the performance of each of the defence lengths is independent and hence the risk, expressed in terms of the Expected Annual Damage (EAD), is given by:

$$EAD = \int \sum_{i=1}^{2^n} P(\boldsymbol{d}_i | \boldsymbol{X}) f_{\boldsymbol{X}}(\boldsymbol{X}) g(\boldsymbol{d}_i, \boldsymbol{X}) d\boldsymbol{X} \quad (1)$$

where n is the number of defence lengths, $f_{\boldsymbol{X}}$ is the joint density of hydraulic loads $\boldsymbol{X}$ over the defence lengths, $\boldsymbol{d}_i$ is the defence system state (a vector of length n that comprises a representation of the state as failed or undamaged of each defence in the system) and g is a function that relates the defence system state and hydraulic loads to the economic damage to property. The sum in i covers all 2^n possible configurations of the defence system state $\boldsymbol{d}_i$.

The derivation of the joint density of the hydraulic loads can be complex to define over large spatial areas and a simplifying assumption is therefore made in current practice. The hydraulic loading conditions are assumed to be fully dependent in terms of recurrence interval (return period) within a flood area (i.e. the multivariate variable of the hydraulic loading is reduced to a univariate distribution). This enables the integration of the density of the hydraulic loads over the consequence function to be undertaken in terms of a single likelihood of hydraulic load using a simple integration procedure:

$$EAD \approx \sum_{j=1}^{q} P\left(\frac{x_{j-1}+x_j}{2} < X \leq \frac{x_j+x_{j+1}}{2}\right)\overline{g}(x_j) \qquad (2)$$

where $\overline{g}(x_j)$ is the expected economic damage for the hydraulic load x_j and q is the total number of loading levels (return periods) used in the analysis. Flood areas are typically less than 10 km^2 and Eqn. 2 is evaluated independently for each flood area. To assess the risk at spatial scales larger than a single flood area, the results for each flood area are aggregated. It is of note however, that important information relating to the nature of flood events can be lost when considering only the EAD. This approach does not, for example, enable assessment of the probability and consequences associated with a single flood event that occurs at spatial scales larger than a flood area, when there is partial dependence between the hydraulic loading conditions. Analysis of single event consequences at large spatial scales (ie bigger than a single flood area) can be of interest and importance for the insurance industry, where single event loss damages are of interest and emergency planners, for example, where large-scale evacuation plans are developed. Further discussion on these issues is provided by Environment Agency (2011b)

Within the analysis described here, the simplifying assumption of full dependence within and between flood areas is replaced with a multivariate extreme value model. This model is described in more detail below. The use of the multivariate approach enables information on the probability and consequences associated with single events to be captured more accurately, whilst also considering the likelihood of the flood defences failing.

Description of the modelling method

Overview

The objective of the new modelling system is to improve the handling of the spatial dependence of flood events within the system risk analysis method and hence to solve Eqn. 1 with an explicit consideration of the dependence, in the extremes, of the hydraulic loading conditions (the vector $\boldsymbol{X}$) at different spatial locations. A flow diagram showing an overview of the new modelling system is shown in Figure 1. Figure 2 shows a conceptual diagram of the primary spatial components within the modelling system. Each stage of the new modelling system is described in more detail below.

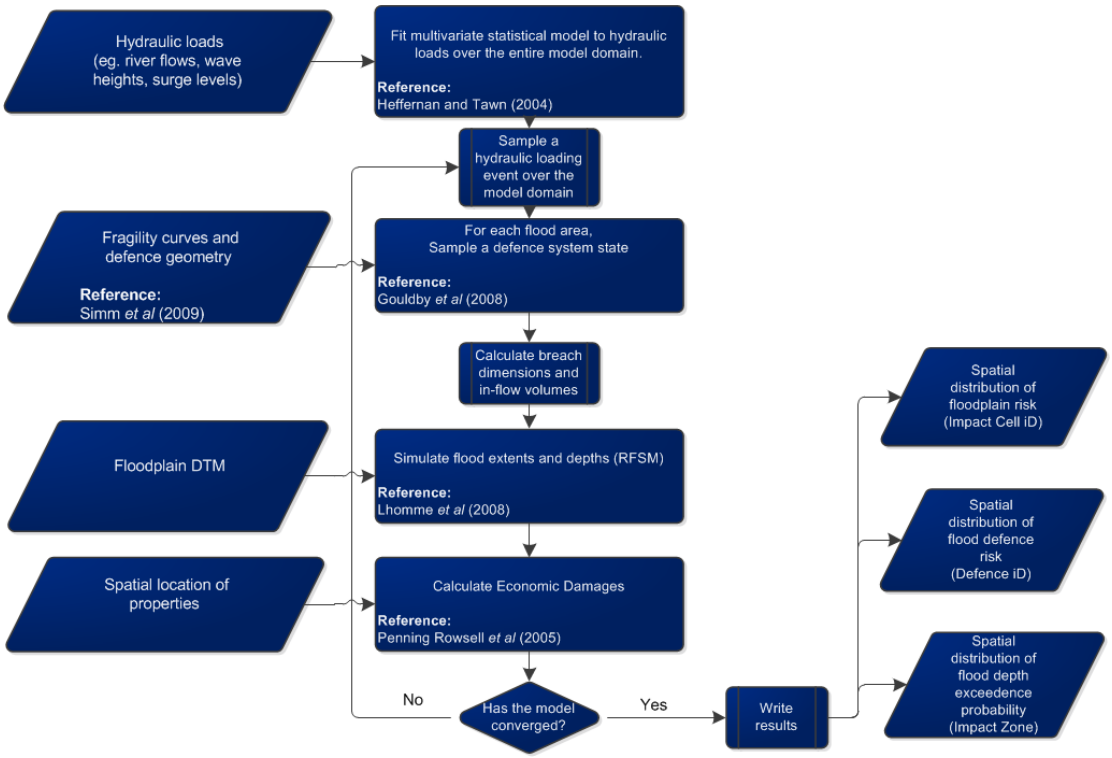

Figure 1

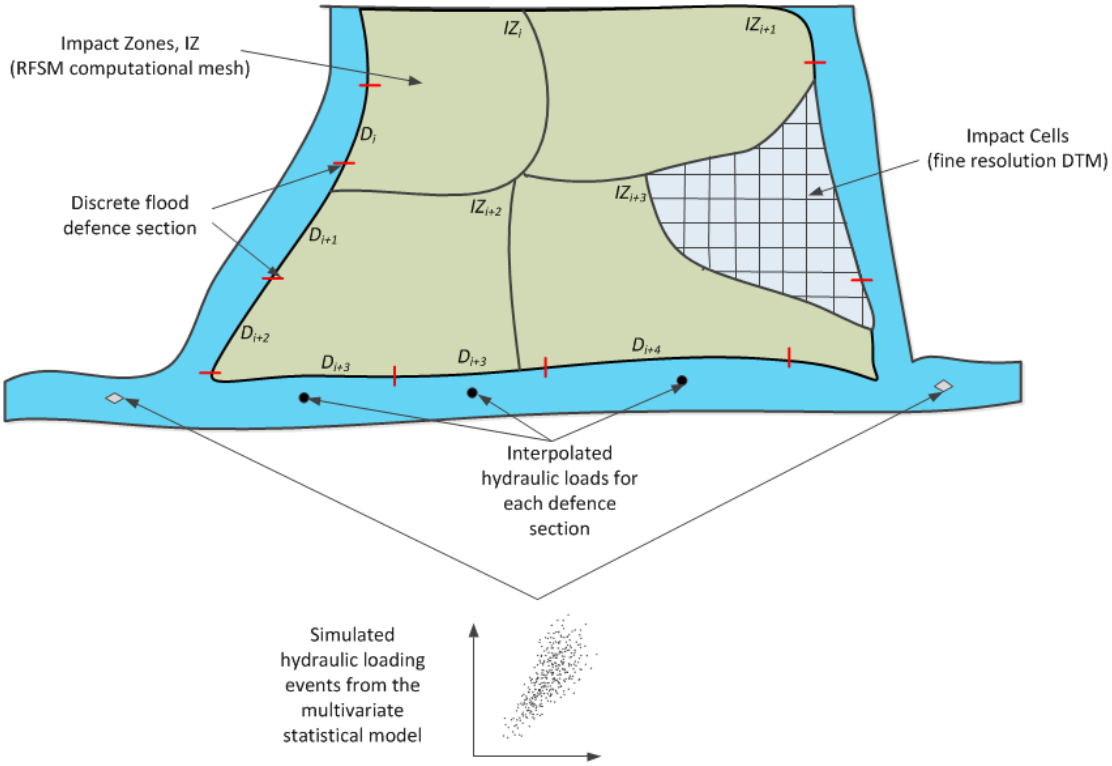

Figure 2

Statistical model for hydraulic loads

There are a wide range of multivariate extreme value models, Coles and Tawn (1991), Joe *et al.* (1992), Coles and Tawn (1994) Ledford and Tawn (1996), for example. All of these models have restrictive assumptions relating to the nature of dependence. More specifically, in the joint tail region, one variable is assumed to be independent

of or asymptotically dependent on the other variables. The Heffernan and Tawn (2004) approach makes no such assumptions and is therefore the model of choice for this study. Further discussion on the motivation for use of the Heffernan and Tawn (2004) method in the context of flood risk analysis is provided in Environment Agency (2011b).

Let $\boldsymbol{X_t} = (X_1, \ldots, X_j)_t$ be a time series of flood related hydraulic loading conditions at a collection of locations within the area of interest. Before dependencies between locations are considered, the extreme loads at each location are studied marginally. For this the standard peaks-over-threshold approach of Davison and Smith (1990), is used: cluster maxima are identified from the time series and the excesses above a suitably high threshold are fitted to the generalised Pareto distribution (GPD). This defines a probability model for large values of the variable X_i:

$$P\{X_i > x \mid X_i > u_i\} = \left[1 + \xi_i \frac{(x-u_i)}{\beta_i}\right]_+^{-1/\xi_i} \quad \text{for } x > u_i, \tag{3}$$

Where the subscript i denotes the spatial location of the data, $\beta_i > 0$, $\xi_i \in \Re$ are the GPD parameters and $[y]_+ = \max(y, 0)$. The threshold u_i is chosen to be just large enough to ensure a stable estimate for the shape parameter ξ_i for all larger thresholds.

In order to separate the marginal characteristics from the dependence analysis, it is usual to standardise the data to common margins using the probability integral transform. This is often referred to as the copula approach. The Heffernan and Tawn (2004) model uses standard Gumbel marginal distributions which are obtained by setting $Y_i = -\log(-\log[\hat{F}_i(X_i)])$ where $\hat{F}_i$ is an estimate of the cumulative distribution function for X_i. For this the GPD fit above the threshold is combined with the empirical distribution $\tilde{F}_i$ of the X_i values to give the following semi-parametric function (first used by Coles and Tawn (1991)):

$$\hat{F}_i(x) = \begin{cases} \tilde{F}_i(x) & x \le u_i, \\ 1 - (1 - \tilde{F}_i(u_i))\left[1 + \xi_i \frac{(x-u_i)}{\beta_i}\right]_+^{-1/\xi_i} & x > u_i. \end{cases} \tag{4}$$

The transformed multivariate time series $\boldsymbol{Y}_t = (Y_1, \ldots, Y_d)_t$ retains the dependence structure of the original data but satisfies $P\{Y_i > y\} = \exp(-\exp[-y])$ for each different location i. The primary aspect of the Heffernan and Tawn (2004) approach is to model the dependence between extreme values of Y_i and typical values of the remaining variables. The analysis is repeated for each site i so that extreme values of all variables are considered.

Let $\boldsymbol{Y}_{-i}$ denote the vector of all variables Y_j excluding Y_i. The Heffernan and Tawn (2004) approach is typically applied using the multivariate non-linear regression model

$$\boldsymbol{Y}_{-i} \mid Y_i = \boldsymbol{a}\, Y_i + Y_i^{\boldsymbol{b}}\, \boldsymbol{Z} \quad \text{for } Y_i > v, \tag{5}$$

where v is a high threshold on Y_i, $\boldsymbol{a} \in [0, 1]$ and $\boldsymbol{b} < 1$ are vectors of parameters and $\boldsymbol{Z}$ is a vector of residuals. Vector arithmetic should be interpreted component-wise so

that each Y_j is modelled as a function of Y_i using parameters $a_{j|i}$ and $b_{j|i}$ and residual $Z_{j|i}$.

The regression parameters $a_{j|i}$ and $b_{j|i}$ are estimated using maximum likelihood under the temporary assumption that $Z_{j|i}$ follows a Normal Distribution with unknown mean and variance. This fit uses all pairs (Y_i, Y_j) corresponding to cluster maxima of $Y_i > v$ to be consistent with the marginal GPD fits made to cluster maxima of X_i. Heffernan and Tawn (2004) show that asymptotically $Y_i > v$ is statistically independent of the residual $Z_{j|i}$. The threshold v is therefore chosen to be just large enough for this condition to hold. Once all parameter estimates have been found a non-parametric estimate of the joint distribution of $\boldsymbol{Z}$ is constructed from the empirical distribution of the sample residuals.

The above description assumes variables Y_i and Y_j occur concurrently so is not appropriate for modelling temporally dependent data with extreme events that are lagged between gauges. Keef *et al.* (2009) overcome this deficiency by fitting the conditional model of $Y_{j,t+\tau} \mid Y_{i,t}$ for a selection of lags τ for each gauge $j \neq i$. This allows the model to be used to simulate new events over a range of lags so that the largest values in each time window need not occur concurrently and this approach has been adopted here.

Statistical simulation of extreme hydraulic loading events

The fitted model provides parameter estimates $a_{j|i,\tau}$ and $b_{j|i,\tau}$ for all locations i, $j \neq i$ and for a range of lags τ. Additionally, for each location i, an empirical sample of joint residuals $\boldsymbol{Z}$ is available, each of which provides values $Z_{j|i,\tau}$ for each $j \neq i$ and lag τ. These can be used to simulate a large number of dependent peak events $\boldsymbol{Y}$, each of which consists of a single peak value for every location in the network with associated lags between peaks. These are then transformed to give samples of spatially dependent peak flow events $\boldsymbol{X}$ on the original scale.

To simulate an event, a conditioning site, i must be selected. The value Y_i is sampled above the threshold v and the remaining Y_j values are sampled from the fitted model for $\boldsymbol{Y}_{-i,\tau} \mid Y_i$. In order to control the proportion of events where each site is most extreme, the value Y_i is constrained to be largest by rejection sampling. Further discussion on this approach is provided in Environment Agency (2011b).

The simulation consists of repeating the following steps, after selecting a conditioning site i:

1. Sample a value Y_i from the standard Gumbel distribution conditioned to exceed v.
2. Independently select one of the joint residuals $\boldsymbol{Z}$ for site i.
3. Calculate $Y_{j,\tau} = a_{j|i,\tau} Y_i + Y_i^{b_{j|i,\tau}} Z_{j|i,\tau}$ for all $j \neq i$ and lags τ.
4. For each j, set Y_j to be the maximum $Y_{j,\tau}$ over selected lags τ.
5. The joint sample $\boldsymbol{Y}$ is rejected unless Y_i is maximum over all gauges.

These simulated events have Gumbel marginal distributions which can be transformed to the original scales using the probability integral transform, inverting the transform applied to the original data using GPD fits and the empirical distribution.

To select the proportion of events where each gauge is most extreme, Lamb *et al.* (2010) propose simulation from the fitted model without rejection and this approach has been adopted here. For each gauge *i*, a large sample of samples is used to estimate $P\{Y_i \geq Y_j \forall j \neq i \mid Y_i > v\}$, the probability that Y_i is largest when *i* is the conditioning gauge. Since all simulated events have at least one threshold exceedance, this can be used to estimate the proportion of all events where Y_i is largest and hence variable X_i is most extreme.

The output from this analysis is a simulated set of hydraulic loading events. Each event comprises a peak flood variable at each location. An example of fluvial flow events simulated from the statistical model and compared to the observed data is given on Gumbel scales in Figure 3. The yellow points are cluster maxima in Y_i from the raw time series above the threshold v (147 cluster maxima in Y_i were found above v = 4.15 (on Gumbel scale) from a 27 year dataset). These were fitted (ignoring lags) to give the blue samples, constrained to $Y_i > Y_j$.by rejection. Similarly, the green points are cluster maxima in Y_j fitted to give the red samples for $Y_j > Y_i$. The diagonal defines the threshold for the rejection during the simulation (i.e. for the blue dots when $Y_j > Y_i$). It is apparent that the dependence in the extremes for site *i* within the simulated data reproduces well that within the observations. Further examples are available within Heffernan and Tawn (2004) and for flood related variables within Lamb *et al.* (2010) and Environment Agency (2011e), for example.

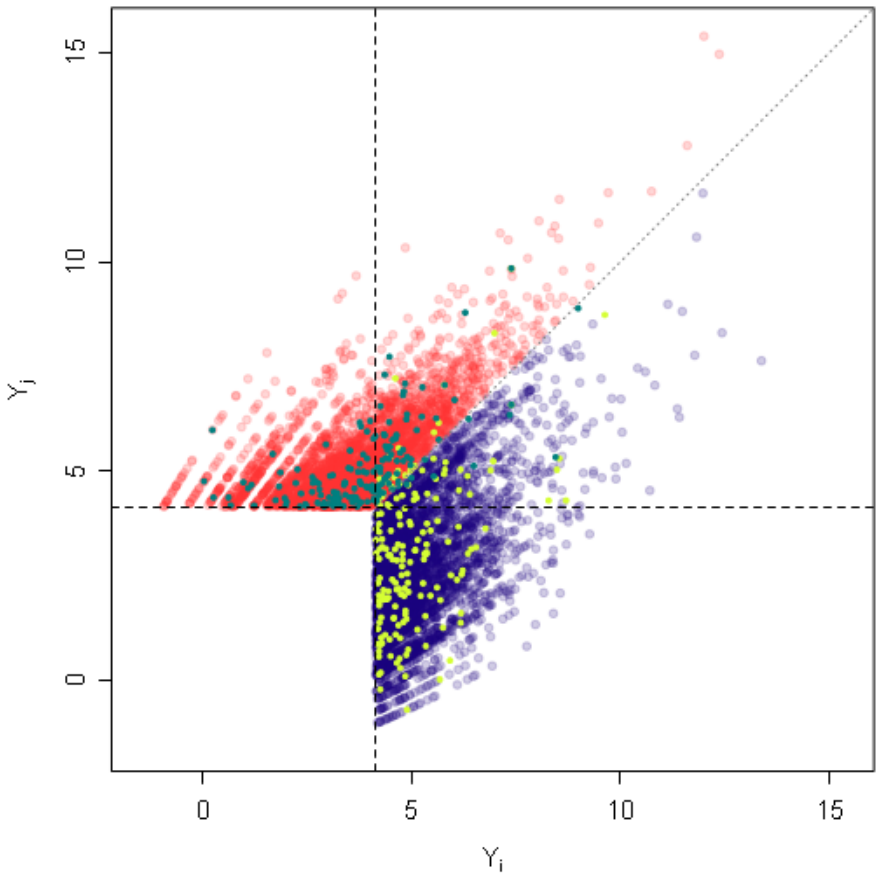

Figure 3

Defence system state reliability and floodplain analysis

The approach used to represent the performance of the flood defences, the propagation of floodwater across the floodplain and the evaluation of economic damages is described by Gouldby *et al.* (2008a) which extends the earlier work of Hall *et al.* (2003) and Environment Agency (2003). A summary description of this method and how it has been integrated with the multivariate extreme value method is provided below.

Each hydraulic loading event that has been simulated from the multivariate statistical model forms the boundary conditions for the flood defence system reliability analysis and subsequent inundation and economic consequence evaluation. The line of flood defences (embankments, for example) that forms the boundary between the river or coast and the floodplain area is discretised into sections that have different performance characteristics (i.e. type of defence, elevation and condition), see Figure 2. Fragility curves are used to define the performance of each defence section, USACE (1996), Simm *et al.* (2009), Schultz *et al.* (2010), Vorogushyn *et al.* (2009), for example, and the performance of each defence section is assumed to be independent from any other. It is assumed that each defence can exist in two possible states, failed (ie structural failure or breached), or undamaged. During a flood event, water can enter the floodplain through any particular defence if it is a breached defence, or if it remains undamaged but is overtopped. As there are a finite number of defence sections and only two possible system states for each section, there are a finite number of defence system states (combinations of failed and undamaged defences). For each hydraulic loading event it is, in principle, necessary to simulate the flood wave propagation and associated economic damages for each (2^n) system state. It is, however, computationally impractical to run an inundation simulation for all of the different defence system states and, for each hydraulic loading event, a Monte Carlo simulation of the defence system states is therefore implemented.

For each simulated defence system state, floodplain discharge volumes are calculated for each flood defence. This water is then propagated across the floodplain using a computationally efficient flood propagation algorithm, the Rapid Flood Spreading Model (RFSM), Gouldby *et al.* (2008a), Lhomme *et al.* (2008). The algorithm uses a pre-process that analyses the natural floodplain topography to distinguish a series of localised depressions. The depressions, termed Impact Zones, are irregular in shape and comprise any number of regularly spaced Impact Cells (the underlying topographical elevation model), see Figure 2. The geometrical properties of the Impact Zones are stored in database tables and these form the computational elements for the inundation model. The volume of water discharged over (or through breached defences), is then spread across the floodplain, using the stored information on the Impact Zones and a final flood extent and floodplain depths for each Impact Cell evaluated.

As the model is volume based, it is exceptionally computationally efficient, at the expense of complete representation of the underlying physical processes. As there is no temporal evolution of the flood wave, it is not possible to compute velocities, for example. Recent research, Jamieson *et al.* (2012), has however, seen the development of a new dynamic model, RFSM EDA, that utilises the same meshing system as the RFSM but implements a new simplified formulation of the shallow-water equations, Bates *et al.* (2010). The implementation of this type of dynamic model within the

system described here, affords a further opportunity for significant improvement. It is likely the type of steady-state modelling system described here will evolve into a more dynamic system in the future. In principle, it would also be possible to utilise the information on temporal lags, generated within the application of the multivariate analysis, to generate time varying hydraulic boundary conditions.

Flood depths output for each Impact Cell are then combined with information from the National Property Database and the widely applied functions, of Penning-Rowsell *et al.* (2005) to determine economic damages.

Within any particular discrete Impact Cell within the floodplain, the probability of exceeding any particular flood depth (h), conditional on the specified hydraulic loading level (x), is approximated by:

$$P(H > h|x) \approx (m_h / m) \quad (6)$$

where m is the total number of defence system state Monte Carlo realisations and m_h is the number that exceed h, under the specified loading level x. Similarly, the conditional probability of exceeding a specific economic damage level (c) is given by:

$$P(C > c|x) \approx (m_c / m) \quad (7)$$

Combining the Monte Carlo realisations for the hydraulic loading with the defence system states, it then follows that the unconditional annual probability of exceeding any particular level of economic damage is:

$$P(C > c) \approx \frac{(l_c / l)}{n_y} \quad (8)$$

where l_c is the number of Monte Carlo realisations that exceed c, l is the total number of Monte Carlo realisations and n_y is the number of years of data that has been simulated. The risk, expressed in the usual terms of EAD is:

$$EAD \approx \frac{\sum_{i=1}^{l} c_i}{n_y} \quad (9)$$

where c_i is the economic damage arising on the ith realisation of the hydraulic loading conditions. The number of realisations required can be controlled in a number of different ways, for example, through specification of convergence criteria on the quantity of interest.

Case study application

Study area description

The case study location is the Eden catchment in the northwest of England (Figure 4). The Environment Agency (2009a) provides an in depth discussion of the flooding problems and ongoing management of flooding in the catchment and this is briefly summarised here. The Eden catchment covers approximately 2400km^2, with the primary watercouses being Eden, Irthing, Eamount, Petteril and the Caldew. Over 90% of the catchment is rural and the total population is around 244,000. The upper catchment (in the South), is dominated by high ground (fells). In the Lower Eden Valley, the floodplain widens, affording storage capacity during times of elevated water levels. In the higher regions to the South, the average annual rainfall exceeds 2800mm and is over 3 times the national average of England and Wales (920mm).

The main population centres are Carlisle, Penrith and Appleby. The floodplain protection varies significantly across the study area and includes high ground in rural areas, embankments and a range of heavily engineered vertical structures within urban areas, Carlisle for example. The study area has been separated into 10016 flood areas and is consistent with those used in the National flood risk assessment of England, Environment Agency (2009b). It is however, of note that the underlying data has been modified to a certain degree and the results shown here do not reflect the absolute magnitude of risk in the catchment.

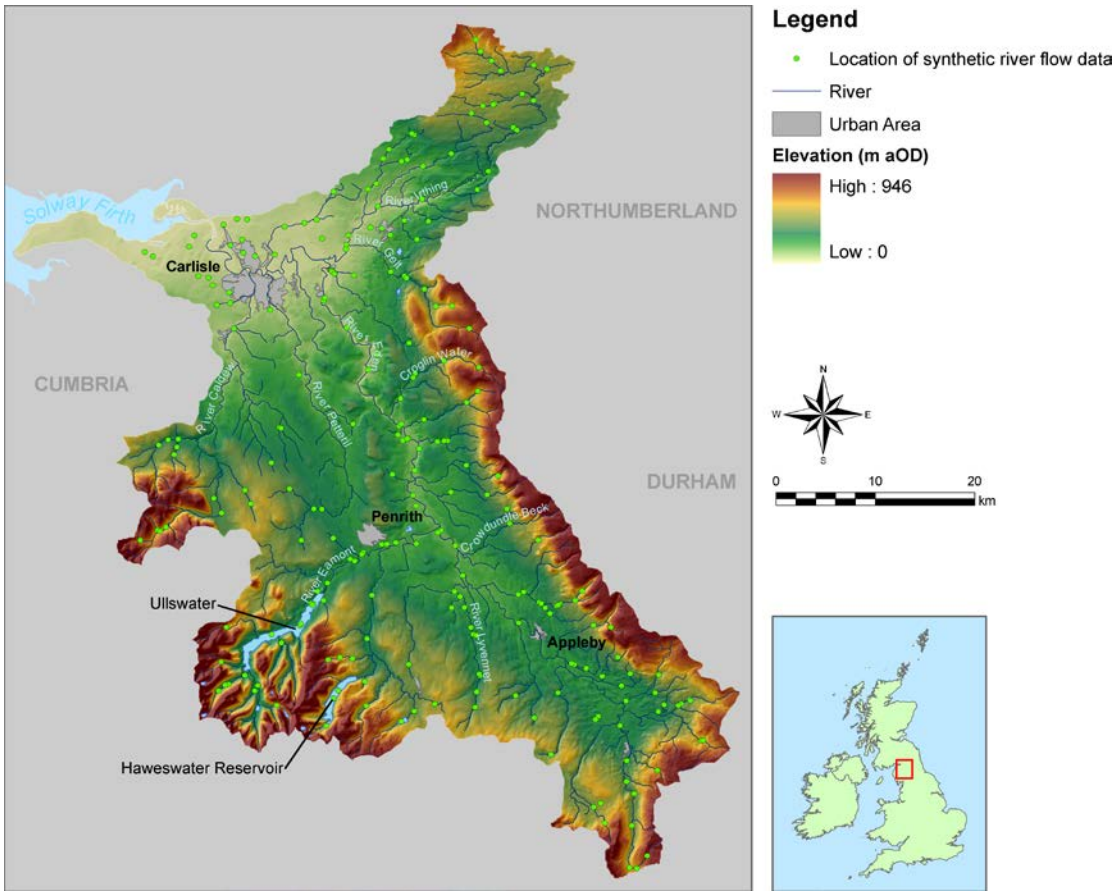

Figure 4

Carlisle has a history of flooding with significant events having been recorded in 1963, 1968, 1979, 1980, 1984 and most recently in January 2005, when nearly 3000 homes were flooded, 3 people died and the resulting flood losses were estimated as £400m, Geographical Association (2009). The flooding arose as a result of a prolonged period (1 month) of high rainfall in the vicinity of Carlisle, saturating the soil and raising local ground water levels. This was then followed by a period of intense rainfall (2 months-worth in 2 days), over the period 6th -8th of January, Geographical Association (2009). Figure 5 shows the hydrograph on the River Eden for this period.

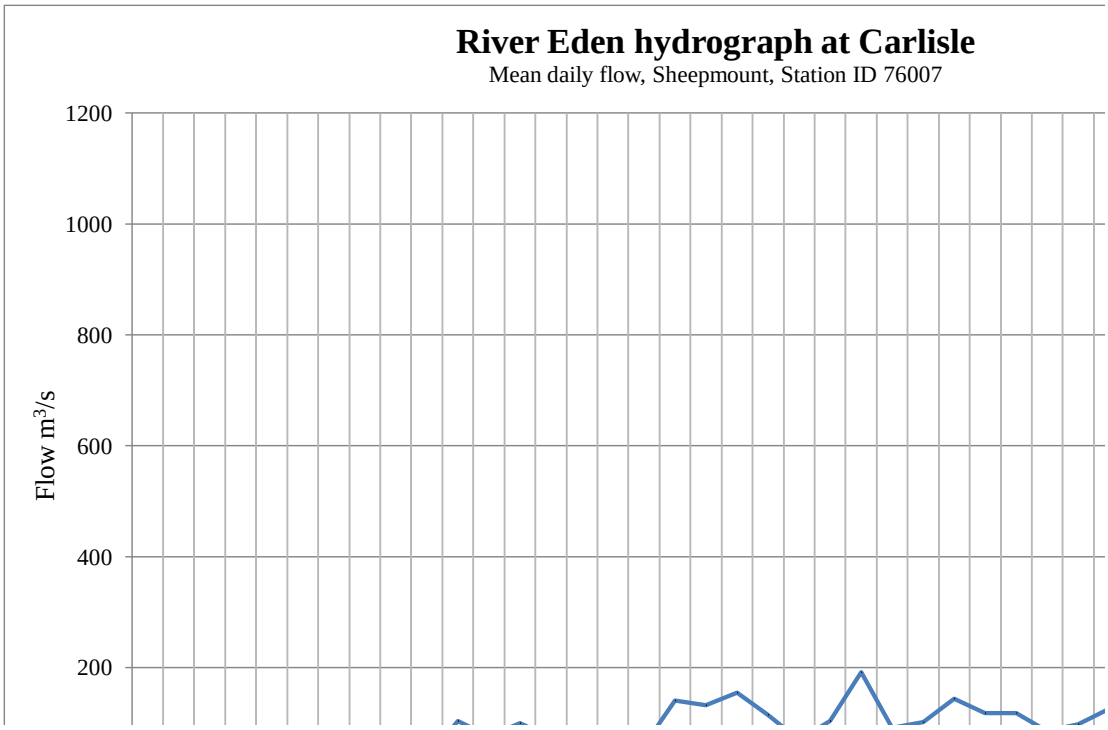

Figure 5

Hydraulic load analysis

Synthetic flow data form the basis of the analysis and these stem from a series of linked models. Time series rainfall, on a 25km spatial grid and an hourly time interval provide the driving data for a gridded hydrological model (Grid-to-Grid, or "G2G", Bell (2007)). These rainfall data, together with estimates of potential evaporation (PE) have been generated from the UK Met. Office Hadley Centre global climate model (GCM), HadCM3, dynamically downscaled to 25km using the HadRM3 regional model, Jones R *et al.* (2004). The G2G Model operates on a 1km grid covering the whole of the UK, and, using a gridded representation of the kinematic wave equation, simulates surface and sub-surface flows. A full description of the G2G model is provided in Bell (2007).

The G2G Model provides 27 years of time series flows on a 1km UK grid along the river network. The gridded data were first interpolated to each of 4119 nodes that span the river network by selecting the largest value of each surrounding grid point at every time step. To reduce the computational burden, rather than applying the statistical analysis to every node, node points that had a value of Pearson's Product Moment Correlation over 0.99 with a remaining node were removed to leave a representative subset of 248 sites. This threshold correlation value was considered sufficiently accurate for use on this case study but it is possible a further reduction in the number of sites could have been achieved using a lower value without loss of accuracy.

The marginal extremes at each of these selected nodes have been analysed separately. Peak flow clusters were identified using the runs method of Smith and Weissman (1994) before the cluster maxima above a high threshold were fitted to GPD. After transformation to Gumbel marginal distributions, cross-correlations were analysed

using node pairs lagged by up to ±6 days. In the majority of cases, the largest correlation was obtained by a lag within ±2 days. Hourly lags of up to ±3 days were therefore used to fit the multivariate statistical model to every pair of nodes in the subset, adopting a similar approach to that of Lamb *et al.* (2010).

Peak flows were then paired with local maxima at every other node so that extreme events that had at least one threshold exceedance could be identified. 709 such events were counted giving an average of 26 extreme events per year. With this, 1000 years worth of hydraulic loading conditions were simulated from the fitted model on the Gumbel scale. Each sample comprised a peak flow level for all 248 selected nodes and had at least one threshold exceedance. Rejection sampling was used to control the proportion of events that are most extreme for each site.

After transformation back to the original scale, linear relationships identified between nodes with large correlations (>0.99) were used to extend the peak flow samples to all 4119 river nodes. These were then converted to water levels using the Conveyance Estimation System, Mc Gahey *et al.* (2008) and mapped to all 34006 discrete river defence sections in the catchment.

Figure 6 shows a comparison of hydraulic loading data (peak fluvial flows) simulated from the statistical model for a subset of stations. The figure shows the range of dependence in the hydraulic loading conditions that is present across the study area and highlights the flexibility (in terms of the range of dependence in the extremes) required of the multivariate model to capture this. Perhaps unsurprisingly, sites in close proximity exhibit a high degree of dependence whilst others, further a-field are only partially dependent on one another.

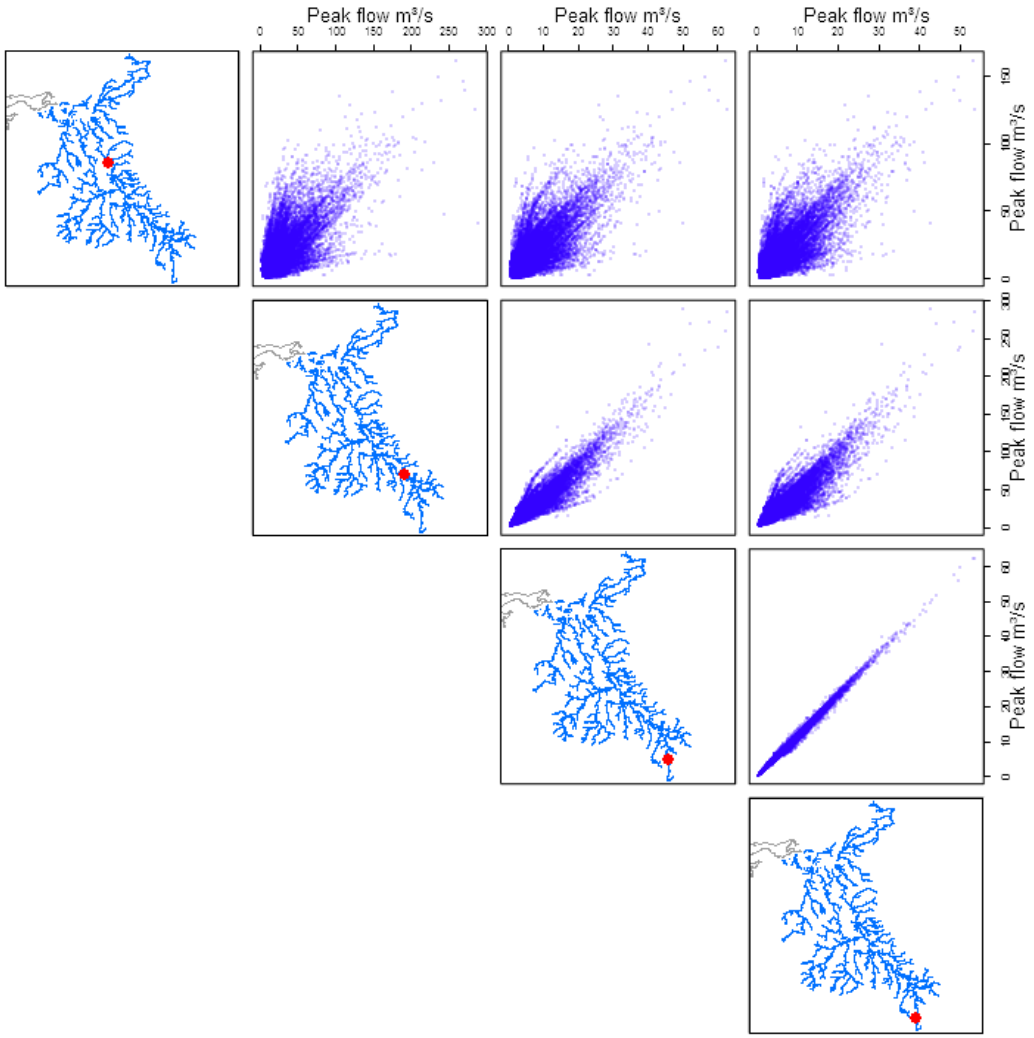

Figure 6

Figure 7 shows the variation in return period of the hydraulic loading levels across the study area for a subset of single realisations from the multivariate model. The spatial variation in the intensity of the flood events is apparent. Some events are spatially diverse and extreme flows arise across the entire study area, whereas other events are very much localised with extremes arising in relatively small areas over the catchment. The event shown in the lower left of Figure 7 is of particular interest. The event comprises relatively high flows in the upstream areas of the catchment (generally > 200 year return period), to the South but the downstream areas, in the vicinity of Carlisle, to the North, flows are significantly less (generally <50 year return period). This highlights the complexity of the hydrological regime in the catchment and gives an indication of the high influence of localised rainfall, in the lower catchment, as evidenced by the 2005 extreme event (Figure 5).

The range of flood events that are shown highlights the communication difficulties that have arisen in the past when describing flood events in terms of the severity of their loading conditions - “The event was a 1 in 100 year (flow) event”, for example. It is apparent that statements about flood events, expressed in terms of the extremes of the hydraulic loading conditions, are often only valid for small spatial areas. Attempting to express widespread flood events, like those that affected England and Wales in the summer of 2007, in terms of return period of the hydraulic loading

conditions, as often seems to be a requirement, can result in misleading information and a general misunderstanding of the nature of the flood event.

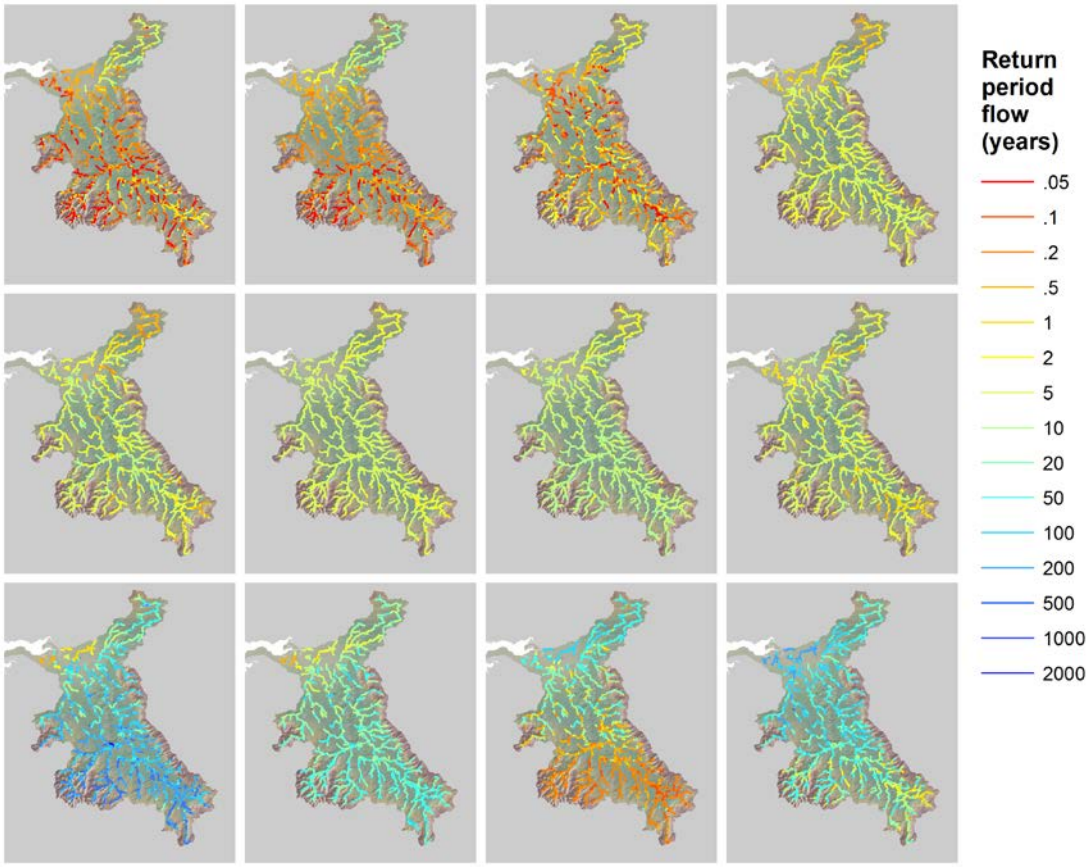

Figure 7

Lewis *et al.* (2011) draw attention to the validity of making an assumption of complete dependence of hydraulic loading level (equal return period) within a flood area with system based flood risk analysis models, for example. This assumption is made to enable a simplified integration of the joint density of the hydraulic loads over the consequence function (Eqn. 2). Their analysis was conducted within the context of coastal systems and it is possible to explore the validity of this assumption further here, within the context of this fluvial system. Figure 8 shows the variation of return period within one of the largest flood areas for the same events shown in Figure 6. The flood area comprises 30 defences, the maximum and minimum return periods and average return period for each of the hydraulic loading events are shown in Table 1. Based upon the synthetic data analysed, it is apparent that even within a flood area there can be significant variation in the return period of the water level and the assumption of equal likelihood can potentially introduce significant bias in some cases. This reinforces the observations on coastal systems of Lewis *et al.* (2011).

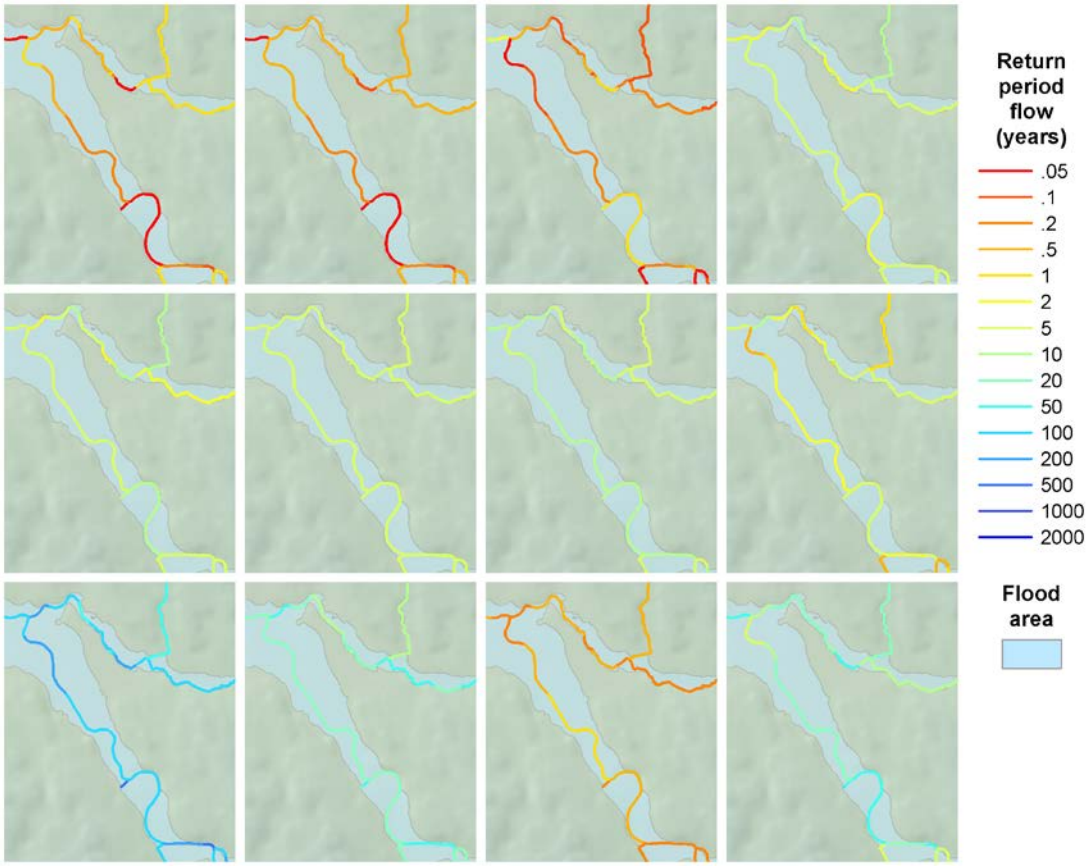

Figure 8

Economic damages and risk estimation

Within the current National Flood Risk Assessment of England and Wales, Environment Agency (2009b), the EAD is derived at the level of a flood area and then aggregated to obtain a regional or national value of risk. The method does not enable estimates of return period damages, for single events that are greater than a flood area. The introduction of the multivariate method does however, enable this. For each realisation of the multivariate model of the hydraulic loads, a Monte Carlo simulation of the defence system states and associated inundation and consequence analysis, within each flood area, has been undertaken. The resulting risk, in terms of EAD, over the whole study area is £19.7 million. Figure 9 shows the spatial variation in the risk. Whilst damages occur throughout the catchment, the greatest concentration of risk is in the north in the vicinity of Carisle, the site of recent and historic flooding.

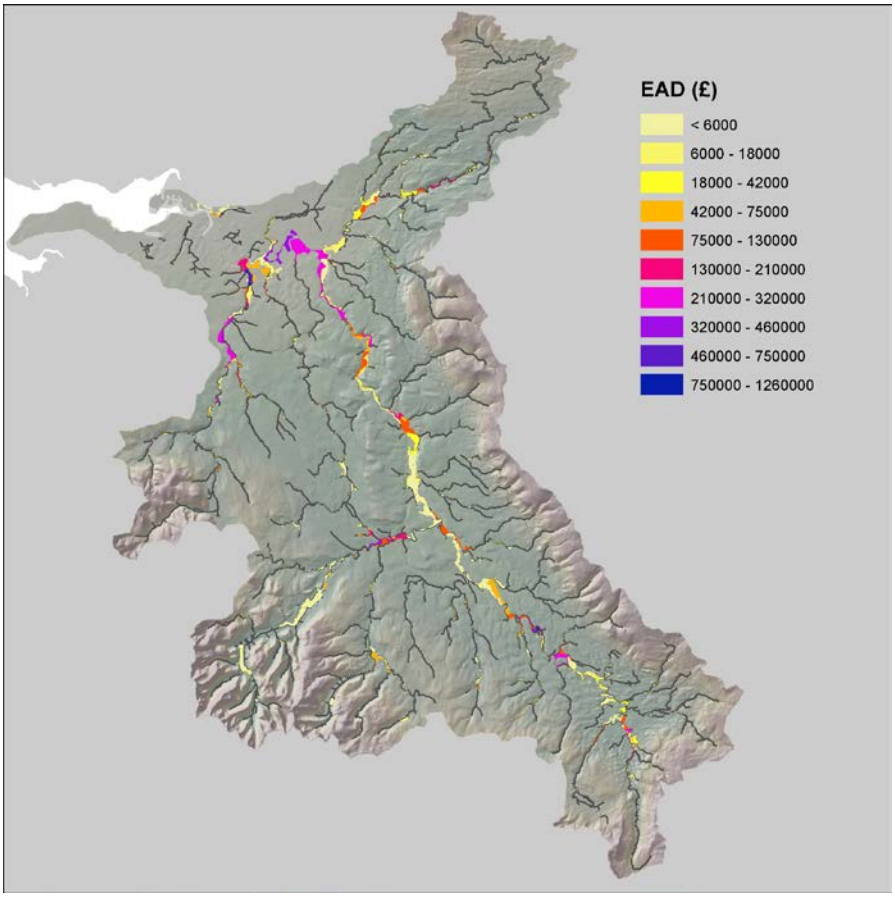

Figure 9

The distribution of damage aggregated over the whole study area is shown in Figure 10. A comparison has also been made under the assumption of full dependence and complete independence of hydraulic load, on a flood area basis. It is interesting to note that in this particular study area the results show the modelled dependence of economic damages to be close to full dependence. This is in contrast to the extreme hydraulic loading conditions that showed a wide range of dependence across the study area. The high dependence in damages results from the localised nature of some extreme rainfall events in the North of the catchment, causing major damage, as evidenced by the event in January 2005. It is important to note that this finding is only applicable for this study area and other study areas will differ. For example, Lamb *et al.* (2010) found the degree of dependence was closer to independence for a study area in the northeast of England.

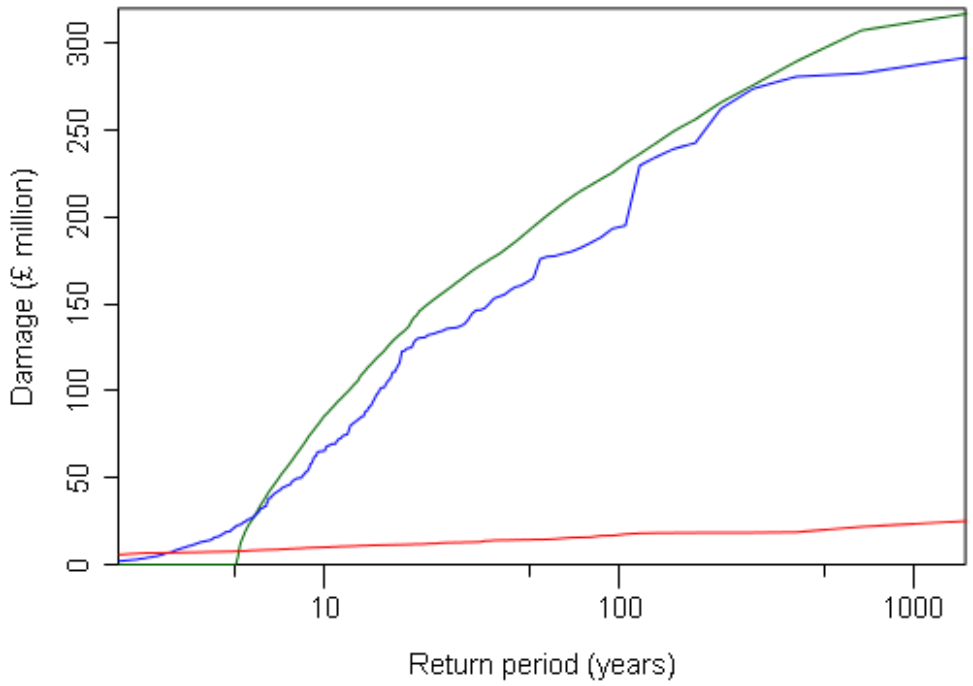

Figure 10

Validation

Validation is an important consideration for any numerical model. Risk however, is an abstract quantity that cannot be measured and hence one of the usual routes of verifying numerical models through comparison with measured data is not possible. Some confidence in the new approach described here can be gained from previous analysis. For example, the systems risk model has been verified for use by the Environment Agency on the major Thames Estuary 2100 study, Gouldby *et al.* (2008b) and the National flood risk assessment of England and Wales Environment Agency (2009b). Lamb *et al.* (2010) and Environment Agency (2011b), provide an in depth exploration of the application of the multivariate method of Heffernan and Tawn (2004) within the context of flooding. Further work is however, required with respect to the validation of probabilistic flood risk models. Environment Agency (2010b) describes a framework for undertaking this type of analysis. In particular, the framework recognises the need to undertake uncertainty analysis that includes both model structural as well as input data and model parameter uncertainties. Whilst prior work on the propagation of input data and parameter uncertainty has had some success, Merz and Thieken (2009a), Gouldby *et al.* (2010), further work on the handling of model structural uncertainties is required.

There are a number of possibilities with regard to assessing model structural uncertainties. One promising approach relates to the development of benchmark data sets that can be used to explore and verify the model components or the whole modelling system. For example, Environment Agency (2010a) describes a range of benchmark tests for 2D inundation models, these type of tests can be used to gain insight on the performance of reduced complexity inundation models (eg. RFSM) that are used within the probabilistic system models. It is of note however, this type of component testing does not necessarily capture the full range of model structural uncertainties. Apel *et al.* (2009), for example, describe the influence of upstream dyke breaches on downstream water levels and hence downstream breach likelihood.

To assess this type of model structural uncertainty, integrated river channel/floodplain models that incorporate probabilistic defence performance and dynamic breach growth are required, Lhomme *et al.* (2010), for example. The development of these benchmarking data sets is the subject of ongoing research which, when complete, is likely to afford more opportunities for validating the type of modelling system described here.

Conclusions

Flooding is a global problem. Effective flood risk management decision making is underpinned by quantitative system models of flood risk. The models that are applied in current practice within England and Wales incorporate a wide range of hydraulic loading conditions, a representation of the likelihood of failure of the flood defence assets and a computationally efficient inundation model. The current models do however, utilise a simplifying assumption to facilitate the evaluation of the flood risk. The hydraulic loading events within a flood area are assumed to be fully dependent in terms of likelihood. This assumption is made to facilitate the calculation of risk in a computationally efficient manner and to overcome the complexities relating to the dependence structure within the extremes of the hydraulic loading conditions.

An artefact of this assumption is the inability of the current method to provide information on the likelihood of damages for single flood events at spatial scales larger than a flood area. Within the current method, risk, expressed as EAD is calculated on a flood area basis and aggregated to obtain risk at larger spatial scales. Information on the probability of exceeding a specified economic damage threshold for a single event is not currently available. This information can be important for the insurance industry and emergency planners, for example. Recent research identified the potential of a multivariate extreme value statistical model to improve this aspect of the existing modelling system.

To overcome these deficiencies within the current method, a new modelling system has been developed. The new system integrates a multivariate extreme value method of the hydraulic loading conditions with the existing modles of flood defence performance, inundation and economic damages. The new modelling system has been applied on a case study site to investigate fluvial flooding in a catchment in the North West of England. A Monte Carlo simulation of the fitted multivariate statistical model enables the hydraulic boundary conditions across the flood defence system to be represented more realistically. The resulting method retains the system characteristics of the current methodology and its ability to reflect the performance of the flood defence infrastructure. This is implemented through a secondary Monte Carlo simulation of the defence system states, conditional on the output of the multivariate model.

This development has enabled the exploration of the assumption of full dependence of hydraulic loading likelihood within a flood area. The analysis shows that in some cases, for a single flood event the return period can vary significantly, even within a flood area. This is likely to introduce a bias in estimates of flood risk that utilise this assumption. This concurs with the findings of recent research relating to coastal hydraulic loading events.

The implementation of the multivariate method enables the probability of single flood event damages to be quantified. This refinement can potentially offer insights into the spatial characteristics of single flood events that are not currently possible with the existing MDSF2 system. It also highlights the limitations of using the EAD. EAD is a relatively simplistic measure of flood risk and analysis of additional information comprised within the full distribution can be of importance.

Some confidence in the system developed here can be afforded through previous application and verification of the different modelling components. Validation of system-based probabilistic models remains a challenge. Ongoing research on the development of benchmark tests for probabilistic models is, however, likely to afford greater opportunity for rigorous validation in the future.

Acknowledgements

This work was supported by the Natural Environment Research Council, Grant Ref. NE/E002420/1 - through the Flood Risk for Extreme Events (FREE) NERC directed mode programme and HR Wallingford´s internal research programme. The authors are grateful to Dr Vicky Bell and Dr Nick Reynard of the Risk Modelling centre at CEH Wallingford, for the support provided with regard to their Grid2Grid Model.

References

Acreman, M. C. (1994). "Assessing the Joint Probability of Fluvial and Tidal Floods in the River Roding." Water and Environment Journal **8**(5): 490-496.

Apel, H., Merz, B. and Thieken, A. H. (2009). "Influence of dike breaches on flood frequency estimation." Computers & Geosciences **35**(5): 907-923.

Apel, H., Thieken, A., Merz, B. and Bloschl, G. (2004). "Flood risk assessment and associated uncertainty." Natural Hazards and Earth System Sciences **4**: 295 - 308.

Bates, P. D., Horritt, M. S. and Fewtrell, T. J. (2010). "A simple inertial formulation of the shallow water equations for efficient two-dimensional flood inundation modelling." Journal of Hydrology **387**(12): 33-45.

Bell, V., Kay A, Jones R, Moore R (2007). "Devlopment of a high resolution grid-based river flow model for use with regional climate model output." Hydrology and Earth System Sciences **11**(1): 532 - 549.

Bruun, J. T. and Tawn, J. A. (1998). "Comparison of approaches for estimating the probability of coastal flooding." Journal of the Royal Statistical Society: Series C (Applied Statistics) **47**(3): 405-423.

Cai, Y., Gouldby, B., Hawkes, P. and Dunning, P. (2008). "Statistical simulation of flood variables: incorporating short-term sequencing." Journal of Flood Risk Management **1**(1): 3-12.

Coles, S. G. and Tawn, J. A. (1991). "Modelling Extreme Multivariate Events." Journal of the Royal Statistical Society. Series B (Methodological) **53**(2): 377-392.

Coles, S. G. and Tawn, J. A. (1994). "Statistical Methods for Multivariate Extremes: An Application to Structural Design." Journal of the Royal Statistical Society. Series C (Applied Statistics) **43**(1): 1-48.

Davison, A. C. and Smith, R. L. (1990). "Models for exceedances over high thresholds." Journal of the Royal Statistical Society, Series B (Statistical Methodology) **52**(3): 393-442.

Environment Agency (2003) Risk Assessment for Flood & Coastal Defence for Strategic Planning R&D Technical Report W5B-030/TR1,
Environment Agency (2009a) Eden Catchment Flood Management Plan: Summary Report 2009 E. Agency
Environment Agency (2009b) Flooding in England: A National Assessment of Flood Risk
Environment Agency (2010a) Benchmarking of 2D Hydraulic Modelling Packages, Environment Agency Report SC080035/SR2, Bristol
Environment Agency (2010b) Validation of probabilistic flood models SC090008/WP1 Phase 1 Final Report – SC090008/WP1/SR1
Environment Agency (2011a) MDSF2 Technical Report, Environment Agency, Science Report SC050051/SR4
Environment Agency (2011b) The risk of widespread flooding – Capturing spatial patterns in flood risk from rivers and coasts, SC060088/R1 Spatial Coherence of Flood Risk – Technical Methodology Report
Environment Agency (2011c) The risk of widespread flooding – Capturing spatial patterns in flood risk from rivers and coasts, SC060088/R2 Spatial Coherence of Flood Risk – Proof of concept summary report
Environment Agency (2011d) The risk of widespread flooding – Capturing spatial patterns in flood risk from rivers and coasts, SC060088/R3 Spatial Coherence of Flood Risk – Results from a national case study
Environment Agency (2011e) The risk of widespread flooding – Capturing spatial patterns in flood risk from rivers and coasts: SC060088/R1 Spatial Coherence of Flood Risk - Technical Methodology Report Environment Agency Bristol
Evans, E., Hall, J., Penning-Roswell, E., Sayers, P., Thorne, C. and Watkinson, A. (2006). "Future flood risk management in the UK." Water Management **159**(WM1): 53 - 61.
Geographical Association (2009). Managing flood risk - Carlisle Case Study. http://www.geography.org.uk/resources/flooding/carlisle.
Gouldby, B., Sayers, P., Mulet-Marti, J., Hassan, M. and Benwell, D. (2008a). "A methodology for regional-scale flood risk assessment." Water Management **161**(3): 169-182.
Gouldby, B., Sayers, P. and Tarrant, O. (2008b). Application of a flood risk model to the Thames Estuary for economic benefit assessment Risk Analysis VI :Simulation and Hazard Mitigation, Caephalonia, WITpress.
Gouldby, B. P., Sayers, P. B., Panzeri, M. C. and Lanyon, J. E. (2010). "Development and application of efficient methods for the forward propagation of epistemic uncertainty and sensitivity analysis within complex broad-scale flood risk system models." Canadian Journal of Civil Engineering **37**(7): 955-967.
Hall, J., Dawson, R., Sayers, P., Rosu, C., Chatterton, J. and Deakin, R. (2003). "A methodology for national-scale flood risk assessment." Proceedings of the Institution of Civil Engineers, Water and Maritime Engineering **156**(3): 235 - 247.
Hall, J. and Solomatine, D. (2008). "A framework for uncertainty analysis in flood risk management decisions." International Journal of River Basin Management **6**(2): 85-98.
Hall, J. W., Sayers, P. B., Walkden, M. J. A. and Panzeri, M. (2006). "Impacts of climate change on coastal flood risk in England and Wales: 2030-2100." Philosophical Transactions of the Royal Society A: Mathematical, Physical and Engineering Sciences **364**(1841): 1027-1049.

Hawkes, P. J., Gouldby, B. P., Tawn, J. A. and Owen, M. W. (2002). "The joint probability of waves and water levels in coastal engineering design." Journal of Hydraulic Research **40**(3): 241-251.

Heffernan, J. E. and Tawn, J. A. (2004). "A conditional approach for multivariate extreme values (with discussion)." Journal of the Royal Statistical Society: Series B (Statistical Methodology) **66**(3): 497-546.

Jamieson, S., Lhomme, J., Wright, G. and Gouldby, B. (2012). "Highly efficient 2D inundation modelling with enhanced diffusion-wave and sub-element topography." Proc. Inst. Wat. Man. **in press**.

Joe, H., Smith, R. L. and Weissman, I. (1992). "Bivariate Threshold Methods for Extremes." Journal of the Royal Statistical Society. Series B (Methodological) **54**(1): 171-183.

Jones R, Noguer N, Hassell D, Hudson D, Wilson S, Jenkins G and Mitchell J (2004) Generating high resolution climate change scenarios using PRECIS M. O. H. Centre Exeter

Keef, C., Tawn J and Svensson C (2009). " Spatial risk assessment for extreme river flows." Appl Stat **58,**(5): 601–618.

Lamb, R., Keef, C., Tawn, J., Laeger, S., Meadowcroft, I., Surendran, S., Dunning, P. and Batstone, C. (2010). "A new method to assess the risk of local and widespread flooding on rivers and coasts." Journal of Flood Risk Management **3**(4): 323-336.

Ledford, A. W. and Tawn, J. A. (1996). "Statistics for near independence in multivariate extreme values." Biometrika **83**(1): 169-187.

Lewis, M., Horsburgh, K., Bates, P. and Smith, R. (2011). "Quantifying the Uncertainty in Future Coastal Flood Risk Estimates for the U.K." Journal of Coastal Research: 870-881.

Lhomme, J., Gutierrez-Andres, J., Weisgerber, A., Davison, M., Mulet-Marti, J., Cooper, A. and Gouldby, B. (2010). "Testing a new two-dimensional flood modelling system: analytical tests and application to a flood event." Journal of Flood Risk Management **3**(1): 33-51.

Lhomme, J., Sayers, P., Gouldby, B., Samuels, P., Wills, M. and Mulet-Marti, J. (2008). Recent development and application of a rapid flood spreading method. Flood Risk 2008, Oxford.

Marsh, T. J. and Hannaford, J. (2007) The summer 2007 floods in England and Wales – a hydrological appraisal CEH Wallingford

Mc Gahey, C., Samuels, P. G., Knight, D. W. and O'Hare, M. T. (2008). "Estimating river flow capacity in practice." Journal of Flood Risk Management **1**(1): 23-33.

Merz, B. and Thieken, A. (2009a). "Flood risk curves and uncertainty bounds." Natural Hazards **51**(3): 437-458.

Merz, B. and Thieken, A. H. (2009b). "Flood risk curves and uncertainty bounds." Natural Hazards **51**(3): 437-458.

Penning-Rowsell, E., Johnson, C., Tunstall, S., Tapsell, S., Morris, J., Chatterton, J. and Green, C. (2005). The Benefits of Flood and Coastal Risk Management: A manual of assessment techniques, Middlesex University Flood Hazard Research Centre.

Roca-Collel, M. and Davison, M. (2010). "Two dimensional model analysis of flash-flood processes: application to the Boscastle event." Journal of flood risk Management **3**(1): 63-71.

Sayers, P., Hall, J. and Meadowcroft, I. (2002). "Towards risk-based flood hazard management in the UK." Civil Engineering **150**: 36 - 42.
Schultz, M., Gouldby, B., Simm, J. and Wibowo, J. (2010) Beyond the Factor of Saftey: Developing Fragility Curves to Characterize System Reliability
Simm, J., Gouldby, B., Sayers, P., Flikweert, J., Wersching, S. and Bramley, M. (2009). Representing fragility of flood and coastal defences: Getting into the detail. Flood Risk Management: Research and Practice. P. Samuels, S. Huntington, W. Allsop and J. Harrop, Taylor and Francis Group, London, UK.
Smith, R. L. and Weissman, I. (1994). "Estimating the extremal index." Journal of the Royal Statistical Society, Series B (Methodological) **56**(3): 515-528.
Tawn, J. and Vassie, I. (1989). " Extreme sea levels: the joint probabilities method revisited and revised." Proc Inst Civ Eng(87): 429–442.
USACE (1996) Risk-based Analysis for Flood Damage Reduction studies Engineer Manual EM 1110-2-1619
Vorogushyn, S., Merz, B. and Apel, H. (2009). "Development of dike fragility curves for piping and micro-instability breach mechanisms." Nat. Hazards Earth Syst. Sci. **9**(4): 1383-1401.
Vorogushyn, S., Merz, B., Lindenschmidt, K. E. and Apel, H. (2010). "A new methodology for flood hazard assessment considering dike breaches." Water Resources Research **46**: 17.
Wahl, T., Mudersbach, C. and Jensen, J. (2012). "Assessing the hydrodynamic boundary conditions for risk analyses in coastal areas: a multivariate statistical approach based on Copula functions." Nat. Hazards Earth Syst. Sci. **12**(2): 495-510.
Woodward, M., Gouldby B, Kapelan Z and Hames D (2012). "Multiobjective optimisation for improved management of flood risk." accepted for publication in ASCE Waterways.
Woodward, M., Gouldby, B., Kapelan, Z., Khu, S. T. and Townend, I. (2011). "Real Options in flood risk management decision making." Journal of Flood Risk Management **4**(4): 339-349.

Word count: 6392

Figure captions

Figure 1 Flow diagram of the new multivariate system based modelling system.

Figure 2 Spatial components of the new multivariate system based model.

Figure 3 Comparison of observed peak flow events (cluster maxima in Y_i and Y_j, yellow and green respectively) against samples from the fitted statistical model (ignoring time lags) for conditioning site *i* and *j* (blue and red respectively) plotted on the Gumbel scale.

Figure 4 Map showing the study area for the case study with the representative nodes spanning the river network. Contains Ordnance Survey data © Crown copyright and database right 2012.

Figure 5 Hydrograph for the River Eden showing elevated flows several weeks prior to the January 2005 event (data source, National River Flow Archive).

Figure 6 Comparison of peak flow events sampled from the statistical model for four sites on the river network.

Figure 7 Variation in return period water levels across the study area for a subset of sampled hydraulic loading events.

Figure 8 Variation in return period water levels within a particular flood area.

Figure 9 Spatial variation in EAD over the study area.

Figure 10 Return period total damage for the study area for the fully dependent (green), partially dependent using the statistical model (blue) and independent (red) cases.

Tables

Table 1 Minimum, mean and maximum return period flows over the 30 defences in the highlighted flood area for each of the events in Figure 5. The events in the figure are numbered in rows beginning in the top-left.

Event Number	Return period (years)		
	Minimum	Mean	Maximum
1	<1	<1	1
2	<1	<1	<1
3	<1	<1	<1
4	2	5	8
5	1	5	8
6	3	5	9
7	6	8	11
8	1	3	14
9	65	145	400
10	8	22	57
11	<1	<1	1
12	3	25	65

Appendix 6 RFSM EDA (Jamieson et al 2012)

Water Management
Volume 165 Issue WM1

A highly efficient 2D flood model with sub-element topography
Jamieson, Lhomme, Wright and Gouldby

ice | proceedings

Proceedings of the Institution of Civil Engineers
Water Management 165 Month 2012 Issue WM1
Pages 1–15 http://dx.doi.org/10.1680/wama.12.00021
Paper 1200021
Received 31/01/2012 Accepted 07/06/2012
Published online 00/00/2010
Keywords: floods & floodworks/hydraulics & hydrodynamics/mathematical modelling

ice Institution of Civil Engineers
publishing

A highly efficient 2D flood model with sub-element topography

1 **Sam R. Jamieson** MSci
PhD Candidate, Heriot-Watt University, Edinburgh in partnership with HR Wallingford, Wallingford, UK

2 **Julien Lhomme** MSc, PhD
Senior Scientist, HR Wallingford, Wallingford, UK

3 **Grant Wright** MEng, PhD
Lecturer, Heriot-Watt University, Edinburgh, UK

4 **Ben Gouldby** BSc
Principal Scientist, HR Wallingford, UK and IH Cantabria, Spain




The need for large- (region-)scale probabilistic simulations means that 2D inundation models are still limited by computational requirements. In addition to parallelisation and physical process simplification, attempts to reduce runtimes typically involve coarsening the computational mesh, which can smooth important topographic features and hence limit accuracy. This paper presents a new 2D flow model that uses an enhanced diffusion-wave, and incorporates sub-element topography in a computational mesh that adapts to the terrain features. The model utilises a fine topographic resolution without having to use a fine computation mesh, and so achieves fast computational runtimes. The model has been tested against the Environment Agency's 2D benchmarking tests, and even though the model is designed to operate at larger spatial scales than those in the benchmarking tests, it is shown to provide comparable accuracy relative to a selection of conventional 2D models, at significantly faster computational speeds. The model therefore has the potential to offer a step change in performance of large-scale probabilistic flood mapping and systems flood risk analysis modelling.

Notation

A_i	impact zone plan area (m^2)
A_p	panel flow area (m^2)
c	celerity of a wave (m/s)
f	an interface between impact zones
g	gravitational acceleration (m/s^2)
h_i	impact zone water depth (m)
i, j	impact zones
n	Manning's coefficient of friction
$\boldsymbol{n}_j$	directional unit vector between an impact zone and its neighbour j
P_p	panel wetted perimeter (m)
p	interface panels/sections
Q_f	interface flow rate (m^3/s)
Q_p	panel flow rate (m^3/s)
R_p	panel hydraulic radius (m)
S_f	interface water surface slope (m/m)
t	time (s)
$\boldsymbol{u_i}$	impact zone velocity vector (m/s)
V_i	impact zone volume (m^3)
w_f	interface width (m)
X_i	impact zone cross-sectional flow area (m^2)
η_f	interface water level (m)
η_i	impact zone water level (m)
α	constant used for scaling the Courant number
β	constant used for velocity calculation
ς_p	frictional wetted height on panel sides (m)
Δx	sub-element (or panel) cell width (m)

1. Introduction

Large-scale flood mapping is a primary requirement of the Floods Directive (EC, 2007), and probabilistic flood risk models that require computationally efficient 2D components are in increasing demand. The Environment Agency of England and Wales' (EA) national flood risk assessment (NaFRA) (Environment Agency, 2009) and modelling decision support framework (MDSF2) (Environment Agency, 2011) have utilised simplified inundation models for almost a decade, due to the number of simulations required to undertake comprehensive risk analyses (Gouldby *et al.*, 2008a; Hall *et al.*, 2003). These risk models have also been successfully applied for a wide range of other purposes (e.g. Evans *et al.*, 2006; Gouldby *et al.*, 2008b; Woodward *et al.*, 2011), and there is increasing demand to improve the reliability of the results, particularly the inundation aspects (National Audit Office, 2011).

It is well established that for a given hydrological input, ground elevation and topographic features dominate the hydraulic inundation process (Romanowicz and Beven, 2003; Zhang and Cundy, 1989). In small-scale studies, particularly urban environments, computational grid sizes must be of the order of 1–5 m to appropriately characterise the underlying topography (Mark *et al.*, 2004). In practice, however, large-scale and probabilistic simulations can rarely be completed at this resolution. Reducing the grid size, for example, has a dramatic effect on the computational cost associated with full shallow-water equation (SWE) models and, counterintuitively, regular grid diffusion-wave models tend to be even slower at such resolutions (Hunter *et al.*, 2008).

While it is evident that 2D inundation simulations over large areas cannot be achieved with grids of equivalent length-scale to natural topographic variation, using traditional grids with coarse resolution can artificially smooth important topographic features. To address this shortcoming, there has been increasing development of models that employ a sub-grid representation with the aim of improving topographic detail while maintaining computational efficiency (Casulli and Stelling, 2011; Hartnack *et al.*, 2009; McMillan and Brasington, 2007; Yu and Lane, 2006b). Yu and Lane (2011) found that post-processing of the DEM to re-introduce the topographic features improves the simulation accuracy of their sub-grid approach. This demonstrates that although accounting for sub-grid mass storage effects, most sub-grid approaches have difficulty representing sub-grid flow blockage effects unless the grid cell boundaries are perfectly aligned with topographic features. An exception to this is the multi-layered approach of Chen *et al.* (2008), which can cope with urban flow blockages within a grid cell. Yet this is limited to simplistic building layouts and it would be difficult to apply to real catchment topography. For coarse modelling this issue was avoided in the past by using manual delineation of flood cells along floodplain features, such as railway embankments and dykes (Estrela and Quintas, 1994; Romanowicz *et al.*, 1996; Zanobetti *et al.*, 1970), but manually creating such grids is subjective and expensive and cannot be practically undertaken at a large scale.

This grid issue has, to some extent, been resolved by the rapid flood spreading method (RFSM) (Gouldby *et al.*, 2008a; HR Wallingford, 2006), wherein computational elements, known as impact zones, are automatically defined to precisely follow topographic features. In addition, the sub-element topography is resolved at the level of the underlying digital elevation model, and so always captures the critical topographic crests causing flow blockage, without the need to manually re-introduce these features.

The RFSM was first implemented with a simple spreading algorithm that conserved volume but did not represent the temporal evolution of the flood wave (direct RFSM). This was later improved with a version that attempted to account for the frictional and dynamic effects of floodplain propagation, using a simplified approach (Lhomme *et al.*, 2009). More recently, attempts have been made to improve process representation by incorporating a time-stepping analytical approximation to the diffusion wave (dynamic RFSM) that is similar in dynamics to the raster storage model Lisflood-FP (Bates and De Roo, 2000). Output from this model compared well with that from a full SWE model on a large-scale site in Ireland (Lhomme *et al.*, 2012), but less well when employed in the EA's 2D hydraulic modelling benchmark tests (Wright *et al.*, 2012). Under these tests, accuracy was constrained due to the use of a constant time step and flow limiters, as has been demonstrated in other diffusive-type models (Hunter *et al.*, 2005).

This paper presents a new version of the RFSM model that overcomes some of the limitations noted above. This new model, RFSM-EDA (RFSM – explicit diffusion wave with acceleration term) – follows the sub-element impact zone approach but uses a new formulation, similar to the diffusion wave but incorporating the local acceleration term of the Saint Venant equations (Bates *et al.*, 2010). An adaptive time step has been implemented, and all flow limiters have been removed. The effectiveness of the model is demonstrated using a selection of the EA's 2D hydraulic benchmark tests (Wright *et al.*, 2012).

2. Model

RFSM-EDA is based on the same mesh concept as the direct RFSM (Gouldby *et al.*, 2008a; Lhomme *et al.*, 2009) and the dynamic RFSM (Environment Agency, 2010, Lhomme *et al.*, 2012). See Figure 1 for a mesh schematic. It incorporates the following primary assumptions.

- The domain can be divided up into discrete and hydraulically consistent topographic depressions, called impact zones (IZs).
- The water surface elevation within each IZ is constant.
- The relationship between water surface elevation and volume in an IZ can be defined by a non-hysteretic relationship.
- The flow rates between neighbouring IZs are calculated linearly across the interface between them, independently of other neighbours.
- The interface can be characterised by a level–width relationship, where the width is assumed to increase with increasing level.

2.1 Pre-processing algorithm

Before computation can begin, the IZs are defined through a pre-processing algorithm. In a first stage, IZs are delineated around collections of cells which, following the line of greatest slope, would drain to the same topographic low point. This produces IZ boundaries defined along topographic crests and high points. In a second stage, the original IZs are modified to ensure that they are above a certain minimum area, and that the interfaces between them are above a minimum communication depth. These modifications are controlled by user-defined parameters; appropriate values will vary depending on the landscape and the DEM resolution. Finally, the level–volume and neighbour level–width

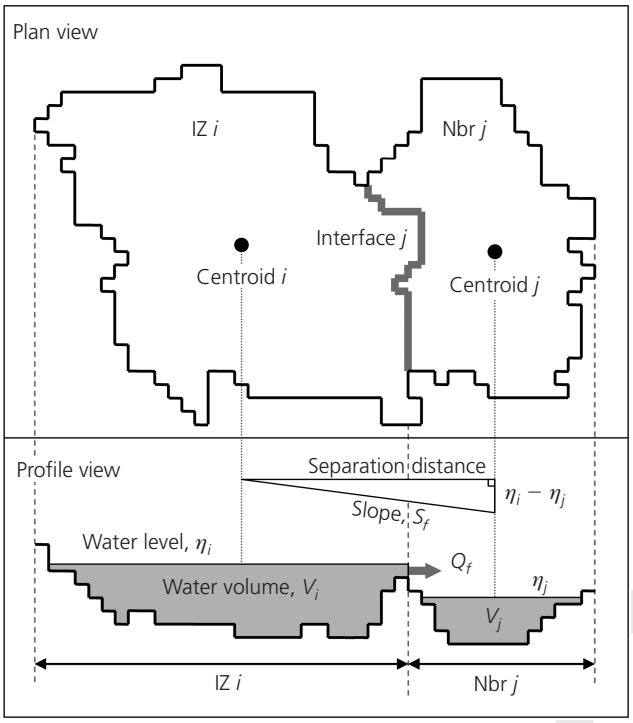

Figure 1. Schematic of an impact zone with a neighbour, in plan and profile. Showing irregular boundaries and selected key variables. Solid grey represents a volume of water

relationships are calculated, and the results are written to a database.

2.2 Governing equations

The derivation of the flow equations stems from the approach of Bates *et al.* (2010). Starting with the one-dimensional Saint Venant equations, advection is assumed negligible and the equations are discretised semi-implicitly, but rearranged into an explicit form. The hydraulic radius is calculated in full including the friction on the side of cells. This differs from other models (e.g. Bates *et al.*, 2010; McMillan and Brasington, 2007; Yu and Lane, 2006a) because the assumption that friction is only encountered on the cell base may not be appropriate in highly variable terrain. A single flow is required for each neighbour interface, *f*, but to avoid sudden changes in hydraulic radius in complex topography, the fluxes are evaluated as the sum of individual fluxes across a number of interface panels, equal to the number of sub-element cells, *p*, in the interface:

$$1.\quad Q_f^{t+\Delta t} = \sum_p \frac{(Q_p^t - \boldsymbol{g}\Delta t A_p^t S_f^t)}{1 + \boldsymbol{g}\Delta t n^2 |Q_p^t| / A_p^t (R_p^t)^{4/3}}$$

where Q_f is the interface flow, Q_p is the panel flow, t is time, $\boldsymbol{g}$ is gravitational acceleration, A_p is panel area, R_p is hydraulic radius of the panel, n is Manning's coefficient and S_f is the water surface slope across the interface. See Figures 1 and 2 for schematic diagrams showing the relationship between the variables.

The panel hydraulic radius is calculated by

$$2.\quad R_p^t = \frac{A_p^t}{P_p^t}$$

The panel area, A_p, is the difference between the interface water level, η_f, and the panel ground level, z_p, multiplied by the sub-element cell width, Δx:

$$3.\quad A_p^t = \Delta x(\eta_f^t - z_p)$$

The panel wetted perimeter, P_p, is the summation of the wetted base (i.e. the width of the sub-element cell) and the wetted height to one or both of the adjacent panels, ς_p:

$$4.\quad P_p^t = \varsigma_p + \Delta x$$

To evaluate A_p, the interface flow level, η_f, is needed, and a number of different approaches can be applied. Using the mean of the levels in the adjacent IZs is problematic because negative depths occur when the downstream level is below the interface crest. The dynamic RFSM (Lhomme *et al.*, 2012) avoids this by switching to the upstream level when the mean level would create a negative depth. However, this can cause sudden and cyclical jumps in the interface depth if the downstream level fluctuates

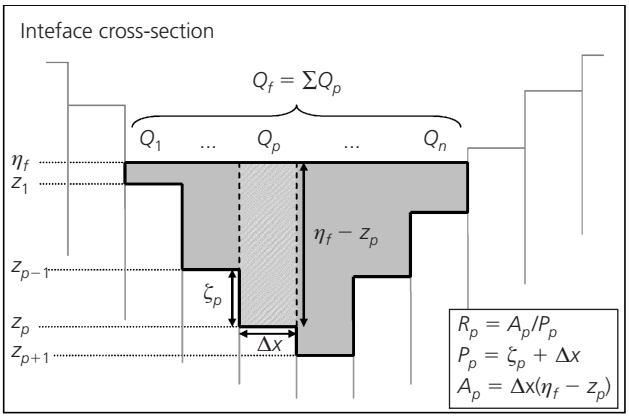

Figure 2. Schematic of an interface between two neighbouring impact zones. Solid grey colouring represents water part-submerging the interface, and the demarked rectangle represents a calculation panel corresponding with an individual sub-element cell

around the level of the interface. In RFSM-EDA a smoother result is obtained by always using the upstream level:

$$\eta_f^t = \max(\eta_i^t, \eta_j^t) \quad (5)$$

The interface slope, S_f, is calculated by dividing the difference in neighbouring IZ water levels by the separation distance between their centroids.

The solution is progressed by applying the conservation of mass:

$$V_i^{t+\Delta t} = V_i^t + \Delta t \sum_j Q_f^{t+\Delta t} \quad (6)$$

where V_i is the volume in IZ i, and j is an IZ neighbour of i. V_i is a function of η_i, the IZ water level, and this relationship is defined in advance in look-up tables created during the pre-processing stage. Therefore, the IZ volume can be efficiently converted into a water level for use in the flux calculations.

2.3 Numerical stability

The scheme is subject to the Courant–Freidrichs–Lewy (CFL) condition, which is satisfied by ensuring that the domain of dependence of the interfaces of an IZ should not exceed the area of the IZ, as used by Guinot and Soares-Frazao (2006). This version of the CFL condition is more appropriate for irregular-shaped elements than that used by Bates *et al.* (2010), because it uses areas rather than lengths. It also differs by including velocity with celerity. The maximum permissible time step, $\Delta t_{\max}$, is given by

$$\Delta t_{\max} = \alpha \min \frac{A_i^t}{\sum_j w_f \max(\|\boldsymbol{u}_i^t\| + c_i^t, \|\boldsymbol{u}_j^t\| + c_j^t)} \quad (7)$$

where α is a constant used to scale the predicted time step, A_i is the surface area of i, w_f is the interface width, $\boldsymbol{u}_i$ is the magnitude of the IZ velocity vector, and the celerity of a wave, c, is given by

$$c_i^t = \sqrt{g h_i^t} \quad (8)$$

where h_i is the depth of water in IZ i.

2.4 Wetting/drying

In some reduced complexity models an algorithm is used to reduce over-rapid wetting or drying (Bradbrook *et al.*, 2004; Yu and Lane, 2006a). As the IZs are assumed to have topographic barriers as crests between them, when an IZ initially wets, the water cannot leave until it fills the volume below the lowest interface level of its neighbours. Similarly, as an IZ dries, inappropriately large flows will not cause a negative depth, as the stored volume below the minimum interface level will absorb the excess flux. These effects, resulting from the IZ shape, provide a natural resistance to model instability. Therefore no special wetting or drying treatments are explicitly represented within the model.

2.5 Velocities

The velocities calculated at the interfaces could be used as a surrogate for the IZ average velocity in flat topography, but this is not appropriate when the IZs have a depression-like shape. In this case the interface velocities are expected to be relatively shallow and fast, compared with deeper and slower flow conditions at the IZ centre. To convert the interface velocities to an area-average velocity vector, an additional step is necessary. Assuming the IZs are of regular shape, the volume of water that has been fluxed out of the IZ (using the results of Equation 1) is divided by the area of a representative cross-section through the centre of the IZ, X_i:

$$\boldsymbol{u}_i^t = \frac{\Delta t \sum_j Q_j^t \boldsymbol{n}_j}{X_i^t} \quad \text{where } Q_j^t > 0 \quad (9)$$

where $\boldsymbol{n}_j$ is the unit vector between the IZ and neighbour centroids, used to provide the velocity as a vector. Whether the IZ shape is assumed cubic, cylindrical or as an inverted cone, the calculation for the IZ cross-sectional area can be written as

$$X_i^t = \beta \sqrt{(h_i^t V_i^t)} \quad (10)$$

where β is a constant which for the aforementioned shapes takes on a value between 0·96 and 1·13. As we assume the IZs to be of variable shapes and sizes, β is given a value of 1 for simplicity. It is important to note that this velocity does not impact on the fluxes between IZs, which are calculated independently. The only impact it has on the model is through the CFL condition (Equation 7).

3. Application

3.1 ■■■■■■

3.1.1 Environment Agency benchmark tests

The EA has produced a set of hydraulic benchmark tests designed to test a range of predictive abilities of 2D inundation models. Details of the test specifications are provided in Wright *et al.* (2012) and Environment Agency (2010), so they are only briefly described in this paper. RFSM-EDA has been assessed on most of these tests, although only the results of tests 2A, 4, 5 and 8A are shown here. Table 1 provides a breakdown of the tests, with a justification provided for those not shown.

Test	Shown in paper?	Reason
1	×	RFSM-EDA, as most models, performs well on this test, but there is little of interest in the results
2A	✓	See Section 3·2
3	×	A test of momentum conservation, which the numerical scheme of RFSM-EDA is not expected to achieve
4	✓	See Section 3·3
5	✓	See Section 3·4
6	×	Dam break scenarios require a full SWE scheme with shock-capturing ability, so RFSM-EDA is not tested
7	×	Dynamic linking with a 1D element has not yet been tested for RFSM-EDA
8A	✓	See Section 3·5
8B	×	Dynamic linking with a 1D element has not yet been tested for RFSM-EDA

Table 1. Benchmarking tests that have been completed, and justification for those not

3.1.2 Comparison with other models

RFSM-EDA has been compared against a number of other models to provide a context for the results, rather than to draw specific conclusions about these individual models. While this is not a rigorous test of the model's validity, in the absence of validation data the model is compared with a range of respected and widely used models. Two finite-volume SWE models are shown, InfoWorks-ICM (Innovyze, 2011; Lhomme *et al.*, 2010) and Tuflow-FV (2nd-order spatial accuracy) (Environment Agency, 2010). Three simplified models are also shown: JFLOW-GPU, a regular grid diffusion-wave model (Bradbrook *et al.*, 2004; Lamb *et al.*, 2009); the dynamic RFSM, also a diffusion-wave model but with the same sub-element representation as RFSM-EDA (Environment Agency, 2010; Lhomme *et al.*, 2012); and Lisflood-ACC, which has a similar numerical approach to RFSM-EDA but is based on a regular grid (Bates *et al.*, 2010; Neal *et al.*, 2011). For these tests all the models adhered to the test specifications apart from the dynamic RFSM, which used an equivalent (though not identical) mesh to 'mesh A' used by RFSM-EDA, described in the following section.

3.1.3 Application of RFSM-EDA

The primary results for RFSM-EDA are created using a mesh significantly coarser than in the other models, but with a sub-element cell resolution corresponding to the specified grid resolution of the tests. This is called mesh A. However, some extra simulations have been carried out using different computational meshes that offer additional insight. Mesh B uses a similarly coarse computational grid, but utilises the finest topographic resolution available in the raw DTM for its sub-element resolution. Mesh C replicates the test specification exactly, like the other models. This means using a fine computational mesh, with each RFSM-EDA mesh element containing one topographic sub-element cell. A summary of the three mesh types for the different tests is provided in Table 2.

For meshes A and B, the results have been produced with significantly coarser meshes than recommended, and this should be noted when considering the results. For example, the comparative models have extracted results from small grid cells containing only the specified test points, whereas RFSM-EDA uses considerably larger computational elements, which may represent the hydraulic conditions not just in the location of the test points but at distal locations as well.

Mesh C has been used for tests 2A and 5 for comparative purposes, but in practice RFSM-EDA would not be used on such a mesh, as there are no benefits in using the IZ methodology when each IZ contains only one sub-element cell. In fact, the additional computational overhead of the sub-element approach (e.g. calling volume/level look-up tables) makes the use of IZs with one sub-element cell, or only a few cells, more costly than using 'traditional' grids.

All the RFSM-EDA simulations were completed on a machine running Windows XP with a 3·0 GHz processor and 8 GB of RAM, connecting to an SQL database on a network server.

3.2 Test 2: Filling of floodplain depressions

Test 2 is designed to demonstrate a model's ability to deal with inundation processes in a low-momentum event. The test is a square domain of 16 topographic depressions, with test points in each, and an inflow hydrograph in the top left corner. This is an extreme test of the IZ schematisation; rather than the specified ~10 000 elements, the RFSM-EDA mesh A uses only 16 automatically generated elements, one per depression. This means that mesh A had 625 times fewer computational elements, with the same 20 m topographic resolution. RFSM-EDA is capable of further increasing the topographic resolution, and mesh B has the same 16 elements, but with a 2 m topographic resolution, 10 times greater than the other models. Mesh C has the recommended 10 000 elements. See Table 2 for details.

Figure 3 shows the model results at test point 4 (closest to the

EA Test	Test specification	Details of RFSM-EDA meshes					
		Mesh A		Mesh B		Mesh C	
	Cell size: m^2 (~no. of elements)	Average IZ size: m^2 (no. of IZs)	Sub-element cell size:m^2	Average IZ size: m^2 (no. of IZs)	Sub-element cell size: m^2	Average IZ size: m^2 (no. of IZs)	Sub-element cell size: m^2
2A	400 m^2 (10 000)	250 000 m^2 (16)	400 m^2	250 000 m^2 (16)	4 m^2	400 m^2 (10 000)	400 m^2
4	25 m^2 (80 000)	2 300 m^2 (861)	25 m^2	Not undertaken		Not undertaken	
5	2 500 m^2 (7 600)	35 000 m^2 (530)	2 500 m^2	Not undertaken		2 500 m^2 (7 643)	2 500 m^2
8A	4 m^2 (97 000)	212 m^2 (1 786)	4 m^2	174 m^2 (2 207)	0·25 m^2	Not undertaken	

Table 2. Details of mesh sizes and sub-element cell resolutions for meshes A, B & C.

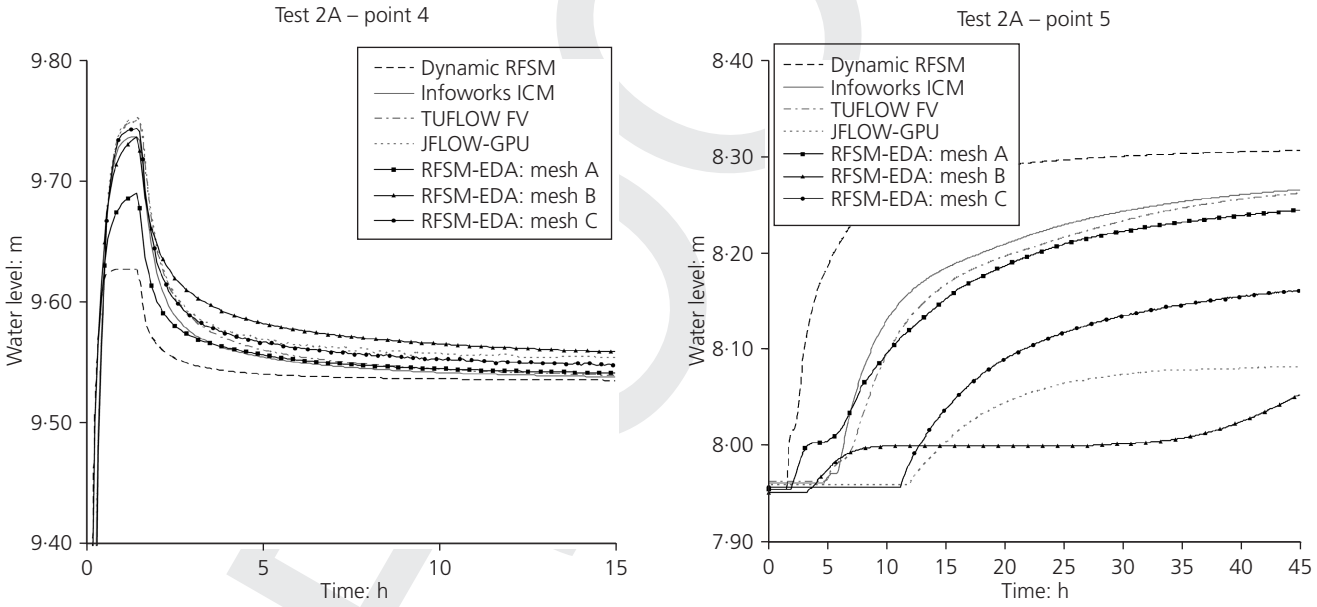

Figure 3. Level plots for test 2 – points 4 and 5

boundary condition) and point 5 (the farthest point from the boundary condition, which receives a significant flow of water). At point 4, RFSM-EDA's mesh A results have a similar profile to the other models, but the peak level is ~4–6 cm lower. The final level matches the other models exactly. At point 5 there is a large spread in the results of all models, not just the ones shown here (Environment Agency, 2010). Even so, RFSM-EDA's results closely match those of Tuflow and InfoWorks, and from 6 h on they remain within 2 cm of Tuflow. RFSM-EDA predicts the water levels to rise ~2·5 h earlier than the other models. This is due to the large IZs of RFSM-EDA. When water over-tops the preceding crest it immediately fills up from the IZ base (the location of the test point). For the other models the water must travel through a number of cells after the crest before it reaches the test location.

Mesh B produces a response that is quite different from the other models (Figure 3). Although it matches the peak level of the other models at point 4, the final level is 1–2 cm higher. This is because, rather than averaging the DEM to 20 m, it utilises all

the topographic information available at a 2 m resolution. Therefore, this mesh depicts the crests with a higher level of accuracy than the models using the averaged 20 m DEM. Once the water has spread over several depressions and reached point 5, there is a noticeable cumulative effect; the water levels rise significantly only after 35 h. For this test, therefore, the topography has a greater impact on the results than the physical complexity of the model.

RFSM-EDA is also used with mesh C, which matches the test specification with 10 000 IZs. As would be expected, the results have a close match to the other models. At point 4 they remain with 6 mm of JFLOW, and at point 5 the results lie in the middle of all the others, and are closest to JFLOW. Although not a model validation, this demonstrates that RFSM-EDA behaves as expected when used with the same computational resolution as the other models.

The mesh A results show a significant improvement over the older dynamic RFSM, which reaches a peak level approximately 10 cm lower than the other models at point 4. At point 5 the dynamic RFSM's levels rise much too fast and finish ~4 cm higher than with InfoWorks and Tuflow.

The RFSM-EDA simulations using meshes A and B were computationally fast, with equal runtimes of ~0·9 s. A large proportion of this time was spent communicating with the SQL database that holds the data, and therefore increasing or decreasing the alpha value had little or no effect on simulation runtimes, and the increased topographic resolution of mesh 'B' did not slow the model relative to mesh 'A'. The depression shape of the IZs meant that there was a natural resistance to mass balance errors. The simulations were completed with alpha values of 1, with median time steps of ~62 s. No instabilities were found and the mass balance errors were 0%. The simulation with mesh C had only one sub-element cell in each IZ, so did not benefit from the IZ depression shape. However, it was also able to use an alpha value of 1 with only a 0·3% mass balance error.

Overall the results of test 2 show that RFSM-EDA can effectively predict propagation of flood waters over a complex domain. This is encouraging given that only 16 computational elements are used.

3.3 Test 4: Rate of propagation over extended floodplains

The speed of propagation of a flood wave is tested in test 4. A completely flat domain is used, with an inflow hydrograph applied at the centre of the left boundary, to produce a semi-circular flood wave. It is not possible to automatically generate the IZs as there is no topographic variation in the domain; a regular grid has therefore been used. The specified resolution is 5 m with approximately 80 000 elements. For this test, RFSM-EDA uses mesh A with 861 elements, 93 times fewer than the specification. There is no value in assessing results of mesh B or C due to the flat topography.

Figure 4 shows 15 cm depth contours at 1 h and 3 h after start of inundation. The coarse resolution means RFSM-EDA is not able to resolve the wetting front to the same level of detail as the other models. However, the speed of propagation is a significant improvement over the dynamic RFSM, which appears too slow and also appears to exhibit some oscillatory behaviour at the wetting front. InfoWorks and Tuflow predict the flow boundary in concentric circles, whereas RFSM-EDA exhibits a very slight preferential flow towards the diagonals, similar to Lisflood-ACC. This has been seen in several models that have the x and y flow directions decoupled (Neal *et al.*, 2011). For all tests completed by RFSM-EDA, this pattern has only been observed on perfectly flat topography when using a regular grid. It is therefore not expected in real topographic environments.

Figure 5 shows the level plot at point 2, 100 m from the inflow. As the RFSM-EDA's grid cells are large, the water reaches test point 2 marginally before the other models, but the form of the curve matches those of the other models well, with a peak level of 26·1 cm compared with 26·6 cm for Lisflood-ACC and 27·5 cm for Tuflow. RFSM-EDA's velocity profile has the correct shape, although the results are too low, with a peak velocity of 0·20 m/s compared with 0·23 m/s and 0·25 m/s for Lisflood-ACC and Tuflow, respectively. This may be due to the assumptions used in the area-averaging for the velocity calculations.

RFSM-EDA completed the test using an alpha value of 3, which produced a runtime of ~13 s, significantly faster than any other model (the fastest other model took nearly six times longer). This was achieved with zero mass balance errors.

3.4 Test 5: Valley flooding

Test 5 simulates a major flood inundation from a dam failure in a valley. The test domain has a constant downward slope with a hydrograph applied at the top of the valley. For mesh A, a regular square grid was adopted as few depressions could be found. The mesh had 530 elements, each 200 m square (except at the domain boundary), whereas the specified resolution was over 14 times this number of elements, with approximately 7600. For mesh C, 7643 IZs where used with one sub-element cell per IZ to match that of the other models.

Figures 6 and 7 respectively show the first and last test points in the domain. The IZs in mesh A generally have 16 sub-element cells in them. The test point will be at one of these cells, but normally at least one of the other 15 sub-element cells will have a lower level. This is why the levels for mesh A can be seen to start from a lower level than the other models. At point 1 the levels finish ~28 cm lower than Lisflood-ACC, and peak ~21 cm lower. It is clear that the Dynamic RFSM did not perform well for these tests, which is probably due to the use of flow limiters.

Mesh C shows that when running at the recommended resolution, RFSM-EDA produces results that are very similar to the other models. In fact, they are almost indistinguishable from those of

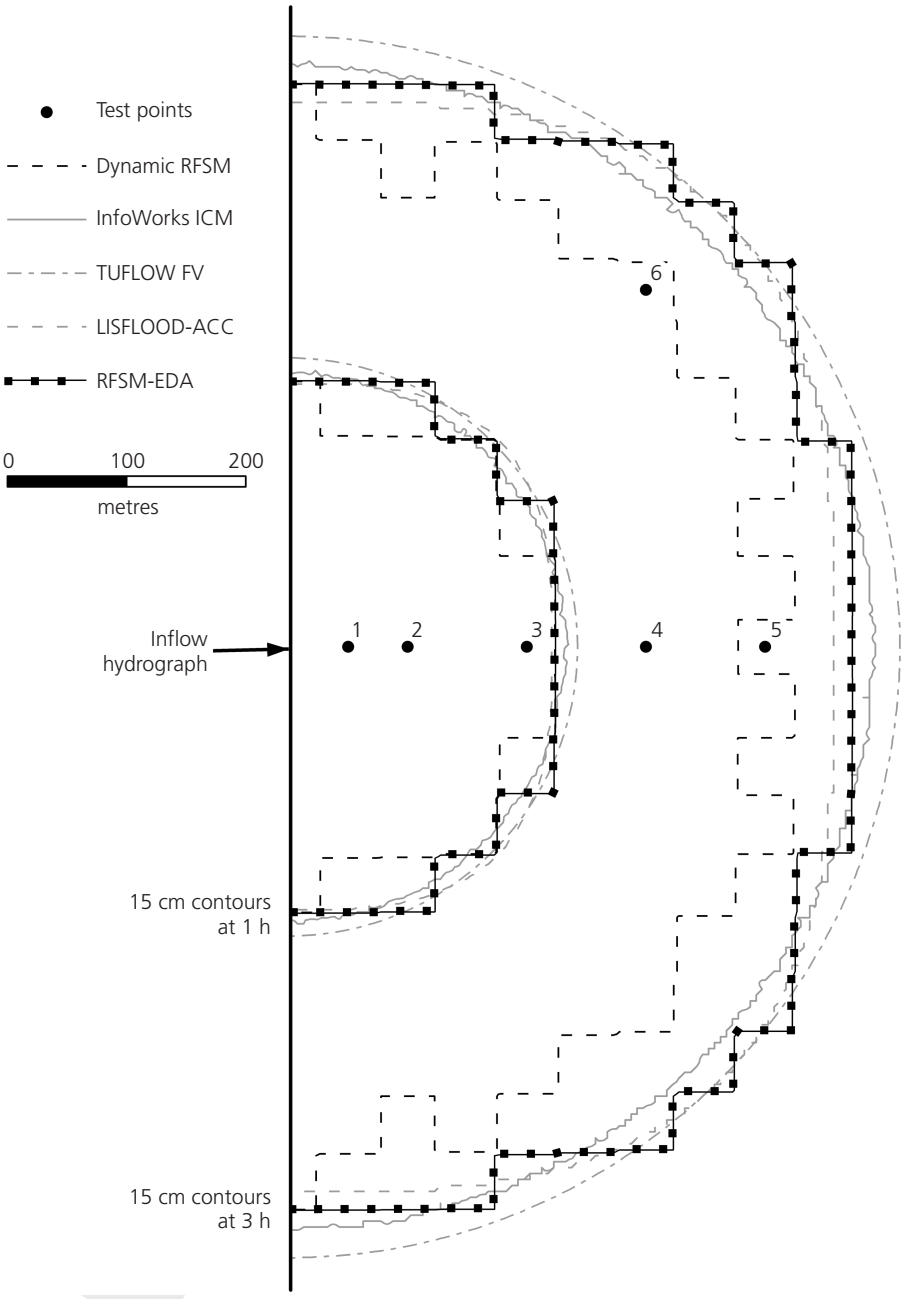

Figure 4. Depth contours (15 cm) at 1 h (inner concentric lines) and 3 h (outer concentric lines) for test 4

Lisflood-ACC. This is to be expected as when there is only one sub-element cell in the IZ the governing equations simplify to an equivalent of Bates *et al.* (2010). The differences seen between RFSM-EDA's results for mesh A and the other models are therefore primarily caused by the size of the IZs. Normally IZs have a natural resistance to over-rapid spreading of water, as each IZ must fill up a depression to the crest level before it can continue to flux. However, on test 5 there is an almost constant slope and very few depressions can be found. The IZs fill up from the lowest sub-element cell, and can immediately continue to flux, causing over-rapid down-slope wetting. This has a cumulative effect down the whole valley. At point 1 (~3·2 km from the inflow) the levels start to rise ~7 min earlier than in the other models, but by point 5 (~15·7 km from the inflow) it is ~50 min too early. The wetting front propagates at 7·1 km/h for RFSM-EDA, and at an average 5·2 km/h for the other models.

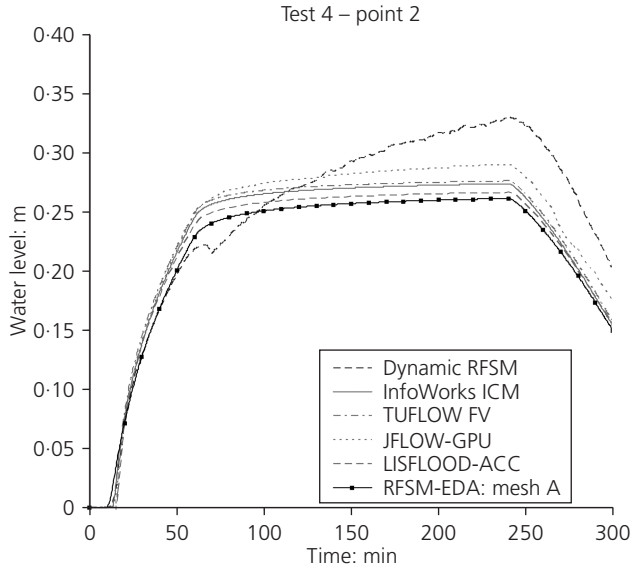

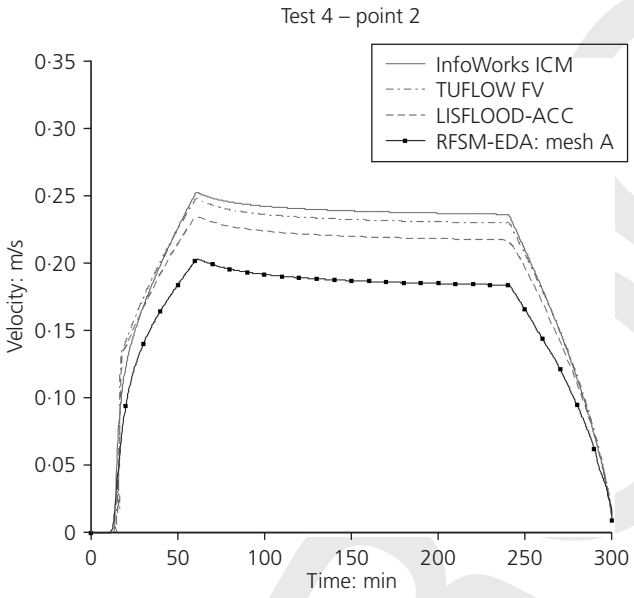

Figure 5. Levels and velocities for test 4 – point 2, 100 m from the inflow

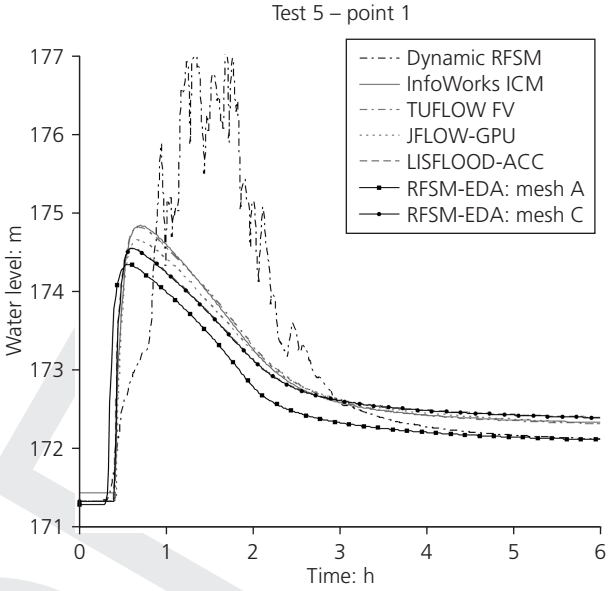

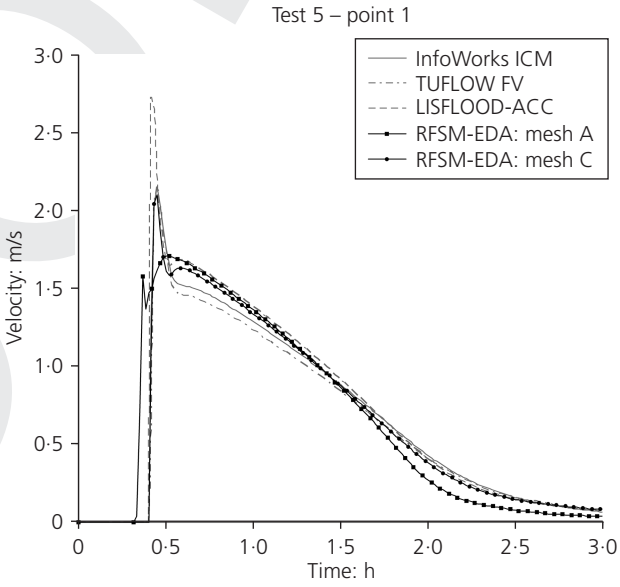

Figure 6. Levels and velocities for test 5 – point 1, near the inflow source

The velocities predicted by RFSM-EDA (mesh A) match the other models well. At point 1 the velocities for RFSM-EDA remain within 0·15 m/s of the other models, except for a ~5 min window at 0·5 h where it peaks ~0·4–1 m/s lower. Adjusting for the time lag, at point 5 the velocities of RFSM-EDA remain within 0·1 m/s of the other models, except for a 15 min window when they are ~0·1–0·4 m/s lower.

RFSM-EDA (mesh A) was run with an alpha value of 2, which resulted in a final mass balance error of only 0·02%. It completes the simulation in ~14 s, which is significantly faster than all other models that undertook the test (ranging from 0·6 to 350 min). The mesh C model was also run with an alpha value of 2, and had zero final mass balance errors.

3.5 Test 8A: Rainfall and point source surface flow

This is a test of high-resolution modelling in an urban environment, initially from a global pluvial event, and subsequently from a surcharging culvert in the top right corner of the domain. The simulation is run long enough to allow the water to settle in the lower areas.

This test case has real topography and RFSM-EDA can therefore use its automatic mesh generation. The resulting IZs have quite

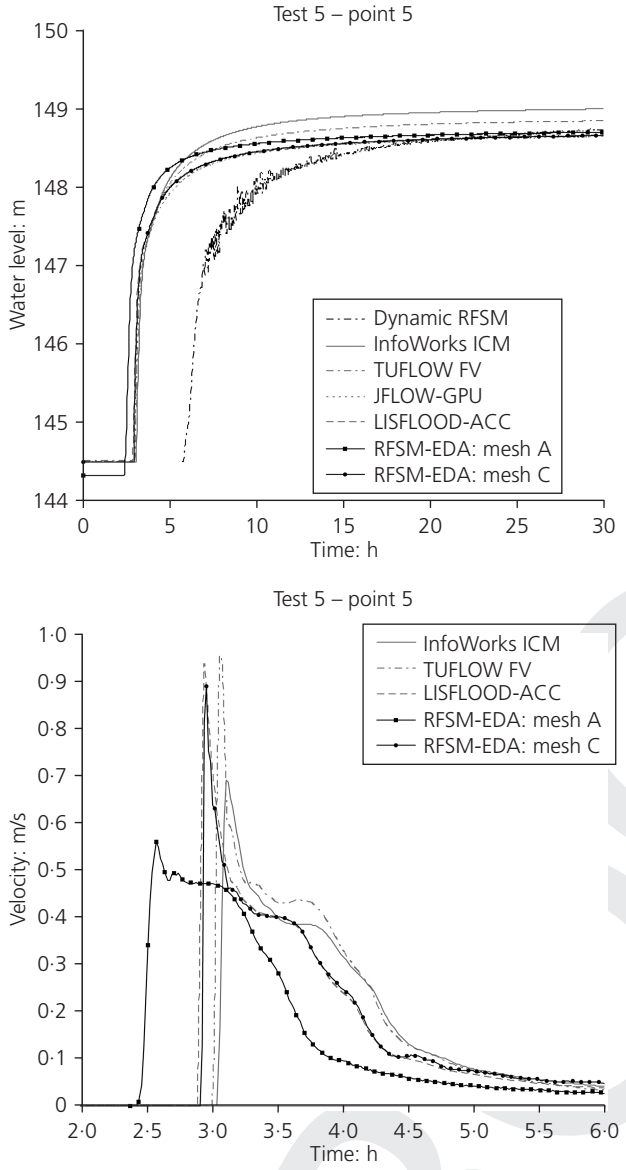

Figure 7. Levels and velocities for test 5 – point 5, at the bottom of the valley

complex shapes and neighbour relations, as shown in Figure 8. Mesh A has 1786 IZs with the recommended topographic resolution of 2 m. This is ~54 times fewer than the specified 97 000 elements. Mesh B is also used, which has 2207 elements and a sub-element resolution of 0·5 m.

The results for RFSM-EDA are good considering that the scale of the test is far smaller than the model was designed for. Results for meshes A and B both have levels approximately 10 cm higher than the other models at point 7 for both the first and second peaks (Figure 9). For point 8 (Figure 10), mesh A results are ~8 cm higher at the first peak and 1–2 cm lower for the second peak, whereas mesh B results are 1–2 cm higher for both peaks. The final levels are similar for all models in point 7, but very widely spread for point 8. This indicates that the different models have likely sampled or averaged the raw DTM in different ways. The dynamic RFSM performs poorly and does not match the shape of the curves as well as RFSM-EDA does. Although the timing of the velocities is good, the magnitudes are lower for both meshes; roughly half that of the other models, with mesh B tending to have greater velocities. The IZs have complex shapes which encompass the major flow routes on the roads (where the test points are located) as well as the areas surrounding the roads. It is likely therefore that the lower velocities are a result of the velocity area-averaging over the large IZs.

While the local response of RFSM-EDA may differ in a few places from the other models, the overall model response is similar, and is illustrated by comparing the depth contours over the domain (Figure 11); note that to avoid complication, only the results of RFSM-EDA (mesh A) and Tuflow FV are shown in Figure 11. RFSM-EDA appears to match Tuflow very well for depths of 20 cm, but the lower depths of 5 cm are not very well depicted in certain parts of the domain, particularly the sloped areas to the east. This is investigated further by calculating the *F*-statistic, which measures the predictive accuracy of the inundated area (Horritt and Bates, 2001) relative to the Tuflow results. Mesh A has an *F* value of 54% for depths greater than 5 cm. When the depth threshold is increased to 20 cm, mesh A has an *F* value of 69%. For mesh B the predictions are 53% and 71%, respectively. Clearly RFSM-EDA has some difficulties simulating the shallow flow paths, but when greater depths are considered it performs much better. There is no major difference in the results of mesh A and B.

RFSM-EDA is run with an alpha parameter of 4 for these tests. For mesh A this gives a runtime of 2·90 min, much faster than any other model, and with a mass balance error of only 0·06%. For mesh B it runs in 4·32 min with a mass balance error of 0·83%. The longer runtime for mesh B is partially because it has ~24% more IZs, but it is also due to the finer sub-element resolution. On average an IZ in mesh B has ~27 sub-element cells in each interface, whereas mesh A has only ~6. This means that simulations using mesh B have a lot more calculations to undertake for the interface fluxes than simulations using mesh A.

3.6 Computational efficiency

Unlike most similar models, the data needed to run RFSM-EDA is stored in an SQL database. This allows for efficient modularisation within probabilistic modelling frameworks like MDSF2, but it can slow down the simulation through read and write access to the SQL server. Whilst this is not generally an issue unless a high frequency of intermediate results are required, it can dominate the performance in very short tests: for example, in test 2A one-fifth of the simulation time is spent in initialisation.

The simulation times for all models/tests are given in Table 3. It is important to note that these results may not present a fair comparison, as computers with varying specifications have been

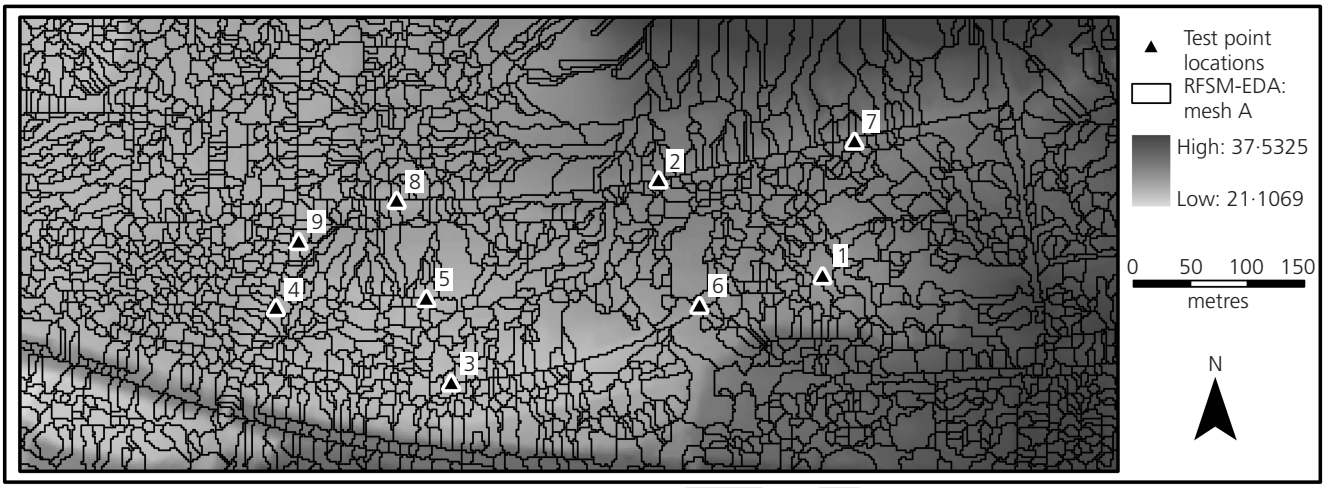

Figure 8. Impact zones in RFSM-EDA mesh A for test 8A, with DEM

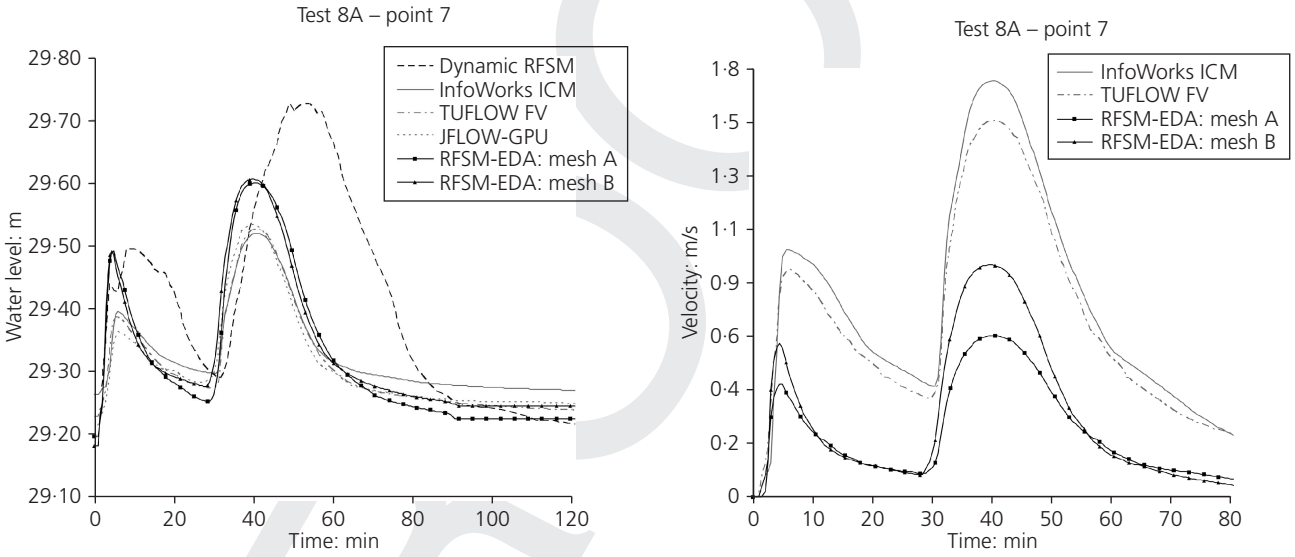

Figure 9. Levels and velocities for test 8a – point 7

used and some of the models also used parallel processing (e.g. Tuflow-FV, InfoWorks-ICM and JFLOW-GPU).

Table 3 clearly shows that RFSM-EDA is fast; the fastest in every test attempted. This has been achieved without the benefit of parallelisation. It performs well in these tests primarily because it was possible to maximise the benefit of the sub-element representation while undertaking the computations on a coarse grid. At larger spatial scales, for which the model has been developed, further benefits are likely to be realised.

It is also expected that using a single flux calculation (based on total interface properties as opposed to the compound section currently used) would significantly improve simulation runtimes.

4. Discussion

RFSM-EDA was designed to be used on large (city/regional) scales with variable (i.e. real) topography. The EA's benchmark tests are small scale and a number have artificially smooth topography. Despite this, the RFSM-EDA has demonstrated an ability to generate results that are in line with those of models that comprise a more complex representation of the physical processes and thus take a longer computational time. Moreover, RFSM-EDA can incorporate even finer-scale topography with

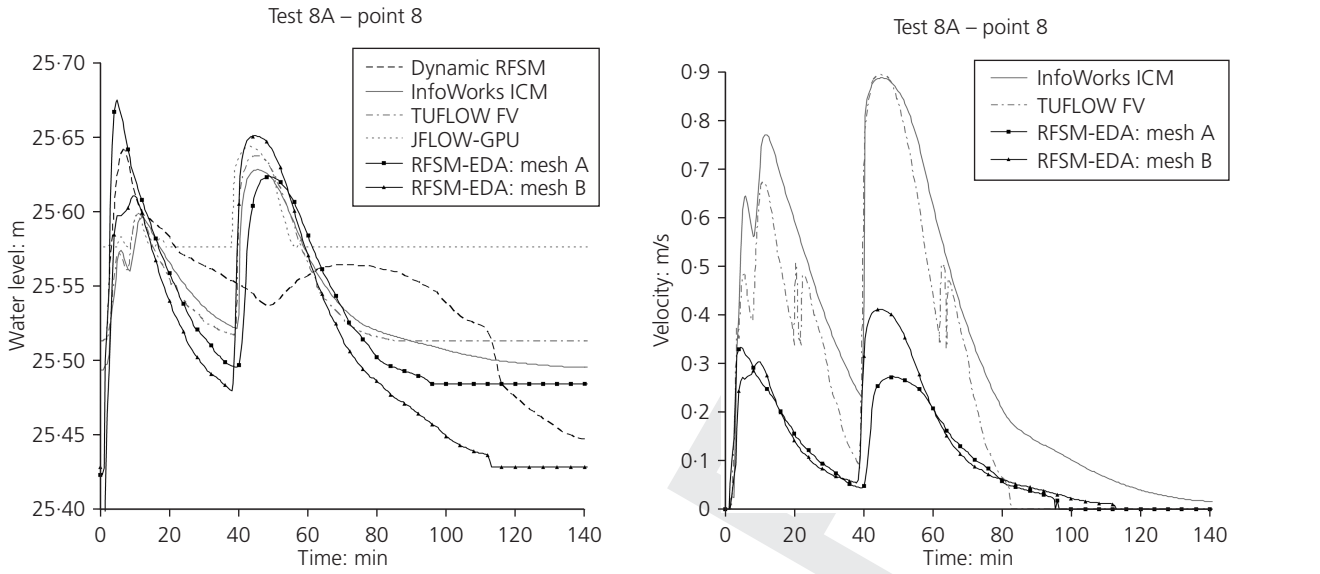

Figure 10. Levels and velocities for test 8a – point 8

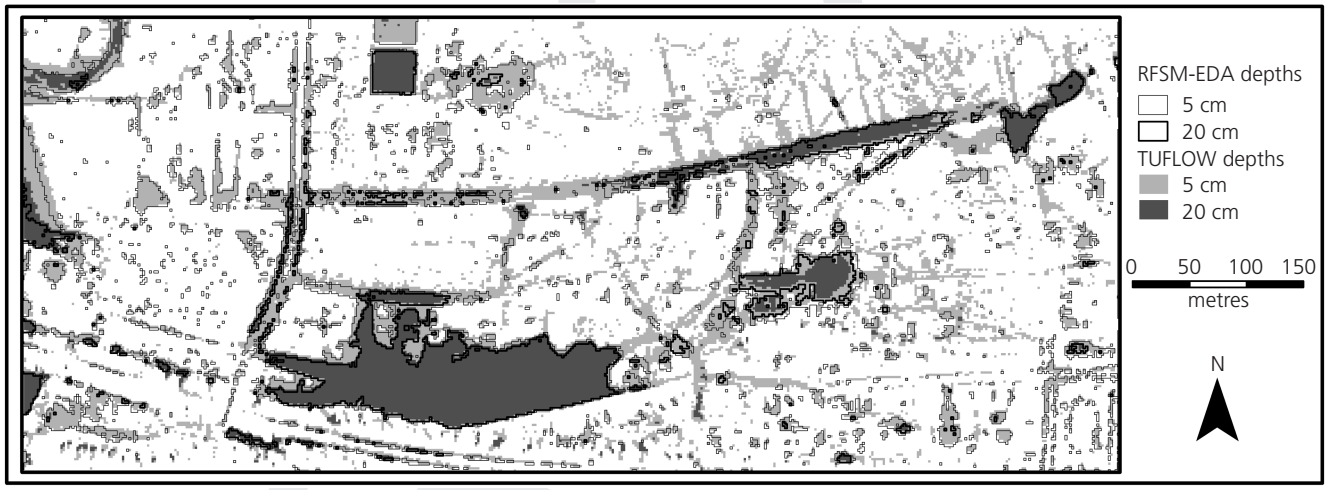

Figure 11. Depth contours for RFSM-EDA and Tuflow FV for test 8A

minimal impact on runtimes. This reduces the need of the modeller to introduce additional uncertainties to the modelling process by averaging or re-sampling the DEM. Given that much of the flood modelling undertaken in the UK is at larger spatial scales and often of a probabilistic nature, it may be appropriate to consider the introduction of additional tests that are able to appropriately verify models that are developed for this purpose.

The schematisation of RFSM-EDA means that water fills from the lowest point in an impact zone. On the relatively rare occasion that natural floodplain depressions do not exist, such as in test 5, water leaves an impact zone immediately upon wetting. This results in an overestimation of propagation speed by 36%. For large-scale probabilistic modelling this source of error is unlikely to be significant, and the results presented herein show that peak levels and flows are predicted reasonably accurately (see Figures 5 and 6). In other situations where RFSM-EDA results differ more markedly from those of the other models presented here, it is worth considering that the EA benchmarking report includes many more model results (Wright *et al.*, 2012), and the peak flood levels of RFSM-EDA are within the spread of these results.

The sub-element representation in RFSM-EDA offers an effective approach for reducing runtime while preserving or, in some cases, increasing topographic accuracy. The results using the

Model	Computation time in minutes for each test			
	2	4	5	8A
RFSM-EDA (mesh A)	**0·015**	**0·21**	**0·23**	**2·9**
Dynamic RFSM	0·19	5·8	9·8	23·3
Tuflow FV	2·64	24·5	2·9	72·6
InfoWorks ICM[a]	0·73	6·5	0·7	27·1
JFLOW-GPU	1·83	2·3	10·2	16·2
Lisflood-ACC[b]	n/a	1·97	0·68	n/a
Fastest other[c]	0·4	1·27	0·6	4
Slowest other[c]	130	282·8	350	307·8

[a] The runtimes are taken from InfoWorks RS, but the results in this paper are from InfoWorks ICM; little difference is expected.
[b] Lisflood-ACC runtimes appear in Neal *et al.* (2011).
[c] Fastest and slowest models other than those shown in this paper, but appearing in Wright *et al.* (2012).

Table 3. Simulation runtimes for different models, fastest in bold type

recommended DEM resolution matched the other models well. In some cases, such as test 2A, using an even higher DEM resolution produced a step change in model response, which implies that the topography has a greater effect on simulation results than process representation. Additionally, because the mesh is automatically aligned to topographic features such as embankments and dykes, it will always respect the effect they have on propagation directions, regardless of grid scale.

The adaptive time step used by RFSM-EDA has shown to be effective for all tests. Unlike Lisflood-ACC, which generally needs alpha values significantly below unity (Neal *et al.*, 2011), RFSM-EDA is stable with a value of 1 or significantly above. The fact that the alpha value could be as large as 4 in test 8A implies that the CFL condition used (Equation 7) may be conservative for this algorithm. It is likely that this is due to the inclusion of the velocity vector in the CFL condition, which is not included in the original model of Bates *et al.* (2010). Although several other diffusive models use velocity in their stability condition, such as Bradbrook *et al.* (2004), an alternative formulation that excludes velocity may be more appropriate for RFSM-EDA.

Although the results have already been shown to be good for these small tests, there is potential for further improvements. In test 5 the propagation speeds are too fast down the valley, which is primarily caused by the large computational elements. Future work should aim to find an approach to limit the propagation speeds for large computational elements. Using a single flux calculation at the interface, rather than a summation of panel fluxes, has the potential to make RFSM-EDA considerably faster still, although the impact on simulation accuracy will require verification. Some investigations may be necessary to see whether predictions of low-depth flow paths can be improved, as in test 8A, but these shallow flow paths are less important for probabilistic risk calculations than greater depths.

The RFSM-EDA has been developed specifically for use at larger spatial scales and within the context of probabilistic simulations. The model provides a step-change in accuracy over previous versions, the dynamic RFSM and the direct RFSM (which is currently used within the Environment Agency's NaFRA and MDSF2 systems). This significant improvement comes with the price of additional computational expense over the direct RFSM. The computational expense is however, a fraction of that associated with alternative models that solve the full SWE on conventional grid systems. The model therefore provides a good compromise between practical computational times, while providing robust flood simulations.

5. Conclusions

RFSM-EDA has been applied to six of the EA's hydraulic benchmarking tests, four of which are shown in this paper. The model was designed to be used on larger domains of naturally varying topography, but nonetheless has performed well given the small-scale nature of the tests. The peak levels predicted by RFSM-EDA differed by less than ± 10 cm from the other models in all cases except for test 5, where they were within ± 50 cm. This is a mesh effect rather than a numerical inaccuracy, as when using an equivalent mesh resolution the results were visually identical to those of Lisflood-ACC. The velocity predictions had a similar form to the other models, though they tended to be 20–60% lower. This is primarily because an impact zone average velocity is used; using a maximum velocity would be more

conservative. RFSM-EDA clearly offers a step change in accuracy over the direct RFSM and dynamic RFSM, while comparing favourably with industry standard codes. As RFSM-EDA can increase topographic resolution without needing to increase the number of computational elements, it is able to improve simulation accuracy further with minimal change in computational burden.

RFSM-EDA was the fastest of all models by a considerable margin on all of the tests (less than a tenth of the average runtime of the models shown here, and between 4% and 73%, depending on the test, of the runtime of the otherwise fastest model). It has the potential to be even faster if simpler flux calculations and parallelisation are implemented. Additional testing on very large regional domains is underway, and it is likely that the benefits of the scheme will become even more apparent as the trade-off between simulation time and grid resolution becomes more severe for conventional models.

RFSM-EDA has completed a selection of the EA benchmarking tests with fast runtimes and results accurate enough for broad-scale flood risk assessments. The tests present a proof of concept, and demonstrate that the model has the potential to be an effective tool for large-scale and probabilistic inundation modelling.

Acknowledgements

Our thanks to Jeff Neal and Paul Bates of Bristol University, and Tom Willis of Leeds University, for providing the Lisflood-ACC results, Ruth Clarke of Innovyze for the Infoworks ICM results, Bill Syme of BMT WBM for the Tuflow FV results, and Rob Lamb of JBA for JFLOW-GPU. Thanks to Nigel Wright of Leeds University who helped coordinate the acquisition of some of the data. This joint Heriot Watt and HR Wallingford research collaboration is funded by HR Wallingford's internal research programme and Herriot Watt's PhD scholarship scheme.

REFERENCES

Bates P and De Roo A (2000) A simple raster-based model for flood inundation simulation. *Journal of Hydrology* **236(??)**: 54–77.

Bates P, Horritt M and Fewtrell T (2010) A simple inertial formulation of the shallow water equations for efficient two-dimensional flood inundation modelling. *Journal of Hydrology* **387(??)**: 33–45.

Beven K and Binley A (1992) The future of distributed models – model calibration and uncertainty prediction. *Hydrological Processes* **6(??)**: 279–298.

Bradbrook K, Lane S, Waller S and Bates P (2004) Two dimensional diffusion wave modelling of flood inundation using a simplified channel representation. *International Journal of River Basin Management* **2(??)**: 211–223.

Casulli V and Stelling G (2011) Semi-implicit subgrid modelling of three-dimensional free-surface flows. *International Journal for Numerical Methods in Fluids* **67(??)**: 441–449.

Chen A, Djordjevic S, Leandro J, Evans B and Savic D (2008) Simulation of the building blockage effect in urban flood modelling. *11th International Conference on Urban Drainage, Edinburgh, UK*, pp. ■■■–■■■.

Environment Agency (2009) *Flooding in England: A National Assessment of Flood Risk*. Environment Agency, Bristol, UK.

Environment Agency (2010) *Benchmarking of 2D Hydraulic Modelling Packages*. SC080035/SR2. Environment Agency, Bristol, UK.

Environment Agency (2011) *MDSF2 Technical Report, Science Report SC050051/SR4*. Environment Agency, Bristol, UK.

Estrela T and Quintas L (1994) Use of a GIS in the modelling of flows on floodplains. In *2nd International Conference on River Flood Hydraulics, York, UK* (White W and Watts J (eds)).

EC (European Parliament and Council of the European Union) (2007) Directive 2007/60/EC of the European Parliament and of the Council of 23 October 2007, On the assessment and management of flood risks. *Official Journal of the European Union*, L288/27.

Evans E, Hall J, Penning-Roswell E *et al.* (2006) Future flood risk management in the UK. *Proceedings of the Institution of Civil Engineers – Water Management* **159(1)**: 53–61.

Fewtrell TJ, Bates PD, Horritt M and Hunter NM (2008) Evaluating the effect of scale in flood inundation modelling in urban environments. *Hydrological Processes* **22(??)**: 5107–5118.

Fewtrell T, Duncan A, Sampson C, Neal J and Bates P (2011) Benchmarking urban flood models of varying complexity and scale using high resolution terrestrial LiDAR data. *Physics and Chemistry of the Earth* **36(??)**: 281–291.

Gouldby B, Sayers P, Mulet-Marti J, Hassan M and Benwell D (2008a) A methodology for regional-scale flood risk assessment. *Proceedings of the Institution of Civil Engineers-Water Management* **161(??)**: 169–182.

Gouldby B, Sayers P and Tarrant O (2008b) Application of a flood risk model to the Thames Estuary for economic benefit assessment. In *Risk Analysis VI:Simulation and Hazard Mitigation* (Brebbia CA and Beriatos E (eds)). WIT Press, Caephalonia, pp. 11–19.

Guinot V and Soares-Frazao S (2006) Flux and source term discretization in two-dimensional shallow water models with porosity on unstructured grids. *International Journal for Numerical Methods in Fluids* **50(??)**: 309–345.

Hall JW, Dawson RJ, Sayers PB *et al.* (2003) A methodology for national-scale flood risk assessment. *Proceedings of the Institution of Civi Engineers – Maritime Engineering* **156(3)**: 235–247.

Hartnack J, Enggrob H and Rungo M (2009) 2D overland flow modelling using fine scale DEM with manageable runtimes. In *Flood Risk Management: Research and Practice* (Samuels P (ed)). Taylor and Francis, London.

Horritt M and Bates P (2001) Effects of spatial resolution on a raster based model of flood flow. *Journal of Hydrology* **253(??)**: 239–249.

HR Wallingford (2006) *Rapid Flood Spreading Methodology (RFSM)*. Thames Estuary 2100 Report DT4. Environment Agency, Bristol, UK.

Hunter NM, Horritt MS, Bates PD, Wilson MD and Werner MGF (2005) An adaptive time step solution for raster-based storage cell modelling of floodplain inundation. *Advances in Water Resources* **28(??)**: 975–991.

Hunter NM, Bates PD, Neelz S *et al.* (2008) Benchmarking 2D hydraulic models for urban flooding. *Proceedings of the Institution of Civil Engineers – Water Management* **161(??)**: 13–30.

Innovyze (2011) *Infoworks 11·5 RS Help*. Innovyze, Broomfield, CO, USA.

Lamb R, Crossley M and Waller S (2009) A fast two-dimensional floodplain inundation model. *Proceedings of the Institution of Civil Engineers – Water Management* **162(??)**: 363–370.

Lhomme J, Sayers P, Gouldby B, Samuels P and Wills M (2009) Recent development and application of a rapid flood spreading method. In *Flood Risk Management: Research and Practice* (Samuels P (ed.)) Taylor and Francis, London, UK, pp.15–24.

Lhomme J, Gutierrez-Andres J, Weisgerber A *et al.* (2010) Testing a new two-dimensional flood modelling system: analytical tests and application to a flood event. *Journal of Flood Risk Management* **3(??)**: 33–51.

Lhomme J, Jamieson S and Gouldby B (2012) A fast 2D diffusive wave model with sub-element resolution for large scale flood mapping. In preparation.

Mark O,Weesakul S, Apirumanekul C, Aroonnet S and Djordjevic S (2004) Potential and limitations of 1D modelling of urban flooding. *Journal of Hydrology* **299(??)**: 284–299.

McMillan H and Brasington J (2007) Reduced complexity strategies for modelling urban floodplain inundation. *Geomorphology* **80(3–4)**: 226–243.

National Audit Office (2011) *Flood Risk Management in England*. The Stationary Office, London, UK.

Neal J, Villanueva I, Wright N *et al.* (2011) How much physical complexity is needed to model flood inundation? *Hydrological Processes* **26**, http://dx.doi.org/10.1002/hyp.8339.

Romanowicz R and Beven K (2003) Estimation of flood inundation probabilities as conditioned on event inundation maps. *Water Resources Research* **39(3)**: http://dx.doi.org/1029/2001WR001056.

Romanowicz R, Beven KJ and Tawn J (1996) Bayesian calibration of flood inundation Models. In *Floodplain Processes* (Anderson MG, Walling DE and Bates PD (eds)). Wiley, Chichester, UK, pp. ■■■–■■■.

Wright N, Neelz S and Pender G (2012) EA 2D Benchmarking Study. *Proceedings of the Institution of Civil Engineers – Water Management*, this issue.

Yu D and Lane S (2006a) Urban fluvial flood modelling using a two-dimensional diffusion-wave treatment, part 1: mesh resolution effects. *Hydrological Processes* **20(??)**: 1541–1565.

Yu D and Lane S (2006b) Urban fluvial flood modelling using a two-dimensional diffusion-wave treatment, part 2: development of a sub-grid-scale treatment. *Hydrological Processes* **20(??)**: 1567–1583.

Yu D and Lane S (2011) Interactions between subgrid-scale resolution, feature representation and grid-scale resolution in flood inundation modelling. *Hydrological Processes* **25(??)**: 36–53.

Zanobetti D, Longeré H, Preissmann A and Cunge J (1970) Mekong Delta mathematical model program construction. *Journal of the Waterways and Harbors Division* **96(??)**: 181–199.

Zhang WH and Cundy TW (1989) Modelling of two-dimensional overland-flow. *Water Resources Research* **25(??)**: 2019–2035.

1: Goulby – is Spain the appropriate location for the second affiliation?
2: Is the use of this "alternative" Greek sigma rather than the usual σ intentional and for a purpose?
3: Woodward et al. 2011 is not listed in References.
4: DEM has not been "defined" – spell out at first use.
5: Head 3 was followed by 3.1.1. A heading 3.1 is required between them. The alternative is to re-number all the sub-head in Section 3.
6: PRODUCTION: this paper is in this issue; see list
7: Where (??) is appended to a volume number, please supply the issue number if there is one.
8: Beven K and Binley A (1992) – This reference does not appear to be cited in the text.
9: Chen et al. 2008 – page numbers in Proceedings? Who si the sponsor/publisher?
10: Estrela T and Quintas L (1994) – Name and location of publisher of Proceedings?
11: Fewtrell TJ, Bates PD, Horritt M and Hunter NM (2008) – This reference does not appear to be cited in the text.
12: Fewtrell T, Duncan A, Sampson C, Neal J and Bates P (2011) – This reference does not appear to be cited in the text.
13: Lhomme J, Jamieson S and Gouldby B (2012) – Include only if "in press" by proof stage. Otherwise delete from list and cite in text as "unpublished".
14: Neal J, Villanueva I, Wright N *et al.* (2011) – include publication details as well as DOI.
15: Romanowicz R and Beven K (2003)– include publication details as well as DOI
16: Romanowicz R, Beven KJ and Tawn J (1996) – page numbers?
17: PRODUCTION: Add details when the issue is paginated.

WHAT DO YOU THINK?

To discuss this paper, please email up to 500 words to the editor at journals@ice.org.uk. Your contribution will be forwarded to the author(s) for a reply and, if considered appropriate by the editorial panel, will be published as a discussion in a future issue of the journal.

Proceedings journals rely entirely on contributions sent in by civil engineering professionals, academics and students. Papers should be 2000–5000 words long (briefing papers should be 1000–2000 words long), with adequate illustrations and references. You can submit your paper online via www.icevirtuallibrary.com/content/journals, where you will also find detailed author guidelines.